ABSTRACT

YADAV, RAMESHWAR. Chemically Crosslinked Polymer Electrolyte Membranes from Fluorinated Liquid Precursors for Application in Fuel Cells**.** (Under the direction of Dr. Peter S. Fedkiw and Dr. Joseph M. DeSimone.)

Chemical crosslinking of polymer electrolyte membrane (PEM) liquid precursors has the ability to support variable acid loading and create intricate structures that are highly effective in suppressing methanol crossover while maintaining reasonable conductivity in PEMs for direct methanol fuel cells (DMFCs). PEM fabrication from photocuring of liquid precursors is another advantage over traditional methods of melt-processing and solvent-casting in which high cost and sophisticated equipment are employed. Linear-chain PEMs have certain shortcomings for application in DMFCs because of methanol crossover from the anode to the cathode, limited conductivity and high cost from processing steps and conditions.

In our approach, photocuring of liquid precursors produces chemically crosslinked PEMs with good mechanical strength and dimensional stability. Styrene functionalization of perfluoropolyethers diols of six different molecular weights (MWs) between 1000-4000 g mol^{-1} yields crosslinkers that afford crosslink density corresponding to their MWs. Copolymerization of the fluorinated liquid crosslinker and a styrene sulfonate ester co-monomer via UV-light initiated free-radical bulk polymerization produces chemically crosslinked PEMs. Conversion of the ester into corresponding sulfonic acid through base/alcohol hydrolysis and ion-exchange in acid solution confers these PEMs excellent proton conductivity.

The variable crosslink density from different MWs of crosslinker provides wide window of compostions to form PEMs with ion-exchnage capacity (IEC) varying from 0.5 to 1.85 meq g^{-1}. The higher end of acid loading is two times that of benchmark Nafion membrane at good mechanical strength and dimensional stability in these crosslinked PEMs. Such high-acid loading in linear-chain PEMs leads to dissolution in polar solvents. Combining low MW (1000 g mol^{-1}) and high MW (4000 g mol^{-1}) crosslinkers in these PEMs improves the mechanical strength further. The fluorinated chain in crosslinked structure from perfluoropolyethers provides thermal stability up to 260 °C that is sufficient for most practical applications of DMFCs.

Due to IEC of 1.85 meq g^{-1}, these PEMs have shown conductivities of 220 to 340 mS cm^{-1} at 100% relative humidity and at 25 to 60 °C, respectively, that are 3-fold higher than that of Nafion 117 conductivity. For methanol crossover reduction, the nature of crosslinked structure has been exploited to obtain PEMs with good methanol barrier and proton conduction properties. An objective of this research was to optimize the composition of PEMs derived from crosslinker with six different MWs and comonomer resulting in low methanol permeability and reasonable conductivity. This combination of low permeability and reasonable conductivity has resulted in the selectivity of 1.36×10^5 S cm^{-1}/cm^2 sec^{-1} that is more than three times that of Nafion 117 selectivity.

Depending on the crosslinker MW and composition, these crosslinked PEMs have conductivities in the range of 10^{-4} to 10^{-1} S cm^{-1} and methanol permeabilities in the range of 10^{-9} to 10^{-6} cm^2 sec^{-1}. Under identical acid content, incorporation of low MW crosslinkers reduces the methanol permeability further by increasing the crosslink density. Nafion 117 has conductivity of $1.04 \pm 0.02 \times 10^{-1}$ S cm^{-1} and methanol permeability of $2.19 \pm 0.63 \times 10^{-6}$ cm^2 sec^{-1} in liquid water and at room temperature.

In addition to crosslinked PEMs in acidic form, photocuring of mixture of liquid precursor and 4-vinylbenzyl trimethyl chloride dissolved in a solvent (3,3,4,4,5,5,6,6,7,7,8,8,8-tridecafluoro-1-octanol) yields a novel crosslinked alkaline anion exchnage membrane (AEMs). Without any optimization in composition, these crosslinked AEMs in hydroxyl form have shown good conductivity of 45 mS cm^{-1} in liquid water and at room temperature for IEC of 1.43 meq g^{-1}. Analogous to crosslinked acidic PEMs, excellent opportunity exists to exploit the crosslinking approach and optimize the composition and processing condition to achieve maximum anionic ion-exchnage capacity, high conductivity and low methanol permeability in these crosslinked AEMs for application in alkaline fuel cells.

Chemically Crosslinked Polymer Electrolyte Membranes from Fluorinated Liquid Precursors for Application in Fuel Cells

by
Rameshwar Yadav

A dissertation submitted to the Graduate Faculty of
North Carolina State University
in partial fulfillment of the
requirements for the degree of
Doctor of Philosophy

Chemical Engineering

Raleigh, North Carolina

2010

APPROVED BY:

Dr. Peter S. Fedkiw Chair of Advisory Committee	Dr. Joseph M. DeSimone Co-chair of Advisory Committee
Dr. Saad Khan Committee Member	Dr. Xiangwu Zhang Committee Member

DEDICATION

This dissertation is dedicated in true spirit to my father Late Sri Gama Yadav who died in summer 2004, and to family members: my mother Srimati Kamala Yadav, twin daughters Sonika and Monika, wife Ritu, brother Raju, and sisters Chinta and Rita for their caring, love and support.

BIOGRAPHY

Rameshwar Yadav was born in Siwan town, Bihar state, India. After his Bachelor of Technology degree in Chemical Engineering from Institute of Technology, BHU, Varanasi, India in 1993-1997, Rameshwar Yadav worked as operation and process engineer with Mangalore Refinery and Petrochemicals Limited, Mangalore, India for four years from 1997-2001 to gain industrial experience. In 2001, Rameshwar Yadav decided to broaden his career prospect in energy-related area and joined N. C. A & T State University, Greensboro, North Carolina for Master of Science degree in Chemical Engineering. To achieve his career goals, Rameshwar Yadav joined Department of Chemical & Biomolecular Engineering, North Carolina State University in Fall semester, 2004 to pursue PhD graduate study in Chemical Engineering under the guidance of Prof. Peter S. Fedkiw and Prof. Joseph M. DeSimone. Rameshwar Yadav's interests include spending time with his family, reading and applying creativity in solving the problems.

ACKNOWLEDGMENTS

I declare unequivocal gratefulness to these many people who have been genuinely supportive of me during my PhD graduate study at NCSU. First, I would like to express my gratitude to my advisors Prof. Peter S. Fedkiw and Prof. Joseph M. DeSimone for their consistent support, guidance and encouragement. In both research and professional areas, my advisors have encouraged me to learn and persevere to achieve the goals. Their thoughtful and constructive comments have been great source in my career development. I am grateful to Prof. Fedkiw for his commitment and time on my PhD study in all these years.

I would like to thank Prof. DeSimone for providing me with an opportunity and support to be engaged in his research group where I have gained immensely in development of polymer materials. I would like to thank Prof. Fedkiw and Prof. DeSimone's group members for their assistance and friendship. These group members have been extremely helpful, especially when I have been travelling from one research laboratory to the other.

I would like to thank Prof. Saad Khan for his willingness to be on my PhD committee. Prof. Khan has always been very kind to me whenever I have asked for his support. I am thankful to Prof. Xiangwu Zhang for his willingness to be on my PhD committee, mentorship and valuable help in my first year of PhD when I was starting this research effort. Prof. Zhang has been very kind and helpful to me whenever I have approached him for his help, advice and lab support.

I would like to thank Prof. Jan Genzer for his help and cooperation. Prof. Genzer's polymer science and technology course helped me greatly in understanding the fundamentals of polymer materials.

Thanks are due to Prof. Keith Beck (Textile Engineering, Chemistry & Science, NCSU) for his valuable help on using his laboratory instruments. Prof. Beck was very generous and supportive when I was conducting the experiments in his laboratory. I gratefully acknowledge the financial support from Department of Energy (DOE) and National Science Foundation-Science and Technology Center (NSF-STC) to pursue these research efforts.

I am extremely grateful to my family members who have motivated me since my childhood to achieve my career goals. Their caring and encouragement has been extremely valuable in achieving this PhD feat.

TABLE OF CONTENTS

LIST OF TABLES

LIST OF FIGURES

CHAPTER 4 CHEMICALLY CROSSLINKED POLYMER ELECTROLYTE MEMBRANES FROM FLUORINATED LIQUID PRECURSORS FOR APPLICATION IN FUEL CELLS

CHAPTER 5 CHEMICALLY CROSSLINKED ANION EXCHANGE MEMBRANES FROM PHOTOCURING OF FLUORINATED LIQUID PRECURSORS AND IONIC COMONOMER

CHAPTER 6 SUMMARY AND RECOMMENDATIONS

APPENDICES

LIST OF ABBREVIATIONS

AEM......................................Anion exchange membrane

AFC......................................Alkaline fuel cell

ASR......................................Area specific resistance

CPE ....Constant phase element

DMFC ....Direct methanol fuel cell

EB ....Electron beam

ePTFE ....Expanded-poly(tetrafluoroethylene)

FID ....Flame ionization detector

EIS..Electrochemical impedance spectroscopy

ETFE ....Poly(ethylene-*co*-tetrafluoroethylene)

EW ....Equivalent weight

FEP.......................................Fluorinated ethylene-*co*-propylene

FTIR-ATR.............................Fourier transform infrared-attenuated total reflectance

GDL ....Gas diffusion layer

IEC ....Ion-exchange capacity

IPN ....Interpenetrating polymer network

MCFC ....Molten carbonate fuel cell

MEA.....................................Membrane electrode assembly

MW ....Molecular weight

NME......................................Nuclear magnetic resonance

NMP......................................*N*-methyl pyrrolidone

PEM......................................Polymer electrolyte membrane

PEMFC..................................Polymer electrolyte membrane fuel cell

PSEPVE................................Perfluoro(4-methyl-3,6-dioxa-7-octene-1-sulfonyl fluoride)

PVA......................................Poly(vinyl alcohol)

P4VP.....................................Poly(4-vinyl pyridine)

PAFC.....................................Phosphoric acid fuel cell

PCTFE...................................Poly(chlorotetrafluoroethylene)

PDMS....................................Poly(dimethyl siloxane)

PEI...Poly(ether imide)

PFPE.....................................Perfluoropolyethers

PTFE.....................................Poly(tetrafluoroethylene)

PVDF....................................Poly(vinylidene fluoride)

RDE......................................Rotating disk electrode

R_f-SSE...................................Styrene sulfonic acid ester

SiC...Silicon carbide

SEBS.....................................Sulfonated ethylene-*ran*-butylene-b-styrene

SOFC.....................................Solid oxide fuel cell

sPEEK...................................Sulfonated poly(ether ether ketone)

SPEES...................................Sulfonated poly(1,4-phenylene ether ether sulfone) sPFPE....................................Styrene-perfluoropolyethers

SSA ....Styrene sulfonic Acid

TFE ....Tetrafluoroethylene

TGA ....Thermo gravimetric analysis

UV...Ultra-violet

YSZ.......................................Yitria (Y_2O_3)-stabilized Zirconia (ZrO_2)

CHAPTER 1

INTRODUCTION

1.1. Fuel Cells

Combustion based-power systems release pollutants, emissions, and greenhouse gases affecting the climate change. Depleting fossil fuel sources, rising fuel prices, growing geopolitical instability, burgeoning world population and expanding economic growth demand development of clean and efficient sources of power supply.[1] Fuel cells are electrochemical devices that have potential to address these challenges through direct conversion of fuel chemical energy into electricity at high efficiency and at low environmental impact. Fuel cells have the potential to supply power to a wide variety of applications ranging from portable power systems to stationary power systems to transportation vehicles. The growth in fuel cells deployment for practical applications indicates that these power devices are at the threshold of widescale commercialization.

In combustion engines, instant oxidation of hydrocarbons and reduction of oxygen from the air produces only thermal energy resulting in limited efficiency by Carnot cycle. On the contrary, fuel cells have physical separation of half-cell reactions that drive electrons away from the electrochemical reactions sites to produce electricity efficiently along with usable water and heat. Among all the power sources, fuel cells have the highest energy density (100-500 Wh/kg) with the lowest power density (10-100 W/kg) as shown in Figure 1.1.1.[2,3]

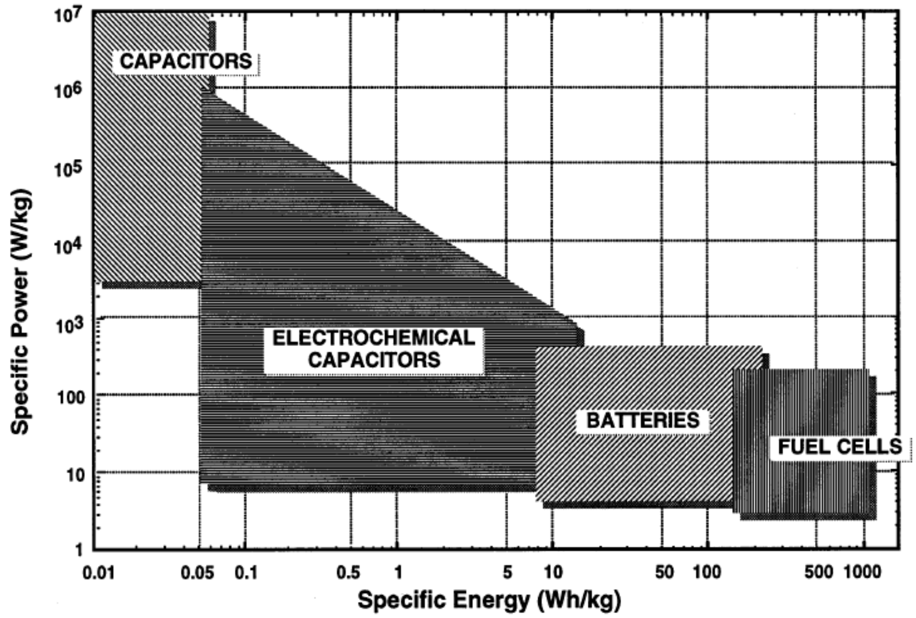

Figure 1.1.1. Ragone plot and comparison of power densities of portable power sources.[2,3]

Unlike batteries and capacitors, fuel cells supply uninterrupted and reliable power at continuous reactants supply. In fuel cells, electro-oxidation of fuels at the anode and electro-reduction of oxygen from the air at the cathode produces electricity, usable heat and water, and CO_2 in case of organic fuels. Based on the types of fuels, fuel cells generate electricity with reduced CO_2 per unit of electricity produced. Use of hydrogen from fossil fuels offers opportunities to sequester, compress, and store CO_2 underground to mitigate the global warming and benefit the environment. There are many types of fuel cells, such as polymer electrolyte membrane (PEM) fuel cells, direct methanol fuel cells (DMFCs), alkaline fuel cells (AFCs), phosphoric acid fuel cells (PAFCs), molten carbonate fuel cells (MCFCs), and solid oxide fuel cells (SOFCs). The electrolytes and operating temperatures classify the type of these fuel cells. Depending on the diverse fuels supply, each type of fuel cells has its own arena of practical application as shown in Figure 1.1.2.

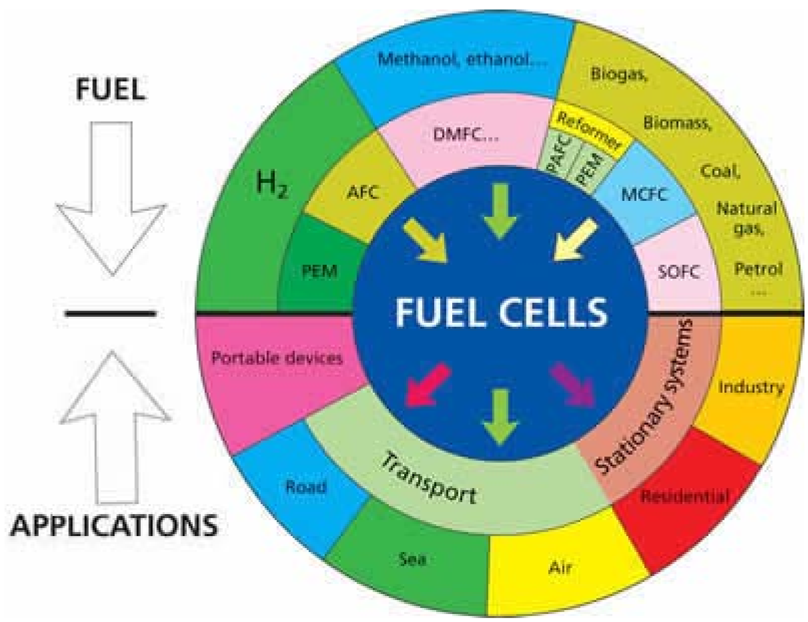

Figure 1.1.2. Types of fuels, fuel cells and their applications.

From Figure 1.1.2, these fuel cells can operate on diverse fuels that include both renewable and fossil fuels to supply power to any practical application. Fuel cells operating on hydrogen from renewable sources add another appealing credential to these power devices. The basic structure of any fuel cells consists of anode for electro-oxidation of reactant fuels, electrolyte for charge carrier transport, and cathode for electro-reduction of oxygen from the air. Figure 1.1.3 illustrates prominent features and comparison of six types of fuel cells.[2,4]

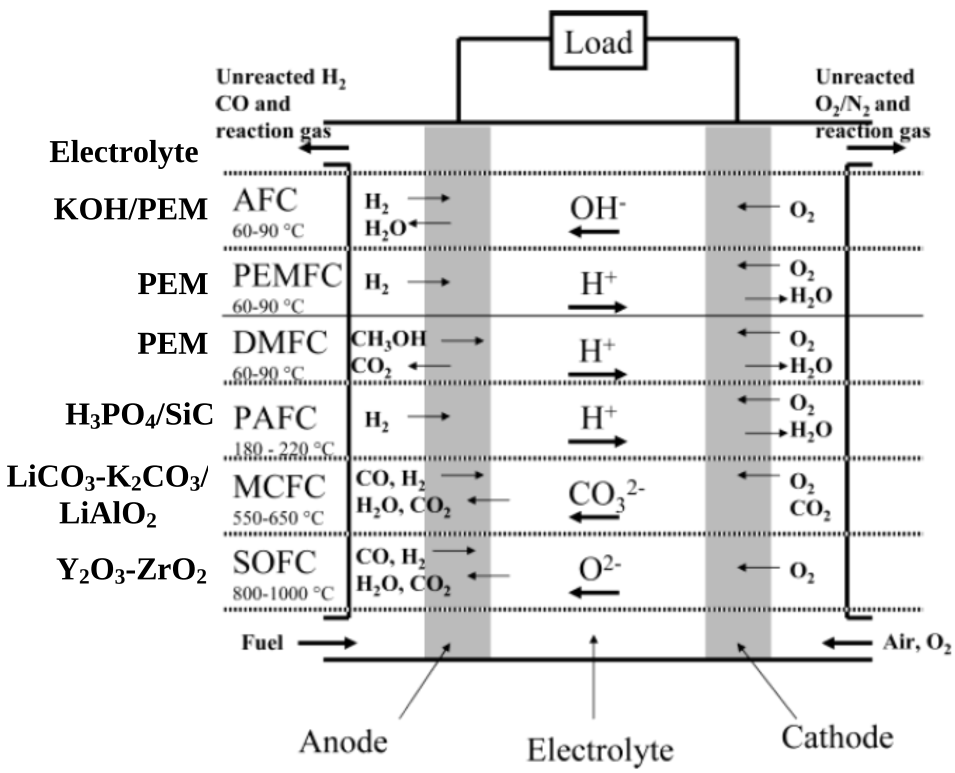

Figure 1.1.3. Comparison of various fuel cells.[2,4]

These fuel cells operate on temperature from 60 to 1000 °C and have their own advantages and disadvantages.[2,4] High-temperature operation in MCFCs (600 °C) and SOFCs (1000 °C) allow direct oxidation or internal reforming of the diverse hydrocarbon fuels producing electricity and practical heat at high efficiency. In MCFCs, the electrolyte is combination of alkali metals (Li, Na, and K) carbonate retained in a ceramic matrix of $LiAlO_2$.[5] These carbonates become conductive at temperature above 600 °C in which charge carrier CO_3^{2-} migrates from the cathode to the anode.[5] SOFCs consist of non-porous metal oxide electrolyte Y_2O_3-stabilized ZrO_2 (YSZ) that attains conductivity at temperature above 800 °C allowing O^{2-} migration from the cathode to the anode.[5] Slow start-up, robust materials requirement, corrosion severity in MCFCs, and thermal expansion and durability in SOFCs are challenges for these fuel cells that have restricted their commercial applications.[4] PAFCs operate in acidic electrolyte retained in silicon carbide (SiC) matrix and at relatively high temperature to achieve good proton conduction.[5] The PAFC suffers from the loss of water vapor due to operation at 200 °C resulting in decline in electrolyte conductivity and performance. Adsorption of mobile phosphate anion on the cathode catalyst reduces the electrode kinetics.[4]

Alkaline fuel cells (AFCs) are low-temperature fuel cells in which hydroxide ion (OH^-) migrates from the cathode to the anode through an alkaline electrolyte. Due to the alkaline electrolyte and elevated pH, electrochemical reactions are facile allowing the use of inexpensive non-noble metal electrocatalysts such as Ni and Ag while accomplishing the comparable performance.[6] In AFC, water consumption at the anode drives water migration from the cathode giving a relatively district advantage in water and flooding management.[6] Conventionally, an AFC operates on liquid KOH electrolyte stabilized in a porous matrix with KOH concentration of 85 wt% for high temperature (250 °) and 35-50 wt% for low temperature (120 °C) operation.[5] This liquid electrolyte is intolerant to CO_2 forming carbonate from mobile metal cation (K^+) and CO_2. Carbonate formation lowers the electrolyte conductivity and precipitates at the cathode hindering mass transfer.[7]

Anion exchange membranes (AEMs) possess several distinct advantages over liquid electrolytes.[8] These membranes have immobilized cationic charges that promote efficient transport of anionic charge carrier. The following benefits: reasonable conductivity, sufficient durability, simplicity in selection and design from polymer materials, good ability to serve as mechanical separator between fuel and oxygen from the air, and choice of thicknesses in membrane electrode assembly (MEA) fabrication have attracted interest in developing the next generation AEMs. Despite so many appealing features of AFCs based on AEMs, conductivity of AEMs is expected to be lower than that of proton exchange membranes (PEMs) at equivalent charge-carrier density. The higher mobility and diffusivity of protons (H^+) than that of hydroxyl ions lead to higher relative conductivity in PEMs (mobility $u_{H+}= 3.63 \times 10^{-3}$, $u_{OH^-}= 2.05 \times 10^{-3}$ cm^2 sec^{-1} V^{-1}, diffusivity $D_{H+}= 9.31 \times 10^{-5}$, $D_{OH^-} = 5.28 \times 10^{-5}$ cm^2 sec^{-1}).[9,10]

1.2. PEM Fuel Cells

PEM fuel cells are efficient (40-80%), low-operating temperature (60-120 °C) and high-power density types of fuel cells suitable for portable, stationary, and transportation power applications. These fuel cells operate on diverse fuels, such as hydrogen, methanol, ethanol, formic acid, dimethyl ether, and others because these fuels are electrochemically active at the operating temperature of PEM fuel cells. In PEM fuel cells, fuels are electro-oxidized at anode releasing protons and electrons. The released protons migrate from the anode to the cathode through PEMs to electro-reduce oxygen from the air. The released electrons travel through the external circuit producing environmentally clean and efficient electricity. The theoretical efficiency and power density of PEM fuel cells are partly realized because of irreversible activation losses from the electrode polarization, ohmic losses predominantly from the ionic resistance of the membrane, and mass transfer limitation at high current density.

The PEM fuel cells are composed of current collector, bipolar plates with flow channels; porous gas diffusion layers (GDLs), electrocatalyst layers, and PEMs. Bipolar plates are designed with machined flow-field to distribute the reactants uniformly and effectively along the electrode surface. Bipolar plates provide structural rigidity and serve as current collector, reactants distributor and separator between fuels and oxidant in a fuel cells stack.[5] Bipolar plates are fabricated from lightweight material such as graphite. In bipolar plates, high electrical and thermal conductivities are essential for efficient electron conduction and heat removal from the system.[5]

Effective electron conduction and transport of reactants and byproducts are essential in GDLs. The porous structure in GDLs allows effective diffusion of reactants and byproducts. The GDLs are made from carbon papers or fabrics incorporating Teflon dispersion or related materials to create hydrophobic atmosphere. Use of carbon provides sufficient electron conduction and hydrophobic Teflon assists in repelling water from the reaction sites. Water removal is important to mitigate flooding which disrupts the diffusion process in PEM fuel cells.

The electrodes so-called catalysts layers (10-30 μm thick) are an important part of PEM fuel cells. The electrode architecture consists of heterogeneous three-phase atmosphere that is essential for electrons, protons, and reactants transport to the catalyst surface. High-surface area, high-catalyst activity, and long-term stability in PEM fuel cells are some of the requirements for a good electrocatalyst. The surface area of electrocatalyst particle varies with particle diameter in the following way:

$$S = \frac{6}{\rho_{Pt} d}$$

where *S* is surface area, *d* is particle diameter and ρ_{Pt} is particle density. Small particle sizes provide large surface that improves the reaction rates. Typically, the electrocatalyst particles (2-4 nm) supported on carbon black particles (30 nm) are dispersed in Nafion dispersion or related ionomer solution to fabricate the electrodes. Ionomer solution assists in proton conduction around the catalyst sites and reduces interlayer resistance at electrode and membrane. Depending on the construction methods, the catalyst-ionomer solution is dried over GDL or membrane to form the MEA. Despite significant progress in MEA assembly, catalysts formulation and MEA fabrication are still delicate projects that require expertise and experience.

In PEM fuel cells, PEM is a central component that serves as proton conductor and mechanical separator for fuels and oxidant. To date, most of the PEMs have been explored for hydrogen-based fuel cells because these fuel cells produce high-power density at high efficiency from facile electro-oxidation of hydrogen. However, these fuel cells face the challenge of hydrogen fuel storage, distribution, and transportation. Hydrogen generation from the fossil fuels leaves inherently some residual carbon monoxide (CO) that poisons the electrocatalysts in PEM fuel cells operating at low temperature. Carbon monoxide adsorbs strongly on the catalytic site reducing the catalyst activity. However, operating PEM fuel cells at high temperature around 150 °C addresses the CO poisoning issue because high temperature is not favorable to CO adsorption on the catalyst site. Besides mitigating the CO poisoning of the electrocatalyst, high-temperature operation improves the overall efficiency of PEM fuel cells.

Despite so much progress in PEM fuel cells, lack of affordable and convenient hydrogen-fuel supply infrastructure has prevented the widespread adaptability of these power devices.[1] Liquid fuels like methanol have advantage over hydrogen because liquid methanol can be easily handled and transported through current infrastructure.[1] Unlike hydrogen gas, liquid methanol fuel and DMFCs have attractive features mostly for portable electronic devices because of simplicity in design and operation.[1]

1.3. Direct Methanol Fuel Cells

DMFCs can be competitive with and viable alternatives to batteries and other power generating devices because of direct electro-oxidation of liquid fuel into electricity. DMFCs are low-temperature power devices because methanol is electrochemically active at such low temperature. Methanol has relatively high volumetric energy density (5000 Wh/L) compared with batteries and hydrogen.[1] This volumetric capacity increases the overall power density of competing electrochemical power sources. DMFCs have promising attributes, such as uninterrupted power supply from a liquid fuel source without any reforming, high power-to-weight ratio, fast start-up, high efficiency, low capital and operating costs, and possible miniaturization for portability. Like traditional PEM fuel cells, electro-oxidation of methanol solution in DMFCs releases protons, electrons, and carbon dioxide as anodic byproduct. The released protons migrate from the anode to the cathode through the PEM to combine with oxygen producing water as cathodic byproduct. Figure 1.3 depicts a schematic diagram of DMFCs. The DMFCs have most of their components in common with traditional PEM fuel cells. The following half-cell reactions describe the electrochemical processes at DMFCs electrodes:

Anode: $CH_3OH + H_2O \rightarrow 6H^+ + 6e^- + CO_2$ $\quad \Delta G^0 = 9.3$ kJ/mol $\quad E_{Anode} = -0.016$ V

Cathode: $3/2\ O_2 + 6H^+ + 6e^- \rightarrow 3H_2O$ $\quad \Delta G^0 = -237.1$ kJ/mol $\quad E_{Cathode} = 1.229$ V

Overall: $CH_3OH + 3/2\ O_2 \rightarrow CO_2 + 2H_2O$ $\quad \Delta G^0 = -nFE = -227.8$ $\quad E_{Cell} = 1.213$ V

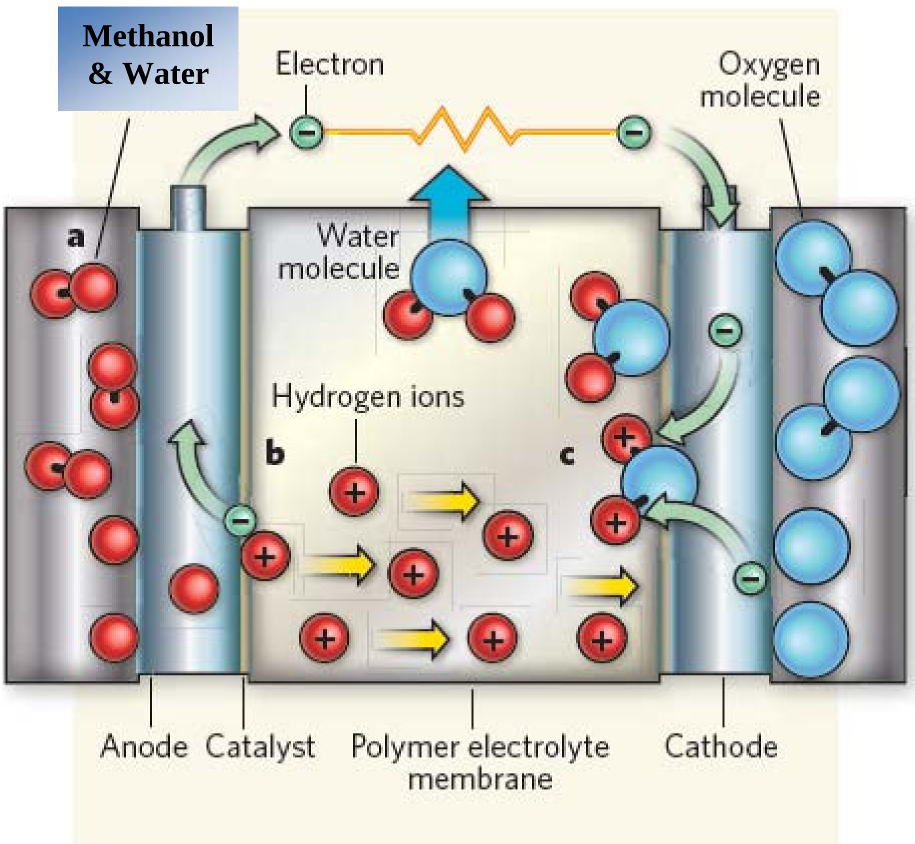

Figure 1.3. Schematic of DMFC.

Equal moles of methanol and water react to produce six protons and six electrons along with byproduct CO_2. At room temperature, DMFCs have theoretical open circuit potential of 1.21 V that gives theoretical efficiency of close to 97%. In methanol electro-oxidation, all the six electrons evolve through multiple reaction steps leading to difficult and sluggish kinetics in comparison with hydrogen electro-oxidation.[8,11] Bimetallic electrocatalyst (Pt-Ru, 1:1) speeds up the methanol electro-oxidation.[8] Aqueous fuel supply due to water as stoichiometric reactant at the anode contributes significantly to water availability in DMFCs. Furthermore, water migration from the cathode to the anode due to water consumption at the anode improves hydration in PEM. As a result, high-ionic conductivity is expected to be available in DMFCs. Methanol crossover from the anode to the cathode has a deleterious effect on DMFCs performance.[1]

1.4. Polymer Electrolyte Membranes

The demanding operating conditions of DMFCs require PEMs to posses these following properties: high-ionic conductivity, low-liquid fuel permeability, low-swellability upon polar solvent uptake, low-oxidant crossover, acceptable thermal, mechanical, chemical, hydrolytic, and electrochemical stability, and affordable cost. Ionic conductivity and methanol crossover have predominant effect on DMFCs performance. Therefore, the membrane in DMFCs must be both an excellent proton conductor and a barrier to methanol transport. Ionic conductivity depends on both charge carrier concentration and its mobility within the membrane at a given operating condition. Concentration of immobilized charges within the membrane determines the proton concentration in a PEM.

For fixed mobility of charge carrier, proton concentration increases the conductivity proportionally in a PEM. Ion-exchange capacity (IEC) and equivalent weight are measured to determine the proton concentration in a PEM. Equivalent weight (EW) expressed as g equivalent^{-1} is the number of grams of dry polymer per mole of acid groups when the polymer is in acid form. IEC is a measure of ionic groups in the polymer expressed as milliequivalents per gram of dry polymer (meq g^{-1}). The expression EW = 1000/IEC relates both IEC and EW. Permeability is used to characterize methanol crossover in the ionic membrane. Permeability is a measure of diffusion and sorption behavior of solvents in the membrane. Permeability is defined as product of $K \times D$ where K is partition coefficient and D is diffusivity.

In DMFCs, methanol permeation occurs through combination of various phenomena such as wetting of the upstream surface, solubility in, diffusion across, and consumption or pervaporation from the downstream surface of the PEM. Hydrophobic environment at upstream surface of PEMs can reduce the surface wetting and methanol crossover. Type and quantity of immobilized acidic groups, type of polymer fluorocarbon *vs*. hydrocarbon, and solvent-host interaction can influence the methanol solubility in PEMs. Structure of polymer such as linear, crosslinked or combination of the two structures can play important role in diffusion across the PEMs. The rate and type of methanol removal from the downstream surface such as selective electro-oxidation of methanol at the cathode or pervaporation can affect the methanol crossover. Here, we have endeavored to control the methanol crossover through crosslinked polymer structure and reasonable acid loading in novel crosslinked PEMs that have potential to produce great performance in DMFCs.

1.5. Objectives and Overview

For widespread adaptability and early commercialization of DMFCs, PEMs with low-methanol crossover and reasonable conductivity are highly sought. Low-methanol crossover allows DMFCs operation at concentrated methanol-water feed enhancing the performance. Preparing PEMs that have low-methanol permeability and reasonable conductivity is challenging because the transport mechanism of water and methanol are similar. Water is integral to the operation of DMFCs because electro-oxidation of methanol requires water to be present at the anode while electro-oxidation of oxygen generates water at the cathode. The polarity of both water and methanol poses challenges to create PEMs with selective transport of water over methanol. This selective transport can lead to enhancement in ionic conductivity and fuel cells performance.

Many polymers with various chemical structures have been explored to develop PEMs for DMFCs. One approach is to incorporate the inorganic fillers such as silica and titania in the membrane to provide barrier to methanol transport. Inorganic fillers do provide such barrier at the expense of the ionic conductivity and membrane homogeneity. Due to lack of interaction between the polymer host and the inorganic fillers, the stability of the composite PEMs is also questionable. Another approach is to incorporate methanol-inhibiting compounds such as poly(vinyl alcohol) in PEMs to retard methanol crossover. However, adding these compounds typically results in a sacrifice in ionic conductivity as these compounds lack intrinsic ionic conductivity. Additional acid loading is incorporated to maintain reasonable ionic conductivity in such PEMs. Moreover, these organic compounds have inadequate chemical stability in the acidic environment of DMFCs.

Linear-chain polymer Nafion 117 is still the benchmark PEM. However, high methanol crossover limits its utility in DMFCs. Nafion 117 can permeate 40% of methanol feed that adversely affects the cathode performance by generating mixed potential. Developing PEMs that have low-methanol permeability and high conductivity without the addition of inorganic fillers or other methanol-inhibiting compounds remains challenging. This dissertation is aimed at addressing some of the membrane challenges that DMFCs faces.

Chemically crosslinked systems provide an avenue to synthesize PEMs with high-ionic conductivity and low-methanol crossover. First, crosslinked structure can support and sustain high-acid loading in comparison with linear-chain polymer. Secondly, crosslinked polymers instead of linear-chain polymers have the ability to provide an intricate barrier and tortuosity to methanol transport. Unlike linear-chain PEMs that suffer from excessive swelling upon solvent uptake, crosslinked structures inhibit the swelling and expansion because crosslinking constrains the mobility of polymer chains and prevents the dissolution of the polymer.

This work presents a novel approach to develop PEMs from fluorinated liquid precursors without involving any solvent. This is the first crosslinked membranes for DMFCs that has been made from fluorinated polymer. Commercially available liquid perfluoropolyethers (PFPE) diols were functionalized with styrene end groups to yield styrene-perfluoropolyether (sPFPE) that is difunctionalized, highly fluorinated, and photocurable liquid precursor. Crosslinkers of six different molecular weights (MWs) were prepared to vary the crosslink density in the PEMs. For incorporating acid groups into the membrane, the styrene sulfonate ester co-monomer (R_f-SSE) was synthesized from sodium *p*-styrene sulfonate. A series of crosslinked PEMs were formed from the mixture of sPFPE and R_f-SSE through UV-light initiated free-radical bulk polymerization followed by hydrolysis and ion-exchange. Methanol solution uptake was measured to characterize the sorption behavior of PEMs. Ionic conducvity in liquid water and methanol permeability were investigated to study the selectivity (ratio of conductivity to permeability) of these crosslinked PEMs for application in DMFCs.

The objective of this research is to investigate the effects of crosslinker sPFPE MWs, crosslinker weight-content, and acid loading on the properties of crosslinked polymer to produce PEMs that have low-methanol permeability while retaining high-ionic conductivity. Six different MWs (1000-4000 g mol^{-1}) of the crosslinker have enabled variable crosslink density in the membrane. This crosslinking approach has resulted in variable acid loading and in achieving the low-methanol permeability with reasonable ionic conductivity.

There are six chapters in this dissertation. The current Chapter 1 presents the fuel cells introduction, advantages, and challenges of hydrogen- and methanol-based PEM fuel cells. In Chapter 2, literature review provides the discussion on Nafion membrane, application of electric field in forming the membrane, effect of thickness on intrinsic properties of ionomers, sulfonamide-based novel polymers for PEM fuel cells, and some family of polymer materials that have been explored for DMFCs. Applying electric field on starting materials during membrane formation is effective in producing PEMs with favorable anisotropic properties. Independent of IEC and structure, PEM properties are dependent on its thickness as Nafion membranes with same IEC and different thicknesses have exhibited.

Ionic conductivity measurement is critical to characterize the PEMs. Chapter 3 describes the analysis of EIS technique. Nafion 117 conductivity is presented in the wide range of temperature and relative humidity that encompass PEM fuel cells operating conditions. Using experimental results of Nafion conductivity, a universal correlation has been developed that calculates the conductivity at any temperature and at any water vapor activity. The correlation also shows that the proton activation energy is dependent on water vapor activity.

Chapter 4 illustrates the synthesis steps, characterizations, and results of crosslinked PEMs. Crosslinked PEMs were synthesized from sPFPE crosslinker and R_f-SSE comonomer. Synthesis procedure involves styrene functionalization of PFPE diols to produce sPFPE. Incorporating a fluorinated tail to styrene sulfonate salt converts it into R_f-SSE ester that is miscible with sPFPE. Photocuring of sPFPE and R_f-SSE mixture yields solid PEM in ester form. Hydrolysis and ion-exchange converts ester into acid group. Low MW crosslinker has the ability to impart high-Young modulus in PEMs. Combination of low- and high-MW crosslinkers provides a good balance of stiffness and flexibility in the membrane.

IEC study has shown that IEC increases with acid content. Solvent uptake is measured to describe the solubility in PEMs. Methanol-solution uptake study shows that crosslinking can be exploited to obtain PEMs with low methanol-solution uptake. Ionic conductivity measured as function of MW and weight-content of crosslinker has confirmed that reasonable ionic conductivity can be achieved in crosslinked PEMs. Most importantly, crosslinked network as opposed to linear-chain network can reduce the methanol crossover substantially. Under identical acid content, incorporation of low-molecular weight crosslinkers can further reduce the methanol permeability due to the resulting increased crosslink density.

Chapter 5 presents a novel approach to produce crosslinked anion exchange membranes (AEMs) from liquid precursor sPFPE and 4-vinylbenzyl trimethyl ammonium chloride. Anion exchange membranes have several advantages over liquid alkaline electrolytes. Photocuring of sPFPE and 4-vinylbenzyl trimethyl ammonium chloride solution dissolved in a solvent converts the homogeneous mixture into a solid AEM without any further processing steps. Chapter 5 shows the synthesis approach and discusses the advantages of crosslinked AEMs derived directly in ionic form.

Chapter 6 provides the research summary and recommendations for future direction to develop novel PEMs and evaluation of crosslinked PEMs in actual DMFCs. Sulfonimide-based crosslinked PEMs can be derived from the sPFPE and a comonomer as described in Chapter 6. Membrane fabrication directly in ionic form has many benefits for MEA fabrication. Chapter 6 shows a scheme to form the crosslinked PEMs directly in ionic form and extend this strategy to construct MEA without any external ionomer dispersion as binder. At the higher end of IEC in crosslinked PEMs (above 1.5 meq g^{-1}), adding methanol-inhibiting compounds, such as poly(4-vinylpyridine), and poly(vinyl alcohol) has promising potential to reduce methanol permeability further while maintaining good conductivity. To circumvent hydrolysis during membrane-fabrication process, the proposed alternative comonomers can be good candidates to copolymerize with sPFPE.

1.6. References

1. G. A. Olah, A. Goeppert., and G. K. S. Prakash, *Beyond Oil and Gas: The Methanol Economy*, **2006**.

2. M. Winter and R. J. Brodd, *Chem. Rev*. **2004**, *104*, 4245-4269.

3. R. Kotz and M. Carlen, *Electrochim. Acta* **2000**, *45*, 2483–2498.

4. M. L. Perry and T. F. Fuller, *J. Electrochem. Soc.* **2002**, *149*, S59-S67.

5. F. Barbir, *PEM Fuel Cells: Theory and Practice*, **2005**, Chapter 1, 1-16.

6. J. R. Varcoe, R. C. T. Slade, G. L. Wright, and Y. Chen. *J. Phys. Chem. B* **2006**, *110*, 21041-21049.

7. E. Gulzow and M. Schulze, *J. Power Sources* **2004**, *127*, 243-251.

8. J. R. Varcoe and R. C. T. Slade, *Fuel Cells* **2005**, *5*, 187-200.

9. A. J. Bard and L. R. Faulkner, *Electrochemical Methods: Fundamentals and Applications, Potentials and Thermodynamics of Cells* **2001**, Second Edition, page 68.

10. E. L. Cussler, *Diffusion: Mass Transfer in Fluid Systems, Diffusion of Interacting Species, Second Edition,* **1997**, Second Edition, Chapter 6, 142-143.

11. R. Liu and P. S. Fedkiw, *J. Electrochem. Soc.* **1992**, *139*, 3514-3523.

CHAPTER 2

LITERATURE REVIEW

2.1. Alternative PEMs

Polymer electrolyte membrane (PEM) is the central component of PEM fuel cells in which the membrane serves as a medium to transport protons from the anode to the cathode. Operating conditions of PEM fuel cells impose array of requirements on these PEMs. For a PEM to be successful, the PEM must have high conductivity and low-fuel crossover as well as other beneficial properties. A good PEM must be both a good proton conductor and a good barrier to fuels, especially methanol in direct methanol fuel cells (DMFCs). In most of the PEMs, proton conduction occurs efficiently under high-water availability. Due to inherent water requirement in PEM and polar nature of methanol, proton conduction and methanol permeation are proportional and coupled with each other. Methanol-crossover phenomenon occurs through concentration gradient, electro-osmotic drag and eventually consumption at the cathode through facile electro-oxidation. For example, methanol crossover through Nafion 117 leads to 40% loss of methanol in DMFCs.[1] This crossover has deleterious effect in that it diminishes the ionic conductivity and produces mixed potential leading to decline in DMFCs performance.

Many PEMs have been developed in response to address the methanol-crossover challenge associated with DMFCs. These PEMs have been realized with their own advantages and disadvantages. Typically, reduction in methanol permeability has resulted in reduction in ionic conductivity as well. Therefore, it is a challenge to produce a PEM with selective transport of water over methanol because both are polar and have similar chemical behavior with PEM. Moreover, water is a stoichiometric reactant at the DMFC anode. Considerable efforts have been directed to understand the chemical structure and morphology of PEM in relation to reduce the permeability while retaining the conductivity.

Usually, polymer membranes are incorporated with acidic groups to form the PEMs. Many membranes such as linear-chain based random and block copolymers, blend membranes, grafted membranes and composite membranes with inorganic fillers have been developed with aim of reducing methanol crossover. To date, despite its unacceptably high-methanol permeability, Nafion 117 is baseline PEM for comparative study of candidate PEMs and remains the benchmark PEM for DMFCs. The section reviews some of reported efforts on polymer materials for PEM fuel cells, especially DMFCs.

2.2. Nafion Membranes

The state-of-the-art membrane, Nafion, is a random copolymer of tetrafluoroethylene (TFE) and perfluoro(4-methyl-3,6-dioxa-7-octene-1-sulfonyl- fluoride) (PSEPVE) in which ion-containing hydrophilic groups PSEPVE (MW = 446 g mol^{-1}) are spaced randomly along the hydrophobic polytetrafluoroethylene (PTFE) backbones.[2] In the synthesis of this copolymer, TFE pressure and PSEPVE concentration determine the equivalent weight (EW) of the Nafion polymer.[2] Despite having PTFE-like backbone, Nafion morphology is semi-crystalline (15-20%) and disordered. The crstallinity is strongly related to EW and disappears below EW of 965 g/equivalent. Nafion is believed to possess disordered morphology in both dry and hydrated states due to the random location of the hydrophilic and hydrophobic moieties. It is speculated that Nafion 117 has molecular weight of 10^5-10^6 Da with approximately 144 units of PSEPVE pendant groups in a typical polymer chain.

Nafion membranes are fabricated from melt-processing (280 °C) of precursor resin that is in sulfonyl fluoride ($-SO_2F$) form because ionic form of Nafion is intractable.[2] In acid form, aggregation and strong ionic crosslinking make Nafion resins intractable for further processing. During membrane fabrication, extrusion can induce micro-structural orientation and anisotropic properties. After melt-extrusion of the polymer resin, hydrolysis in a 15 wt% of KOH or NaOH base solution containing optional 30 wt% of DMSO to speed up the hydrolysis, for about one hour at 80 °C and ion-exchange in aqueous nitric acid (10 wt%) convert the $-SO_2F$ groups into sulfonic acid ($-SO_3H$). The glass transition temperature of Nafion 1100 EW in acid form is 110 °C. However, glass transition temperature of Nafion in

Li^+, Na^+, and K^+ salts form is 215, 235, and 225 °C, respectively. Figure 2.2 shows the chemical structure of Nafion polymer in which the pendant group terminated by sulfonic acid in PSEPVE is responsible for conductivity.

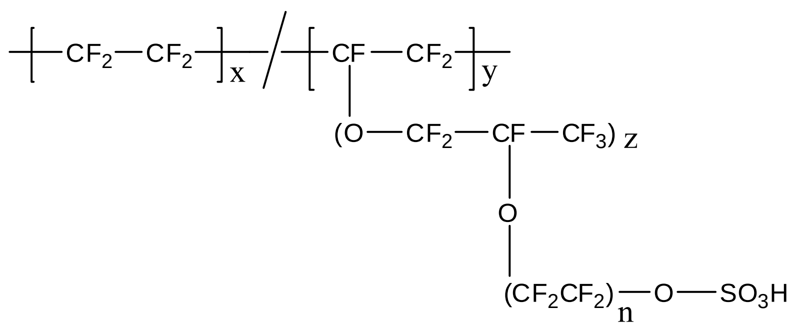

Figure 2.2. Chemical structures of Nafion (x = 6-13, y = 1, z = 1, n = 2), 3M (x = 6-13, y = 1, z = 0, n = 4) and Solvay-Solexis (x = 6-13, y = 1, z = 0, n = 2) membranes.

Like Nafion membrane, 3M and Solvay-Solexis have introduced two other commercial membranes that have Nafion-like PTFE backbone and different sulfonic acid pendant groups (Figure 2.2). In these other commercial membranes, shorter pendant groups than that in Nafion membrane have allowed high-acid loading leading to increase in conductivity.[2-4] However, these other membranes are still under developmental stage for applications in PEM fuel cells.

In addition to polymer membranes, Nafion dispersion is obtained by heating the acidic Nafion polymer in aqueous methanol/ethanol under high pressure. Nafion polymers of lower EWs dissolve at lower temperature than the higher EWs. For example, Nafion polymer of 1100 g/equivalent requires heating above 240 °C in polar solvents to dissolve and form the dispersion. The Nafion dispersion finds its application in formulation of fuel cells catalyst and in preparing relatively thinner membranes so-called dispersion-cast membranes.[5,6]

Both hydrogen and oxygen have higher solubility in Nafion membrane than in pure water where as lower solubility in Nafion than in PTFE.[2] The Nafion resembles strong acid such as trifluoromethane sulfonic acid (CF_3SO_3H) due to perfluorosulfonic acid group with pKa of -6. It is believed that the structural nature of Nafion leads to hydrophobic-hydrophillic phase separation that is interconnected by nanochannels. These nanochannels are believed to control the transport properties in Nafion membrane. Degree of hydration determines the size of these nanochannels, which in turn affects the conductivity. Upon contact with water, Nafion membrane surface changes from hydrophobic to hydrophillic as seen by drop in contact angle.[2]

The Nafion 117 has good protonic conductivity of 100 mS cm^{-1} in liquid water and at room temperature and this conductivity increases with temperature up to 80 °C under high-water availability. However, at and above 80 °C, Nafion is less than optimally efficient due to the loss of water. Nafion 117 is expensive because of the many processing steps involved in its manufacture, and suffers from some shortcomings, such as methanol crossover, low-ionic conductivity under dry conditions, limited IEC (0.91 meq g^{-1}) and insufficient thermal stability above 80 °C. Methanol crossover causes a reduction in the ionic conductivity, swelling of the PEM, and mixed electrode potential at the cathode. In DMFCs that are typically oparted at low-methanol concentration, Nafion 117 can permeate 40% of the methanol. Delamination in the membrane electrode assembly (MEA) that can stem from cyclic swelling and deswelling upon methanol uptake is another potential consequence of methanol-crossover. Nafion 117 exhibits higher swelling in aqueous methanol than in pure water as it lacks an intricate barrier to methanol crossover resulting from its linear-chain polymer structure.

2.3. Electric Field Aligned Membranes

The proton prefers to travel along the shortest path in the polymer electrolyte membranes (PEMs) due to ionic resistance. Tortuous conductive path for proton transport can be altered favorably in transport direction to reduce the ionic resistance. For a given IEC, applying electric field with sufficient strength during the membrane formation can be effective in aligning the immobilized charges permanently in the field direction. Electric field can induce orientation of immobilized ions and align the hydrophillic ionic domains permanently to improve the ionic conductivity for a given IEC in the membrane. The electric field can control the microstructure in the polymer materials with favorable anisotropic properties. These interconnected domains aligned in proton-transport direction can lead to efficient proton-transport. Membranes formed under electric field have demonstrated improved performance in PEM fuel cells. It is important to emphasize that starting materials for membrane formation must be ionic because electric field can be effective mostly on ionic functional groups that are associated with the starting materials.

Besides strength of electric field, other parameters such as nature of solvent and thermal condition during membrane fabrication play an important role in creating the anisotropic structure in the polymer. For example, applying sufficiently high temperature improves the homogeneity in the membrane.[7,8] It is also necessary that dielectric constant of ionic particles must be higher than that of solvent for effective particle orientation.[9] The magnitude and frequency of electric field can determine the size of domains that can be realized in electric field treated PEMs.[10] Electric field has proven to be effective in controlling the structure of composite materials based on inorganic fillers.[11] In composite polymer materials, the inorganic particles can rotate, translate or aggregate to form chains along the field-direction that can be exploited to improve the ionic conductivity in PEMs.[11] It has been reported that electric field can eliminate resistive grain boundaries improving the ionic conducvity of ceramic-based membranes for intermediate temperature fuel cells.[12]

Depending on the membrane-fabrication approach, traditionally, non-ionic monomers or polymers are processed to fabricate the PEMs. Lack of ionic groups in polymer materials at membrane-fabrication stage has curtailed the wide application of electric field. However, some PEMs have been fabricated from ionically conductive polymer materials and inorganic fillers under application of electric field.

Liu and Yates demonstrated the application of electric field to orient ionic domains in sulfonated poly(ether ether ketone) (sPEEK) polymer that was dispersed in non-proton conductor poly(dimethyl siloxane) (PDMS) liquid.[11,13] sPEEK and PDMS combination, though not suitable for actual PEM fuel cells, were used to demonstrate the novel approach to form the membranes with electric field induced selective properties. Thermal curing accompanied by electric field was applied to orient and lock the ionic domains in the field direction permanently. Strength of electric field controlled the chaining of particles in the field direction.[11] AC instead of DC electric field is more effective in uniform distribution of particles and chains through the membranes.[11,13] The electric field polarizes the ionic sPEEK particles in the field direction leading to dipole formation. These diploes form extended chain in the field direction that are fixed permanently after thermal curing of sPEEK and PDMS.

Optical microscopy study, as shown in Figure 2.3.1, has revealed that sPEEK particles orient in the field direction.[11] In through-plane alignment, sPEEK particles formed regular extended chain instead of random chains in in-plane alignment (Figure 2.3.1).

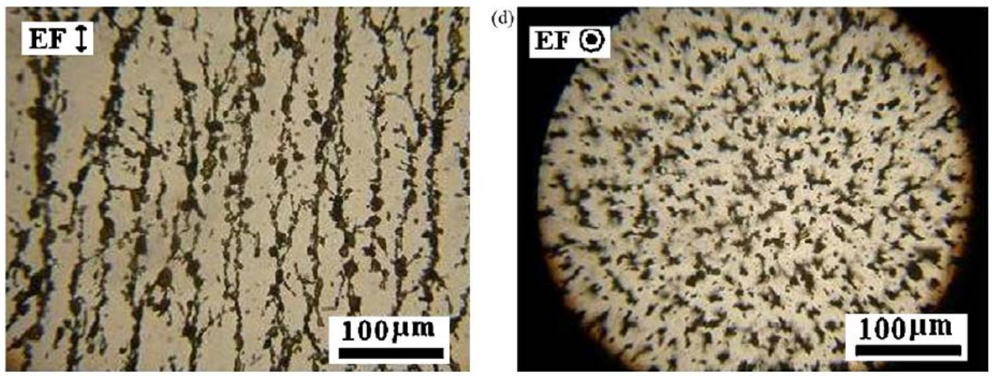

(a) (b)

Figure 2.3.1 Optical microscopy images of sPEEK particles in PDMS membranes (a) In-plane aligned under electric-field (b) Through-plane aligned under electric-field.[11]

In addition to improving the ionic conductivity in the direction of interest, electric field aligned membranes display anisotropic swelling with low area expansion that provides dimensional stability to the membranes under PEM fuel cells operating condition.[13] Due to significant improvement in conductivity and other associated properties of the membranes, reduction in concentration of ionic particles below percolation threshold can be achieved with application of electric field.[11, 13] Figure 2.3.2 shows the substantial improvement in ionic conductivity of Nafion-based membranes that were processed under electric field.[9] Significant improvement in ionic conductivity was accomplished through application of ionic conductivity.

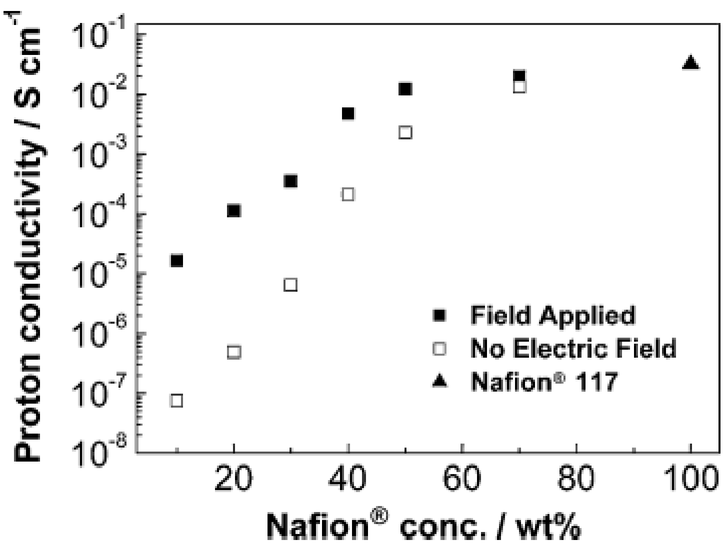

Figure 2.3.2. Through-plane proton conductivity of Nafion/SEBS composite membranes as a function of Nafion content.[9] SEBS is polystyrene-*b*-poly(ethylene-ran-butylene)-*b*-polystyrene.

Karthikeyan *et al*. characterized composite membranes prepared from Nafion dispersion and montmorillonite under application of electric field.[8] Montmorillonite has high aspect ratio of more than 100 and is effective in reducing the methanol crossover if orientated in the transport direction.[8] However, excessive inorganic fillers such as montmorillonite lead to mechanical instability in composite materials. In such situation, controlling the orientation of particles with electric field is an effective means to create anisotropic materials with favorable properties. Atomic force microscopy study showed that montmorillonite particles were orientated in the field direction in Nafion polymer matrix.[8] Lin *et al*. showed that applying electric field on Nafion-dispersion cast membrane reduced ionic aggregation and formed straight fibril-like structures along the membrane thickness.[7] Comparison of electric field and non-electric field based membranes showed that ionic domains were arranged in a regular way spanning the membrane thickness. Ionic conductivity improved by 23% in the membrane that were formed under the electric filed.[7]

Gasa *et al*. used electric field to improve the ionic conductivity of PEMs obtained from blending of sulfonated poly(ether ether ketone) (sPEEK) and poly(ether imide) (PEI).[10] Electric field aligned blend membrane exhibited significant rise in conducvity over isotropic membrane obtained from neat sPEEK. At 50 wt% of sPEEK in PEI matrix, ionic conducvity increased significantly due to electric field induced alignment in the blend membrane.[10] During MEA construction in which Nafion dispersion used as binder is dried, applying electric filed has shown to improve the performance of MEA in PEM fuel cells.[14] Electric field treated MEA exhibited improvement in DMFC power density from 42 to 60 mW cm^{-2}.[14] Electrochemical impedance spectroscopy study confirmed that electric field treatment on MEA reduced the ohmic resistance.

2.4. Effect of Thickness on Intrinsic Properties of PEMs

The intrinsic properties of ionic membranes depend on their thicknesses as reflected by variation in conductivity with thickness.[15-18] Reducing thickness of membrane is a common approach to achieve the low-ohmic resistance in PEM fuel cells. However, this unusual variation of conductivity with thickness is not expected in a homogeneous material. This thickness phenomenon can have serious implications on the performance of PEM fuel cells. Processing conditions and treatment history can induce anisotropy in the membranes leading to thickness-dependent intrinsic properties.[17]

To date, no plausible theory has been put forth that explains variation in intrinsic property of membrane with its thickness. Tsampas *et al*. proposed that conductivity in Nafion membranes is due to proton migration in bulk as well as proton tunneling between adjacent sulfonate groups.[18] Nafion membranes, N112, N115 and N117 that have almost identical equivalent weights, have revealed to possess thickness-dependent properties.[15-18] For example, ionic conductivity of Nafion membranes at 90 °C and in liquid water increased almost linearly from 81 to 160 mS cm^{-1} for increase in thickness from 55 to 206 μm.[15] Figure 2.4 clearly shows that the conductivity increases with thickness of various Nafion membranes.[16]

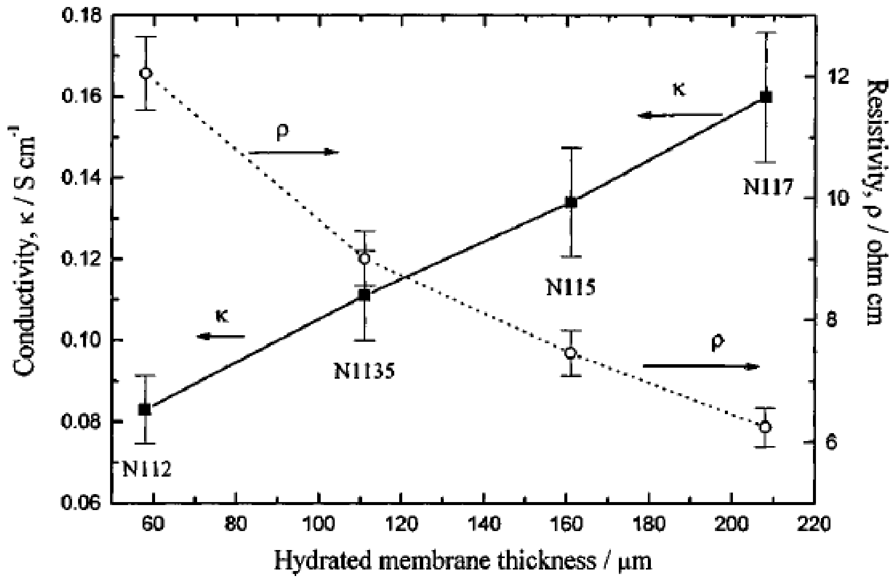

Figure 2.4. The variation in the conductivity and resistivity of the Nafion 1100 EW series of membranes with thickness in 1M H_2SO_4 and at 25 °C.[16]

Silva *et al*. demonstrated similar behavior of Nafion membranes conductivity with thcinkess.[17] They speculated that difference in structural changes due to production process and water uptake could be attributed to these thickness-dependent properties in Nafion membranes.[17] The surface property of membrane can differ from that of bulk due to processing conditions.[19] This variation from the membrane surface to bulk may be manifesting in thickness-induced properties in the membranes.

These thickness-dependent properties were also observed in other type of commercial perfluorosulfonic acid membranes such as Aciplex-S (EW 1025 g/equivalent). In-situ study on these membranes by both magnetic resonance imaging (MRI) technique and electrochemical impedance spectroscopy (EIS) techniques were consistent in revealing that thinner membranes showed variation in conductivity with thickness.[20] MRI technique provided clear evidence of hydration varying with thickness in these Aciplex-S membranes (56, 117, and 340 μm). It was demonstrated that the thickest Aciplex-S membrane absorbed 3.5 times higher water and exhibited the highest conductivity than the thinnest membrane.[20] Composite membranes derived from Nafion dispersion and silica have also exhibited variation in water uptake and conductivity with thickness.[19]

This unusual thickness-dependent behavior can compromise the benefit of thinner membranes that have been claimed to reduce ohmic resistances in PEM fuel cells. Moreover, reduction in thickness can exaggerate the fuel crossover in DMFCs. Therefore, it is advantageous to employ thicker membranes in DMFCs because they have both high conductivity and low-methanol crossover rate. Despite convincing variation in intrinsic properties with membrane thickness, understanding of this thickness-induced phenomenon remains unresolved and may justify further investigation. It is also important to emphasize that, to date, literature lacks any suggestion on optimizing the membrane thickness to achieve optimum performance in PEM fuel cells.

2.5. Sulfonimide-based PEMs

Perfluorinaed and immobilized sulfonamide/sulfonimide are strong and stable acidic polymer materials[2,21,22] with greater thermal stability than the Nafion membranes.[23,24] Polymers containing these functional groups have shown to exhibit greater thermal stability (400 °C), stronger acidity, excellent chemical and electrochemical inertness and less susceptibility to dehydration and oxidative degradation than the corresponding sulfonic acids. In sulfonamide/sulfonimide-based polymer membranes, the functional group ($-SO_2-NH-R$) ionizes into a proton forming hydronium ion in presence of water [21, 22] and a stable anion that is immobilized. The stability of this immobilized anion leads to strong acidity in sulfonamide/sulfonimide. The acidity of sulfonamide/sulfonimide is comparable and even better than that of fluorosulfonic acid.[22,25] Unlike perfluorosulfonic acid, variety of functional groups can be attached to the sulfonimide group to obtain high acidity.[26] In drying of alcohol through pervaporation process, sulfonimide-based membranes have exhibited preferential permeation and higher selectivity of water over alcohol.[27] In PEM fuel cells, sulfonimide-based ionomers have been mentioned to promote the kinetics of oxygen electro-reduction.[26,28]

In polymer membranes for direct methanol fuel cells (DMFCs), incorporating sulfonamide/sulfonimide functional groups can lead to both high-ionic conductivity and low-methanol crossover. This novel strategy of reduction in methanol crossover has advantage over other methods in which reduction in methanol crossover is accompanied by reduction in ionic conductivity. However, to date, there are not many reported studies on methanol crossover across sulfonamide/sulfonimide-based polymer membrane that can be potentially a good candidate for DMFCs. Sulfonimide-based membranes have been tested mostly for hydrogen-based PEM fuel cells. Figure 2.5.1 shows the chemical structure of a perfluoro sulfonimide-based membrane that was developed for PEM fuel cells.[29-31] This membrane is a copolymer of tetrafluroethylene (TFE) and 3, 6-dioxa-Δ^7-4-trifluoromethyl perfluorooctyl trifluoromethyl sulfonimide and resembles Nafion membrane in chemical structure.[29-31] The comonomer is also called bis(perfluoroalkyl) sulfonyl amide.

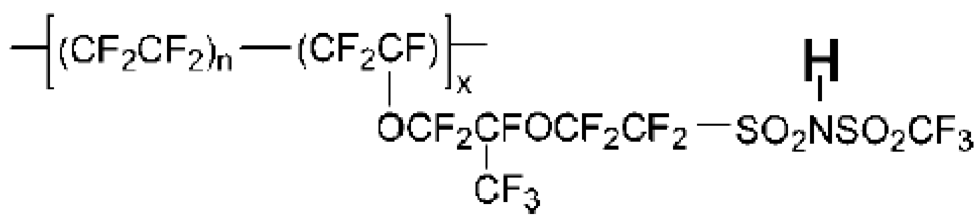

Figure 2.5.1. Chemical structure of perfluoro sulfonimides membrane.[29-31]

DeMarteau *et al*. and others have shown that perfluoro bis-sulfonimides (R_f-SO_2-NH-SO_2-R_f) have properties analogous to corresponding sulfonic acid.[21,24,28] Like traditional PEM materials, these sulfonimide-based membranes also require water for proton conduction and display analogous decline in conductivity with temperature over 100 °C due to loss of water.[21] Their properties are dependent on thermal and hydration conditions.[30] However, infrared spectroscopy study showed that sulfonic acid is more sensitive to hydration than the sulfonimide acids especially at low water uptake.[23,32] At 100% relative humidity and at room temperature, these membranes have conductivity of 100 mS cm^{-1} that is about two times that of Nafion membrane.[29] At equivalent weight of about 1100 g/equivalent and at 100% relative humidity, these membranes showed hydration of 48 water molecules per sulfonimide group that is more than two times of Nafion membrane.[30]

Feiring *at al*. reported a sulfonimide-based styrene monomer that can be polymerized with many comonomers to obtain polymer membranes for fuel cells.[25] Figure 2.5.2 shows the chemical structure of the monomer in which lithium ion (Li^+) can be replaced with proton by ion-exchange with acid solution. The reactivity and perfluoro functional group make this monomer a good candidate to afford membranes for PEM fuel cells. Despite its promising properties, no copolymer of this monomer has been reported for PEM fuel cells.

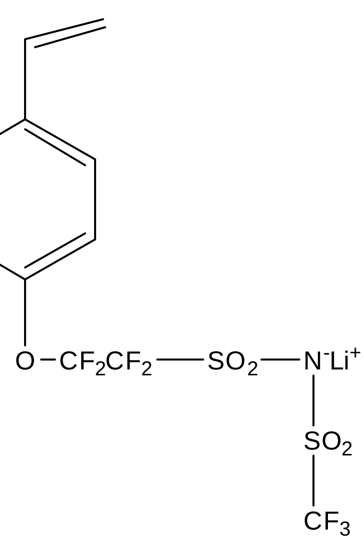

Figure 2.5.2. Chemical structure of sulfonimide-based styrene monomer.[25]

Due to high conductivity like perfluoro sulfonic acid, sulfonimide/sulfonamide-based polymer membranes can potentially outperform Nafion membrane in DMFCs because of their ability to prefer water to methanol while retaining the ionic conductivity. Many parameters govern the solubility and diffusion across the membranes.[27] In sulfonimide-based polymer, hydrogen bonding of water with sulfonimide creates favorable atmosphere for water over alcohol.[27] One poly(amide-sulfonamide)-based membrane showed water selectivity factor of 46 over methanol.[27] Selectivity factor is ratio of weight fraction of permeate to feed streams for water and methanol.

Chemical structure and morphology of polymers, acid loading, and type of acidic functional group can influence the methanol crossover. In case of sulfonimide-based polymer membranes, it is hypothesized that these functional groups can be more effective than corresponding sulfonic acid in forming intricate network and tortuous network leading to reduction in methanol crossover. The behavior of sulfonimide/sulfonimide-based polymer membrane in PEM fuel cells and pervaporation process applied in alcohol drying suggest that these membranes hold the promises to address the challenge of methanol crossover in DMFCs.

2.6. Membranes for DMFCs

2.6.1. PVA Based Membranes

Poly (vinyl alcohol) (PVA) membranes which have preference to permeate water over alcohol find application in pervaporation process.[33] Addition of poly(vinyl alcohol) in PEMs creates methanol barrier properties at the expense of proton conductivity. Pivovar *et al*. investigated PVA membrane crosslinked with succinic anhydride as crossliking agent.[1] Heating of PVA and ethanol/water solution (20 wt%) produced crosslinked structure in these membranes. Due to lack of intrinsic ionic conductivity in PVA, it is essential to soak these membranes in acid solution. Ionic conductivities of these membranes were measured in 1 mol/L sulfuric acid solution and at room temperature. Depending on the crosslinking, ionic conductivity varied from 14 to 53 mS cm^{-1} and methanol permeability at 1 mol/L methanol solution varied from 1.40×10^{-7} to 5.50×10^{-7} cm^2 sec^{-1}.[1]

Conductivity of PVA-based membranes showed linear variation with sulfuric acid concentration. This conductivity variation suggests that these membranes require addition of acid for proton transport. Doping of acids in these membranes raises the issues of corrosion in DMFCs. For concentrated-methanol solution, PVA membranes are better barrier than the Nafion membranes. Pivovar *et al*. also studied conductivity and permeability of other pervaporation membranes.[1] In these membranes, conductivity and methanol permeability were proportional as shown in Figure 2.6.1. Any decrease in permeability resulted in simultaneous decrease in conductivity.

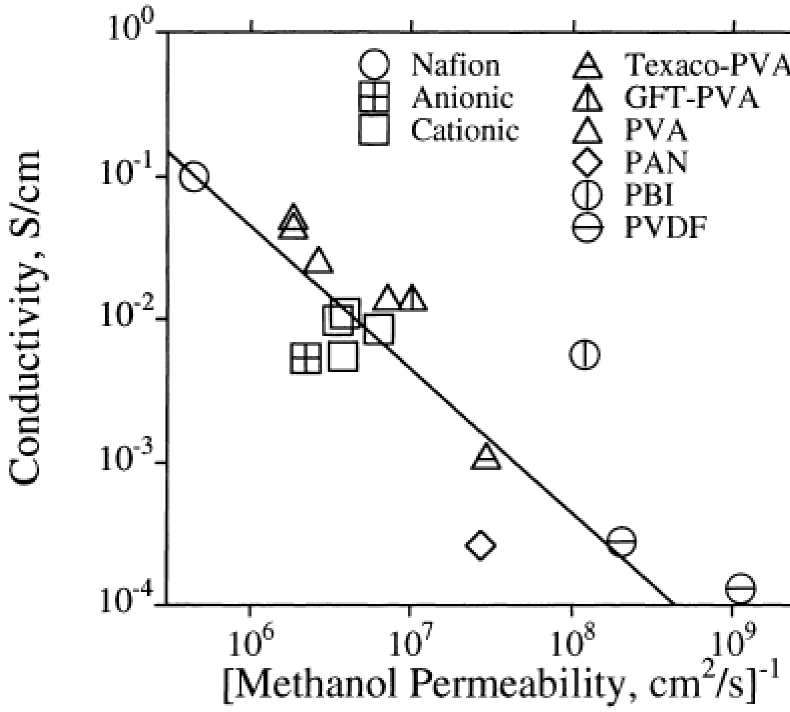

Figure 2.6.1. Conductivity and permeability of pervaporation membranes.[1]

2.6.2. Blend Membranes

Blending of Nafion with fluorinated ethylene-propylene (FEP) is effective in providing the barrier to methanol transport. Lin *et al*. prepared blend membrane from Nafion resin in sulfonyl fluoride form and FEP resin by melt-processing, hot-processing and hydrolysis.[34] Figure 2.6.2 shows the effect of FEP volume fraction on proton conductivity and methanol permeability. Increasing the FEP fraction from 0 to 40 vol% decreased the conductivity from 95 to 22 mS cm^{-1} at 25 °C in water equilibrated membranes and methanol permeability from 3.7×10^{-6} to 1.8×10^{-6} cm^2 sec^{-1} at 1 mol/L methanol solution and at 60 °C.[34] Depending on the volume fraction of FEP, these membranes exhibited selectivity of 1 to 30 relative to unblend Nafion membrane.[34]

Blending of acidic and basic polymers creates hydrogen bridges between acidic and basic groups that can transport protons. Water soluble polymers become insoluble after blending with basic polymers.[35] Ionic crosslinking with basic polymer prevents the dissolution of acidic membranes. Walker *et al*. reported methanol crossover across blend membranes of sulfonated and aminated (polysulfone udel) (PSU), poly(ether ether ketone) (PEEK) and PBI in which ionic crosslink structures reduced methanol crossover.[35] Figure 2.6.3 shows the structure of acid and base polymers that were used to prepare the blend membranes.

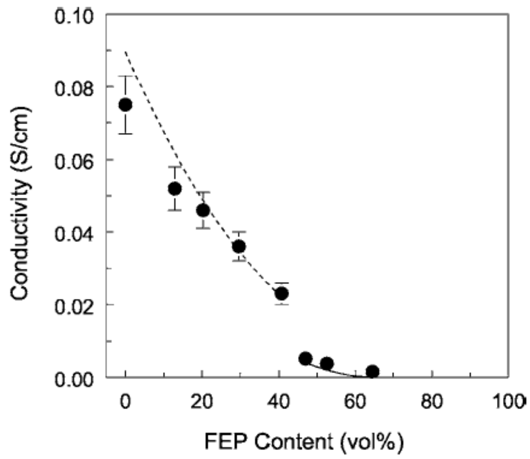

Figure 4. Through-plane proton conductivity of Nafion/FEP blended membranes at room temperature as a function of the volume percent FEP. Closed circles are experimental data; (— — — —) predicted conductivity from Eq. 4 and 5; (———) predicted from Eq. 5 and 7.

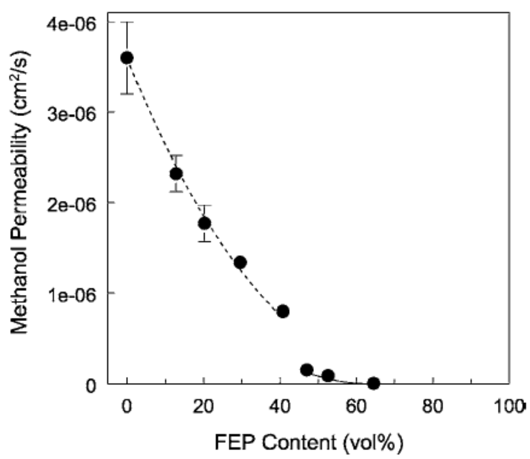

Figure 6. Methanol permeability in Nafion/FEP blended membranes as a function of volume percent FEP (1.0 M methanol at 60°C). Closed circles are experimental data; (— — — —) predicted permeability from Eq. 8; (———) predicted permeability from Eq. 9.

Figure 2.6.2. Nafion and fluorinated ethylene-propylene (FEP) blend membranes.[34]

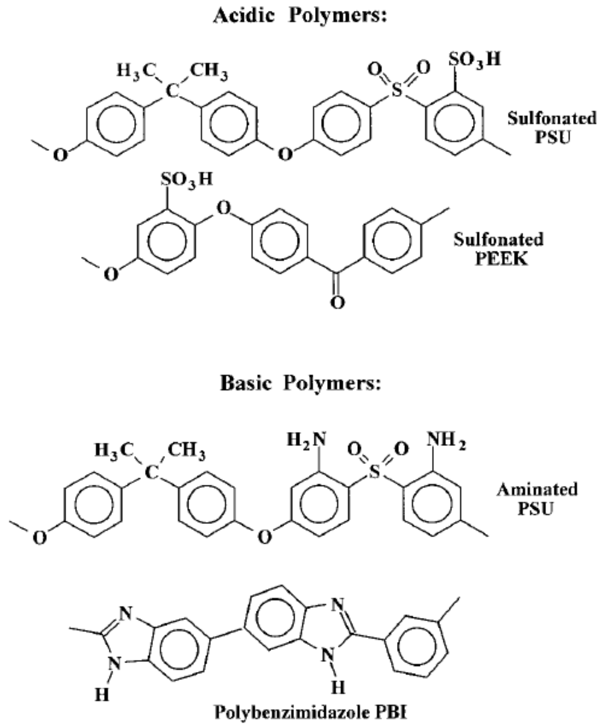

Figure 2.6.3. Polymer components of the acid-base blend membranes.[35]

Despite lower thicknesses (30-100 μm) and higher IECs (0.9-1.46 meq g^{-1}) than that of Nafion 117, blend membranes showed lower steady-state methanol flux of 7.5×10^{-7}-3.0×10^{-6} g(CH_3OH) cm^{-2} sec^{-1} than that of Nafion 117 of 2.4×10^{-5} g(CH_3OH) cm^{-2} sec^{-1}.[35] The membrane from sulfonated-PSU and aminated-PSU displayed the lowest steady-state methanol flux of 7.5×10^{-7} g(CH_3OH) cm^{-2} sec^{-1} among all the blend membranes.

Acid-base blend membranes from Nafion 117 and poly(4-vinyl pyridine) (P4VP) can form ionically crosslinked structure that is effective in reducing methanol crossover.[36] Dip-coating of Nafion 117 membrane with P4VP forms acid-base complex on the surface of membrane that reduces methanol crossover.[36] Woong *et al*. modified Nafion 117 membrane with P4VP/*N*-methyl pyrrolidone (NMP) solution to provide barrier to methanol transport.[36] In one set of modification, Woong *et al.* dip-coated Nafion 117 membrane with P4VP/NMP solution. In the other set of modification, they recoated modified-Nafion 117 membrane with Nafion dispersion.[36]

It is believed that nitrogen in P4VP interacts with sulfonic acid in Nafion 117 to form acid-base complex leading to ionic crosslinking in the Nafion membrane.[36] This surface modification showed reduction in both conductivity and methanol permeability in modified-Nafion 117 membrane. Properties of modified-Nafion membrane were dependant on the concentration of P4VP/NMP solution and dipping time.[36] For example, increasing the concentration of P4VP/NMP solution from 1 to 7 wt% for 5 minutes of dipping time decreased the conductivity (liquid water and room temperature) of modified-Nafion 117 from $3.787 \pm 0.548 \times 10^{-3}$ to $1.713 \pm 0.389 \times 10^{-3}$ S cm^{-1}. The same modified-Nafion 117 membrane showed reduction in methanol permeability (room temperature and 2 mol/L methanol solution) from $6.933 \pm 0.241 \times 10^{-7}$ to $3.469 \pm 0.130 \times 10^{-7}$ cm^2 sec^{-1}.[36]

2.6.3. Composite Membranes Based on Fillers

The three-dimensional silica embedded in polymer matrix can reduce methanol crossover in composite membranes. Sasajima *et al*. filled the sulfonated poly(1,4-phenylene ether ether sulfone) (SPEES) polymer with macroporous silica to reduce the methanol permeability in composite membranes.[37] Three-dimensional ordered silica matrix suppressed the swelling in the composite membrane. For example, water uptake reduced from 2230 wt% in unfilled SPEES to less than 100 wt% in composite membrane at filling ratio of 40%.[37] Filling ratio is a measure of SPEES in porous silica. Increasing the filling ratio from 14 to 46% reduced the methanol permeability from 2.8×10^{-6} to 1.6×10^{-6} cm^2 sec^{-1} at 30 °C and at 2 mol/L methanol solution. In same composite membranes, conductivity (30 °C and Rh 100%) decreased from 6.0×10^{-2} to 6.5×10^{-6} S sec^{-1}.[37] Despite high ion-exchange capacity of pure SPEES (3.13 meq/g), conductivity of composite membranes was lower than that of Nafion membrane.

Conductivity and permeability of Nafion membrane showed stronger dependence on water and methanol concentration than these composite membranes. These results suggest that reduction in methanol permeability can be achieved at the expense of conductivity. It was argued that methanol transport occurs by vehicle mechanism and proton transport by hopping mechanism. Three-dimensional silica reduced the water uptake, swelling and suppressed the methanol transport by affecting the vehicle mechanism.[37]

Song *et al*. prepared nanocomposite membrane from Nafion dispersion and montmorillonite (MMT) clay from the aim of reducing methanol crossover through exfoliated MMT in polymer matrix.[38] The MMT clay layers improve the thermal and mechanical strength of the composite membrane while providing tortuous pathway to methanol transport.[38] X-ray diffraction study revealed no diffraction in the composite membranes containing 1-20 wt% of MMT in comparison with pristine MMT. This lack of diffraction peak suggested that MMT was exfoliated and dispersed in the Nafion polymer.[38] Stress-strain study for 3 wt% of MMT showed that tensile strength improved from 30 MPa in neat Nafion membrane to 45 MPa in the composite membrane. Thermal stability of composite membrane also increased with MMT weight.

Ionic conductivity (liquid water and room temperature) of the composite membranes showed strong dependence on MMT weight. Conductivity decreased from 0.078 to 0.02 S cm^{-1} for MMT weight of 1 to 10%.[38] For the same composition, methanol permeability decreased from 1.0×10^{-7} to 3.0×10^{-8} cm^2 sec^{-1}.[38] At concentrated-methanol feed, DMFC based on composite membrane (1 wt% MMT) produced peak power density of 100 mW cm^{-2} at 70 °C and 10 mol/L methanol solution. For comparison, DMFC based on Nafion 117 produced 90 mW cm^{-2} at 70 °C and 3 mol/L methanol solution.[38]

2.6.4. Surface-Modified Membranes for DMFCs

Modification of Nafion 117 membrane surface by electron beam (EB) and plasma polymerization of a barrier film can reduce the methanol crossover while keeping the bulk part of the membrane intact.[35,39] Surface modification can reduce the pore size leading to selective transport of proton over methanol.[39] Hobson *et al*. modified the surface of as-received Nafion 117 membrane by low-dose EB with an accelerating voltage of 35 kV and exposure of 600 μC cm^{-2}.[39] This surface deforming reduced the methanol crossover by 7% in the modified-Nafion membrane. Decrease in methanol crossover was attributed to removal of hydrophillic domains from the membrane surface by EB radiation.[39] In DMFCs test, these membranes showed improved performance over unmodified Nafion membrane. However, increasing the methanol feed concentration from 6.4 to 10 wt% produced modest increase in the peak power density from 18 to 25 mW cm^{-2} indicating that surface modification is useful mostly for dilute methanol-feed concentration.

Walker *et al*. created a methanol barrier film (0.3 μm) on Nafion 117 membrane surface through plasma polymerization of hexane-hydrogen mixture.[35] Adding hydrogen with hexane improved the flexibility of plasma-created film because pure hexane-based film was brittle due to dissimilar expansion of Nafion membrane and plasma-created film. Untreated Nafion membrane showed higher methanol flux of 2.4×10^{-5} than that of plasma-treated membrane of 3.7×10^{-6} $g(CH_3OH)\ cm^{-2}\ sec^{-1}$.[35] Plasma-treated membranes exhibited longer time (1000 sec) to reach steady-state methanol flux than the untreated Nafion 117 membrane (500 sec) confirming the methanol barrier property at the surface of modified membrane.

2.7. Summary

Despite expensive effort to develop candidate PEMs that can meet DMFCs challenges, reduction in methanol permeability has been achieved by reduction in conductivity in these candidate PEMs. This behavior suggests that developing a PEM with high-conductivity and low-methanol permeability poses enormous challenges.

2.8. References

1. B. S. Pivovar, Y. Wang, and E. L. Cussler, *J. Membr. Sci.* **1999**, *154*, 155-162.

2. W. Grot, *Fluorinated Ionomers* **2008**.

3. V. Arcella, C. Troglia, and A. Ghielmi, *Ind. Eng. Chem. Res.* **2005**, *44*, 7646-7651.

4. A. Ghielmi, P. Vaccarono, C. Troglia, and V. Arcella, *J. Power Sources* **2005**, *145*, 108-115.

5. D. E. Curtin, R. D. Lousenberg, T. J. Henry, P. C. Tangeman, and M. E. Tisack, *J. Power Sources* **2004**, *131*, 41-48.

6. S. Banerjee and D. E. Curtin, *J. Fluorine Chem.* **2004,** *125*, 1211-1216.

7. H. L. Lin, T. L. Yu, and F. H. Han, *J. Polym. Res.* **2006**, *13*, 379-385.

8. C. S. Karthikeyan, M. Schossig, E. Radovanovic, M. C. Goncalves, H. Wittich, K. Schulte, and S. P. Nunes, *Macromol. Mater. Eng.* **2003**, *288*, 175-180.

9. X. Wei and M. Z. Yates. *J. Power Sources* **2010**, *195*, 736-743.

10. J. V. Gasa, R. A. Weiss, and M. T. Shaw, *J. Membr. Sci.* **2008**, *320*, 215-223.

11. D. Liu and M. Z. Yates, *J. Membr. Sci.* **2008**, *322*, 256-264.

12. D. Liu, K. Savino, and M. Z, Yates, *Adv. Funct. Mater.* **2009**, *19*, 3941-3947.

13. D. Liu and M. Z. Yates, *J. Membr. Sci.* **2009**, *326*, 539-548.

14. Z. T. Wang, Y. X. Wang, L. Xu, Q. J. Gao, G. Q. Wei, and J. Lu, *J. Power Sources* **2009**, *186*, 293-298.

15. V. Rao, K. A. Friedrich, and U. Stimming. *Handbook of Membrane Separations: chemical, pharmaceutical, food and biotechnological applications* **2009**, 759-820.

16. S. Slade, S. A. Campbell, T. R. Ralph and F. C. Walsh, *J. Electrochem. Soc.* **2002**, *149*, A1556-A1564.

17. R. F. Silva, M. D. Francesco, and A. Pozio, *J. Power Sources* **2004**, *134*, 18-26.

18. M. N. Tsampas, A. Pikos, S. Brosda, A. Katsaounis, and C. G. Vayenas, *Electrochim. Acta* **2006**, *51*, 2743-2755.

19. P. Dimitrova, K. A. Friedrich., B. Vogt, and U. Stimming, *J. Electroanal. Chem.* **2002**, *532*, 75-83.

20. K. Teranishi, S. Tsushima., and S. Hirai, *Electrochem. Solid-State Letters* **2005**, *8*, A281-A284.

21. A. J. Appleby, O. A. Velev, J. G. LeHelloco, A. Parthasarthy, S. Srinivasan, D. D. DesMarteau, M. S. Gillette, and J. K. Ghosh, *J. Electrochem. Soc.* **1993**, *140*, 109-111.

22. A. Oishi, H. Matsuoka, T. Yasuda, and M. Watanabe, *J. Mater. Chem.* **2009**, *19*, 514-521.

23. C. K. Byun, I. Shariff, D. D. DesMarteau, S. E. Creager, and C. Korzeniewski, *J. Phys. Chem. B* **2009**, *113*, 6299-6304.

24. M. W. Perpall, D. W. Smith Jr., D. D. DesMarteau, and S. E. Creager. *J. Macromol. Sci., Part C: Polym. Rev.* **2006**, *46*, 297-313.

25. A. E. Feiring, S. K. Choi, M. Doyle, and E. R. Wonchoba, *Macromolecules* **2000**, *33*, 9262-9271.

26. M. K. Rahman, G. Aiba, M. A. B. H. Susan, and M. Watanabe, *Electrochim. Acta* **2004**, *50*, 633-638.

27. W. H. Chan, C. F. Ng, S. Y. L. Leung, X. He, and O. C. Cheung. *J. Appl. Polym. Sci.* **1997**, *65*, 1113-1119.

28. S. C. Savett, J. R. Atkins, C. R. Sides, J. L. Harris, B. H. Thomas, S. E. Creager, W. T. Pennington, and D. D. DesMarteau. *J. Electrochem. Soc.* **2002**, *149*, A1527-A1532.

29. J. J. Sumner, S. E. Creager, J. J. Ma, and D. D. DesMarteau. *J. Electrochem. Soc.* **1998**, *145*, 107-110.

30. J. R. Atkins, C. R. Sides, S. E. Creager, J. L. Harris, W. T. Pennington, B. H. Thomas, and D. D. DesMarteau. *J. New Mater. Elecltrochem. Sys.* **2003**, *6*, 9-15.

31. S. E. Creager, J. J. Sumner, R. D. Bailey, J. J. Ma, W. T. Pennington, and D. D. DesMarteau. *Electrochem. Solid-State Letters* **1999**, *2*, 434-436.

32. Y. Yang, A. Siu, T. J. Peckham, and S.Holdcroft. *Adv. Polym. Sci.: Fuel Cells I* **2008**, *215*, 55-126.

33. B. Smitha, S. Sridhar, Y. V. L. R. Kumar, and M. Ramkrishna. *J. Polym. Mater.* **2005**, *22*, 433-444.

34. J. Lin, J. K. Lee, M. Kellner, R. Wycisk, and P. N. Pintauro. *J. Electrochem. Soc.* **2006**, *153*, A1325-A1331.

35. M. Walker, K. M. Baumgartner, M. Kaiser, J. Kerres, A. Ullrich, and E. Rauchle, *J. Appl. Polym. Sci.* **1999**, *74*, 67–73.

36. J. C. Woong, S. Venkataramani, and S. C. Kim, *Polym. Int.* **2006**, *55*, 491–499.

37. K. Sasajima, H. Munakata., and K. Kanamura, *J. Electrochem. Soc.* **2008**, *155*, B143-B147.

38. M. K. Song, S. B. Park, Y. T. Kim, K. H. Kim, S. K. Min, and H. W. Rhee, *Electrochim. Acta* **2004**, *50*, 639–643.

39. L. J. Hobson, H. Ozu, M. Yamaguchi, and S. Hayase, *J. Electrochem. Soc.* **2001**, *148*, A1185-A1190.

CHAPTER 3

Analysis of EIS Technique and Nafion 117 Conductivity as Function of Temperature and Relative Humidity

Rameshwar Yadav [§] and Peter S. Fedkiw [§, #]

[§]North Carolina State University, Raleigh, NC, USA

Abstract

This work presents an analysis of electrochemical impedance spectroscopy (EIS) technique and conductivity of Nafion 117 membrane at relative humidities of 10-100% and at temperatures 25-80 °C. A correlation is developed to calculate the conductivity of Nafion 117 over the temperature and water vapor activity range measured. The correlation also captures the effect of water vapor activity on the activation energy of proton transport. The two-probe EIS technique was employed to measure the in-plane membrane resistance. The effect of platinum electrode dimension was investigated. An equivalent circuit that captures the impedance spectra was used to resolve the ionic resistance. Electrode-membrane area analysis showed that the EIS technique might be effective in through-plane ionic conductivity measurement for small electrode area. The capacitive behavior of Nafion 117 with water-uptake was observed and analyzed. The two- and four-probe methods are compared and yield essentially identical Nafion 117 conductivities (two-probe 79 ± 6%, four-probe 82 ± 1% mS cm^{-1}) in liquid water and at room temperature.

[#] ECS Fellow; corresponding author
Email: fedkiw@eos.ncsu.edu

3.1. Introduction

Ionic conductivity of a polymer electrolyte membrane (PEM) is of paramount significance since it affects the ohmic loss in fuel cells. Nafion 117 possesses the benchmark conductivity for comparison of new PEM candidates. Many studies have reported Nafion 117 ionic conductivity, and even at the same condition of temperature and water activity, the results vary.[1-18] The characterization of new PEMs suggests use of consistent methods to obtain agreeable results of Nafion 117.

Generally, the electrochemical impedance spectroscopy (EIS) technique with a two- or four-probe method is employed to extract the ionic resistance from an equivalent circuit model of the PEM. In the two-probe method, interpretation of low-ionic resistance from impedance spectra can be challenging because the PEM-electrode interfacial impedance can obscure the PEM impedance. However, the two-probe method can be suitable for high-ionic resistance. The four-probe method can separate interfacial contact impedance and is appropriate for low-ionic resistance, but this method requires more sophisticated equipment than the two-probe method. In four-probe method, measurement in certain frequency range can produce impedance spectra free from artifacts. It is also essential to eliminate artifacts in impedance spectra from the four-probe method to obtain conductivity that is identical with that from the two-probe method.

Many publications report Nafion 117 ionic conductivity at various water content and temperatures.[1-18] Because of different measurement techniques, Nafion 117 conductivity varies significantly at identical measurement conditions of membrane history, treatment protocol, temperature, and water content (Table 3.1, Refs. 1-18). For example, Nafion 117 conductivity at 20 °C varied from 63 to 90 mS cm^{-1} in liquid water and from 51 to 96 mS cm^{-1} at 100% relative humidity.[1-6] Nafion 117 conductivity increases with relative humidity and temperature. However, it was reported that Nafion 117 conductivity reached maximum at 60 °C in the temperature range of 25-100 °C.[9-10] The conductivity decreased with temperature from 20 to 45 °C and increased with temperature from 45 to 80 °C for a given relative humidity as reported by Sone *et al*. [6] Apparently, there is a lack of comprehensive and agreeable results on Nafion 117 conductivity at PEM fuel cells operating conditions ranging from 10 to 100% relative humidity and 25 to 80 °C temperature.

Many perceive that through-plane ionic conductivity is representative of proton conduction in an actual fuel cell. Conventionally, an in-plane conductivity measurement is preferred over a through-plane measurement because, for fixed ionic conductivity, dimensions of the PEM used in the conductivity cell can be adjusted to obtain a measurable ionic resistance with the EIS technique. In the through-plane configuration, for a fixed area of electrodes, the PEM thickness acting as inter-electrode distance sets the ionic resistance, which is typically too low to measure by the EIS technique.

Extrapolation of the semi-circle arc or the low-frequency linear spectra on a Nyquist plot to the real-axis yields the ionic resistance. In a typical Nyquist plot for PEM, change in shape and size of impedance spectra arc occurs because of impedance variation with water uptake and temperature. A single equivalent circuit that can capture the impedance at different water content and temperature can be useful for ionic conductivity measurement.

Table 3.1 Nafion 117 Conductivity				
T (°C)	**Phase**	**Conductivity (mS cm^{-1})**	**EIS Method**	**References**
20	Liquid	63	2P, TP	[1]
	Liquid	77	2P, IP	[1]
	Liquid	90	2P, TP	[2]
	Vapor (93%)	14	CP, IP	[3]
	Vapor (92%)	36	2P	[4]
	Vapor	51	2P	[4]
	Vapor	55	4P, IP	[5]
	Vapor	66	CP, IP	[3]
	Vapor	96	4P, IP	[6]
23	Liquid	90	4P, IP	[7]
25	Liquid	48	2P, TP	[8]
	Vapor	61	2P, IP	[9]
	Vapor (98%)	75	4P, IP	[10]
30	Liquid	87	2P, IP	[11]
	Liquid	100	2P, IP	[12]
	Vapor (95%)	19	2P, IP	[13]
	Vapor (95%)	47	4P, IP	[13]
	Vapor (90%)	62	4P, IP	[14]
	Vapor	62	2P, IP	[12]
45	Vapor	45	4P, IP	[6]
50	Vapor	112	2P, IP	[9]
	Vapor	135	4P, IP	[11]
65	Liquid	79	2P, TP	[8]
70	Vapor	71	4P, IP	[6]
75	Vapor (95%)	34	2P, TP	[15]
80	Vapor	105	2P, TP	[16]
90	Liquid	184	2P, IP	[17]
	Vapor (98%)	61	4P, IP	[10]
	Vapor (95%)	20	2P, IP	[13]
	Vapor (95%)	72	4P, IP	[13]
95	Liquid	25	2P, TP	[18]
	Vapor (98%)	33	2P, TP	[18]
	Vapor	81	2P, IP	[9]

2P-two-probe, 4P-four-probe method, IP-in-plane configuration, TP-through-plane configuration, CP-coaxial-probe method, Vapor-100% relative humidity, and Liquid-liquid water. Membrane samples were prepared under similar treatment protocol.

Distortion in impedance spectra will lead to a misinterpretation of PEM ionic resistance. A uniform current distribution at the PEM-electrode interface can produce distortion-free impedance spectra resulting in improved ionic conductivity measurement. Excessive contact area at PEM-electrode interface can lead to non-uniform current distribution resulting in distortion of impedance spectra. Reduction in contact area can provide a uniform current distribution and attenuate the distortion in impedance spectra. The EIS technique can also be applied to study the change in dielectric properties of PEM due to water uptake. PEM capacitance is dependent on water content because of the high-dielectric constant of water (78.6).[19-20] As a result, the PEM impedance and time-constant (*RC*) can vary with capacitance. For fixed dimension of PEM, this variation appears as change in shape and size of PEM impedance spectra.

Conductivity measurement requires good control of relative humidity and temperature. Use of a dynamic flow system of wet and dry gases to control the relative humidity requires expensive apparatus, good flow control, accurate humidity sensor, and can be cumbersome. A simple method to control RH, however, is the equilibration of vapor above aqueous salt solutions such as lithium chloride. Because of strong variation of liquid water activity with salt concentration, control of relative humidity in any custom-built enclosure can be achieved effectively with aqueous lithium chloride salt solutions.[21-23]

This work presents an analysis of the EIS technique for conductivity measurement of Nafion 117 as a function of relative humidity and temperature. An equivalent circuit that encompasses the impedance spectra at all measurement conditions is described. Advantages of in-plane conductivity measurement and challenges associated with through-plane conductivity measurement are critically analyzed and discussed. For fixed ionic conductivity, effect of electrode area on through-plane resistance is analyzed.

3.2. Experimental

An apparatus based on ASTM E104-02 was employed to measure ionic conductivity of a PEM as function of relative humidity and temperature.[24] Ratio of headspace volume to active surface area of salt solution was set to be below 25 cm.[24] The apparatus consists of a glass vessel with a detachable top cover. Six PEM-sample holders were attached to a perforated ceramic plate onto which conductivity cells were fixed. A hygrometer (Fisher Scientific) displayed the relative humidity and temperature. A tapered hole at the center of the top cover allowed twelve wires to pass through a silicone rubber stopper for electrical contact. A needle valve at the top cover allowed control of atmospheric pressure in the system.

Figure 3.2.1 shows a schematic of a typical conductivity cell. Figure A.2 in Appendix A.2 shows the photos of conductivity cells and apparatus. The cells were made of Kel-F (PCTFE-polychlorotrifluoroethylene). A 1-cm square window hole at the center of each lower and upper block allowed access of water vapor to membrane. The two-probe EIS technique (frequency range 1Hz-1MHz and AC voltage 10-50 mV) was employed to record impedance spectra using a Zahner IM6e potentiostat. Experimental impedance data were analyzed with ZSimpWin Version 2.00 software (Princeton Applied Research) and an equivalent circuit $(R_1Q_1)(R_2Q_2)$ that is described in Impedance Analysis section.

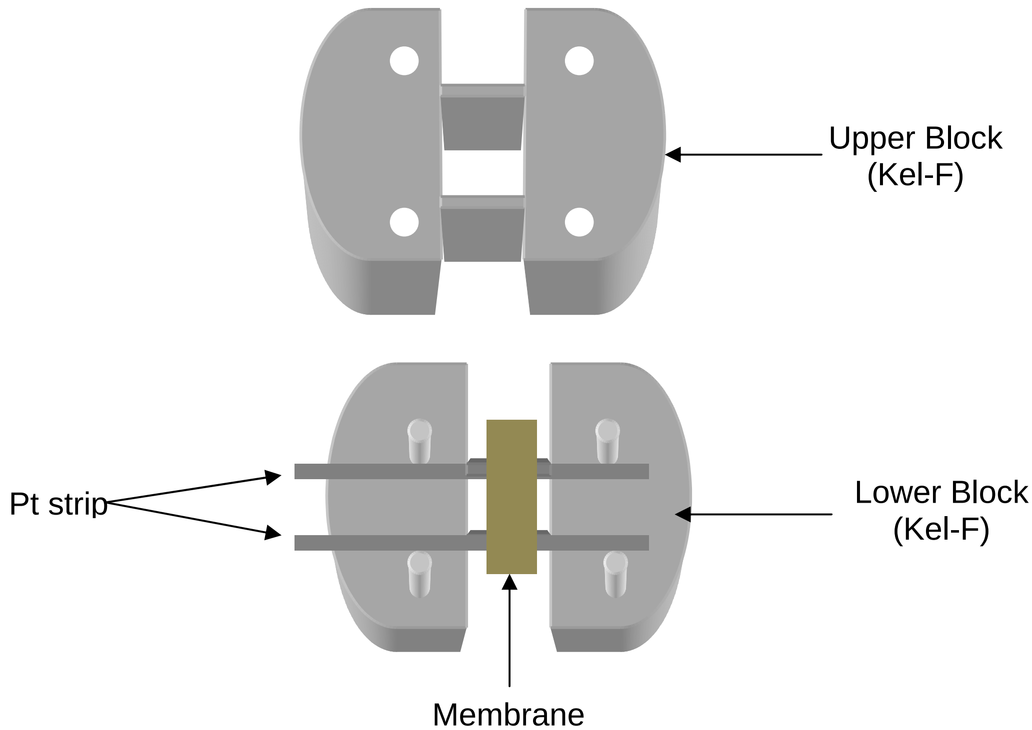

Figure 3.2.1. Schematic of conductivity cells. Typical membrane sample was 15-mm long and 6-mm wide. Effective width of platinum electrode was 1 mm.

Nafion 117 membrane was treated in the following sequential way: boil in 3 wt% hydrogen peroxide solution for one hour, rinse with deionized water (18 MΩ), boil in deionized water for one hour, boil in 0.5 M sulfuric acid solution for one hour, boil in deionized water, rinse with deionized water, boil in deionized water, and soak in deionized water at room temperature. In each step, temperature was monitored to prevent overheating of the membrane above the glass transition temperature of Nafion 117 (110 °C).[6] Use of a rectangular punch of width 6 mm and length 15 mm ensured uniformity in dimensions of membrane sample. Average thickness of the membrane was obtained by measurements at several locations using a digital micrometer (Appendix E, Mitutoyo Corporation). During conductivity measurement, time to equilibrate the membrane with the environment was determined by tracking the conductivity with time until conductivity showed no significant change. Typically, membranes attained equilibrium with water vapor in 48 hours (Figure A.3, Appendix A.3) and with liquid water in 24 hours.

Water vapor sorption in the PEM from is achieved by controlling the water vapor activity by means of salt solution. Percentage relative humidity *% RH*, as shown in Equation (3.2), is 100 times the ratio of partial pressure of water, P^{vap}, to the vapor pressure of water, P^{sat}, both at system temperature T.[25] Water activity a_w is related to the relative humidity as shown in Equation (3.2).[25] Equation (3.2) describe the water activity and its relationship with salt molality.[25]

$$\%RH = 100\frac{P^{vap}}{P^{sat}} = 100a_w = 100\exp(-\frac{\phi_i^{(m)} M_s m_i \nu}{1000}) \qquad (3.2)$$

where $\Phi_i^{(m)}$ is osmotic coefficient, v is number of dissociated salt ions, m_i is salt molality, and M_s is solvent molecular weight. There are many organic and inorganic salts that can be utilized to control water vapor activity in a closed system.[24,26-28] For water vapor activity in the range of 0.10-1.0 and 0.75-1.0, lithium chloride and sodium chloride salts, respectively, are adequate in the temperature range of 25 to 80 °C. We observed that water vapor activity in the range of 0.75-1.0 could be achieved in shorter time by sodium chloride salt than by lithium chloride salt.

In this work, we used lithium chloride salt for water vapor activity control in the range of 0.10-0.60, sodium chloride salt for water vapor activity control in the range of 0.75-0.85, and deionized liquid water for water vapor activity of 1.0. Figures 3.2.2 and 3.2.3 were generated from Equation (3.2) and osmotic coefficient data from literature.[29-30] As illustrated in Figure 3.2.2 and 3.2.3, relative humidity increases with temperature and decreases with increase in salt molality. From Figure 3.2.2, relative humidity from 10-100% can be achieved at any temperature between 0-100 °C by varying the lithium chloride molality. In the high range of relative humidity, sodium chloride salt can be more effective than lithium chloride salt.

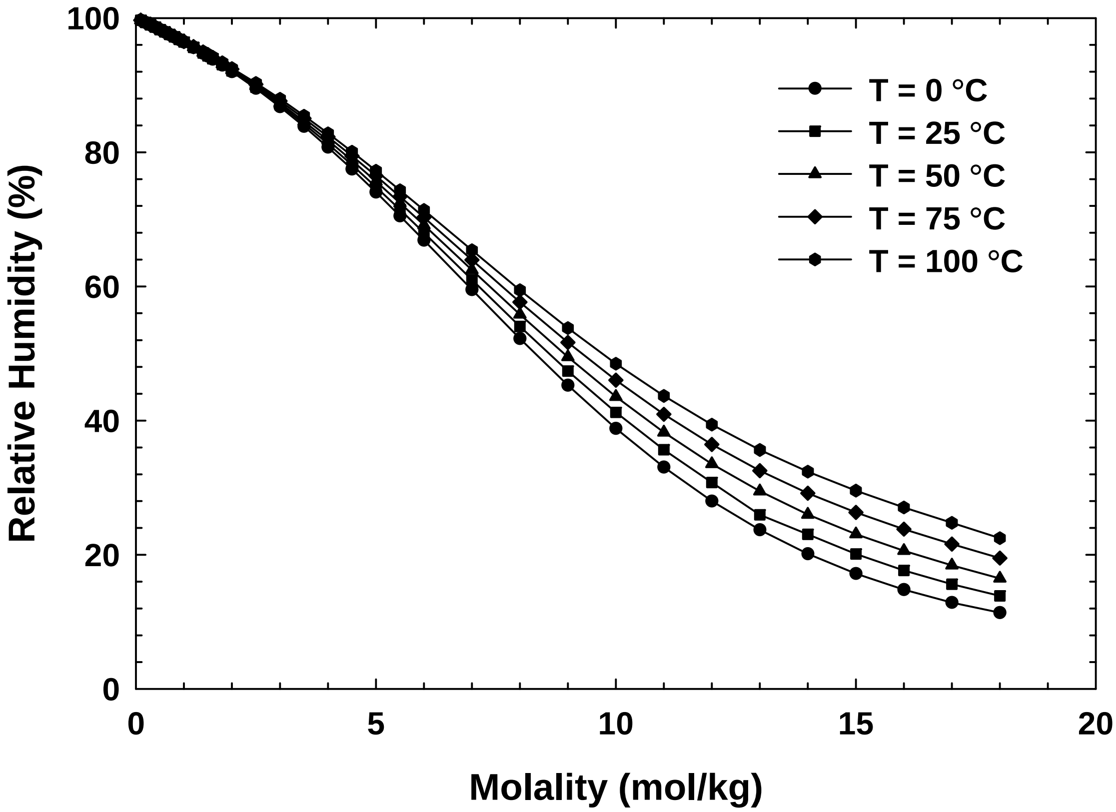

Figure 3.2.2. Calculated relative humidity behavior with lithium chloride (LiCl) salt molality at various temperatures from Equation (3.2) by using osmotic coefficient of lithium chloride salt.[29]

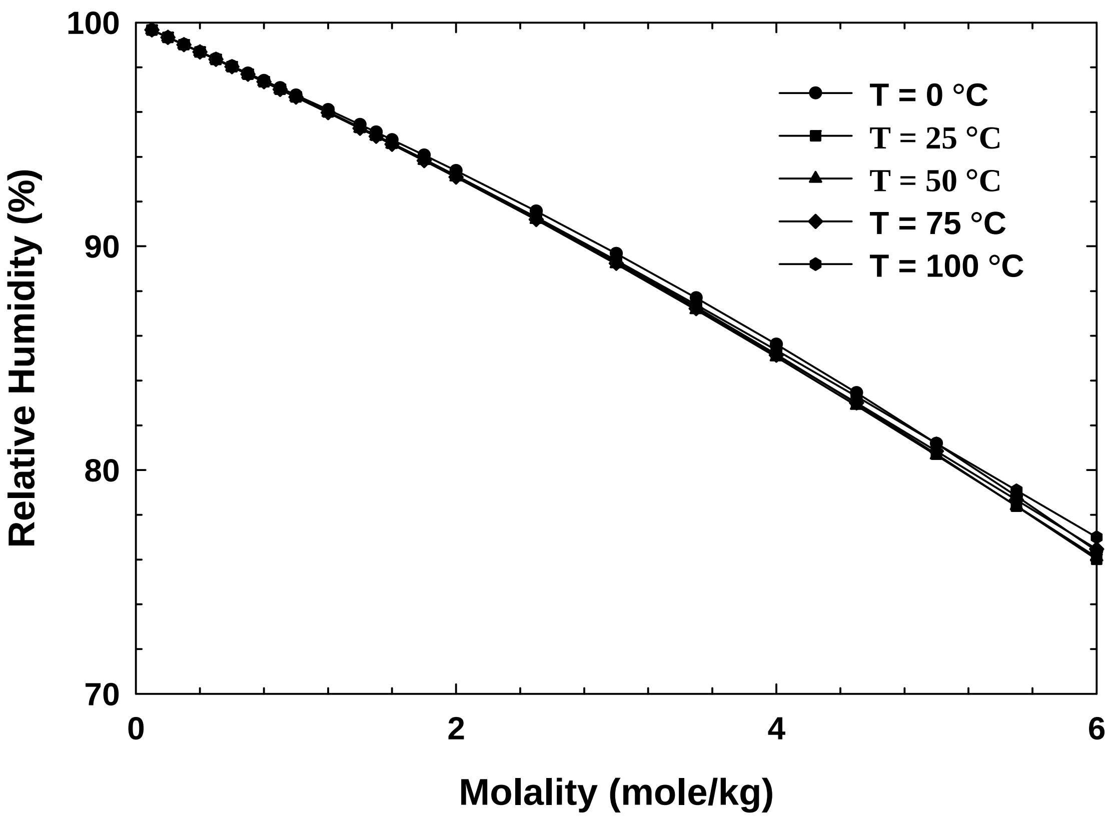

Figure 3.2.3. Calculated relative humidity behavior with sodium chloride (NaCl) salt molality at various temperatures from Equation (3.2) by using osmotic coefficient of sodium chloride salt.[30]

3.3. Impedance Analysis

The following expression describes relationship between ionic conductivity (S cm^{-1}), resistance (ohm), and PEM dimensions (cm):

$$\sigma = \frac{L}{RA} \tag{3.3}$$

where σ is ionic conductivity, R is ionic resistance, L is inter-electrode distance between voltage-sensing electrodes, and A is PEM area normal to current flow. In in-plane configuration, PEM width w multiplied by thickness t is the PEM area normal to current flow ($A = wt$). In a typical Nyquist plot for PEM, extrapolation of semi-circle arc or low-frequency linear spectra to the X-axis gives the ionic resistance. Alternatively, an equivalent circuit is fit to the data in order to resolve the ionic resistance.

An equivalent circuit model $(R_1Q_1)(R_2Q_2)$ was fit to impedance data at all measurement conditions. Appendix A.1 provides the equivalent circuit diagram and an analytical expression for equivalent impedance of PEM and interface system. The equivalent circuit captures a system with two time-constants one for the PEM itself and the other for the interface. Inherently, resistor, R_1, in parallel combination with constant phase element, Q_1, represents impedance of PEM. Resistor, R_2, in parallel combination with constant phase element, Q_2, represents interfacial impedance. The constant phase element captures the electrode surface roughness and system heterogeneity.[31] The impedance of a constant phase element is given by $1/(Q^0(\omega j)^n)$ where Q^0 and n are frequency-independent parameters. The parameter n is 1 for ideal capacitor and varies between 0 and 1 for non-ideal capacitive elements. The equivalent circuit $(R_1Q_1)(R_2Q_2)$ can be resolved into real and imaginary parts to represent the equivalent impedance of the PEM and interface system.[32,33]

3.4. Through-plane and In-plane Ionic Conductivity

Ideally, the through-plane ionic conductivity should be investigated. However, in through-plane ionic conductivity measurement by two- or four- or coaxial-probe method, the voltage-sensing electrode distance L (Equation 3.3) is determined by the membrane thickness that typically varies from approximately 20 to 200 μm for commercial and candidate PEM. Because of the PEM thickness acting as voltage-sensing inter-electrode distance L, through-plane ionic resistance can vary only with electrode surface area A that is normal to ionic current flow. In-plane conductivity cell configuration relative to through-plane configuration offers spatial advantage because inter-electrode distance can be adjusted to obtain measurable in-plane ionic resistance.

For fixed value of the ionic conductivity, Figure 3.4 shows the variation of through-plane ionic resistance with electrode circular surface area A using a conductivity of 100 mS cm^{-1} and a 200 μm thick membrane. $R_{Through\text{-}plane}$ shown in Figure 3.4 is based on circular shape of membrane sample. For any other regular shape of membrane sample, qualitative effect of through-plane area on $R_{Through\text{-}plane}$ would be similar to that in Figure 3.4.

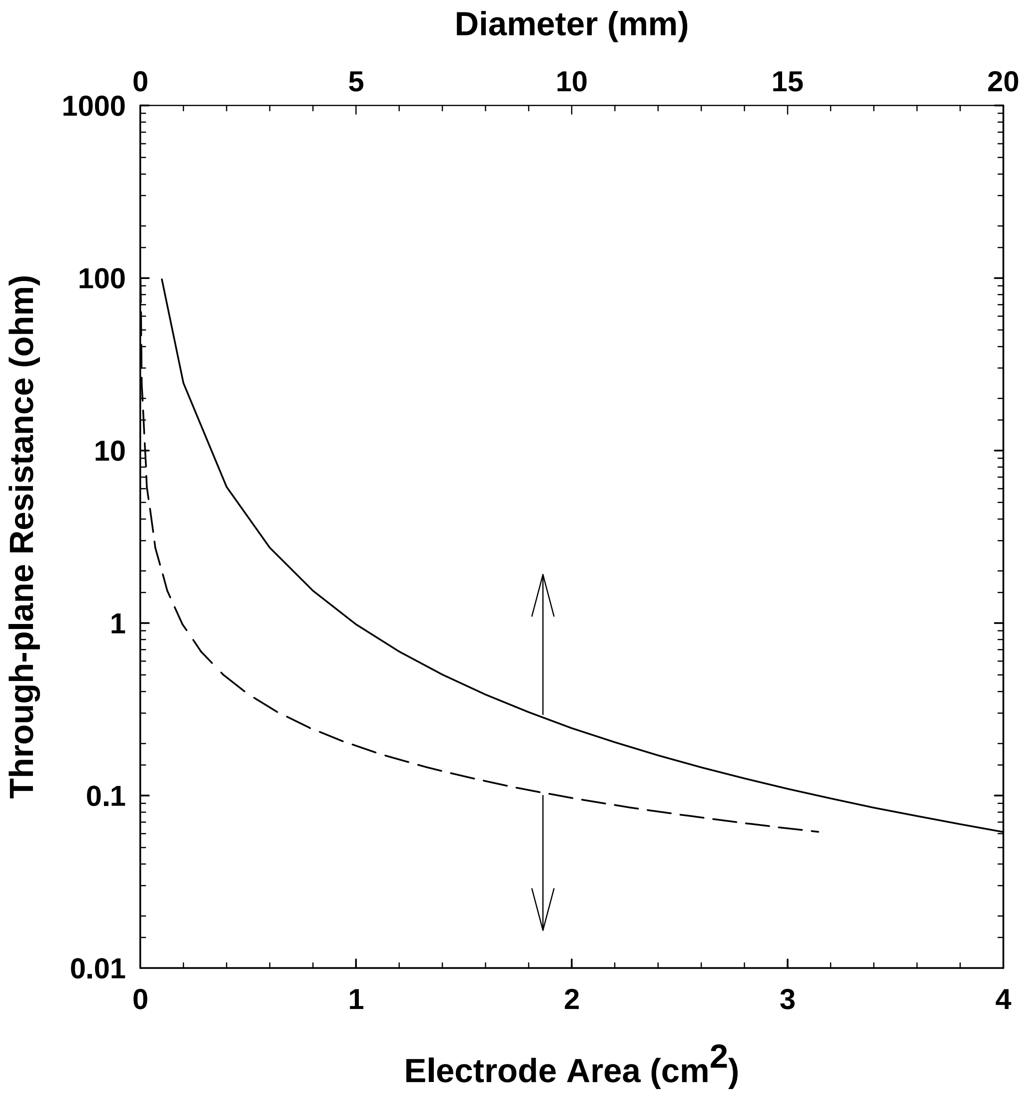

Figure 3.4. Effect of electrode surface area on through-plane ionic resistance. Through-plane resistance of Nafion 117 was calculated from Equation (3.3) using conductivity of 0.10 S cm^{-1} and thickness of 200 μm.

In through-plane configuration, theoretically, electrode surface area can be reduced or enlarged to any extent. However, dimensions of electrolyte can influence the current distribution between the electrodes. For identical area of electrodes and PEM, current distribution is uniform on the electrodes. However, current distribution can become non-uniform if contact area of electrode and membrane is not identical. Non-uniform current distribution can affect the ionic resistance measurement. For electrolytes like PEM with relatively high-ionic conductivity, geometrical effect of contact area on current distribution between electrodes may be negligible. In generating Figure 3.4, we assumed a uniform current distribution independent of PEM and electrode area.

Enlarging the electrode surface area can reduce the ionic resistance to low value that can be challenging to interpret from impedance spectra. For example, increasing the electrode diameter from 1 to 5 mm reduces the ionic resistance from 100 to 1 ohm which would be more difficult to measure by the EIS technique. Depending on convenience, a suitable contact area between PEM and electrodes might be employed to obtain measurable ionic resistance by the EIS technique with two- or four- or coaxial-probe method.

3.5. Effect of Electrode Dimension

In impedance measurement by EIS technique, non-uniform current distribution can occur at PEM-electrode interface with large area because of PEM deformation from applied compressive force and water uptake. Applied compressive force can hinder water transport resulting in PEM deformation and surface heterogeneity. The two-probe EIS technique can display the non-uniform current distribution behavior that arises from physical deformation and surface heterogeneity at PEM-electrode interface. In a Nyquist plot from two-probe method, distortion in impedance spectra can be signature of non-uniform current distribution. This distortion in the impedance spectra can lead to misinterpretation of impedance data.

Uniform presence of water throughout the PEM can improve the current distribution and attenuate the distortion in the impedance spectra. Small contact area at PEM-electrode interface can improve the current distribution and attenuate the distortion in the impedance spectra. Small contact area can enhance water-transport at PEM-electrode interface that can improve current distribution and produce artifact-free impedance spectra. In the conductivity cell, a narrow Pt strip electrode has advantages in providing small contact area that can reduce physical deformation and surface heterogeneity at PEM-interface. In this work, 10 and 1-mm wide Pt strips electrodes were employed to study the effect of electrode dimensions on impedance spectra.

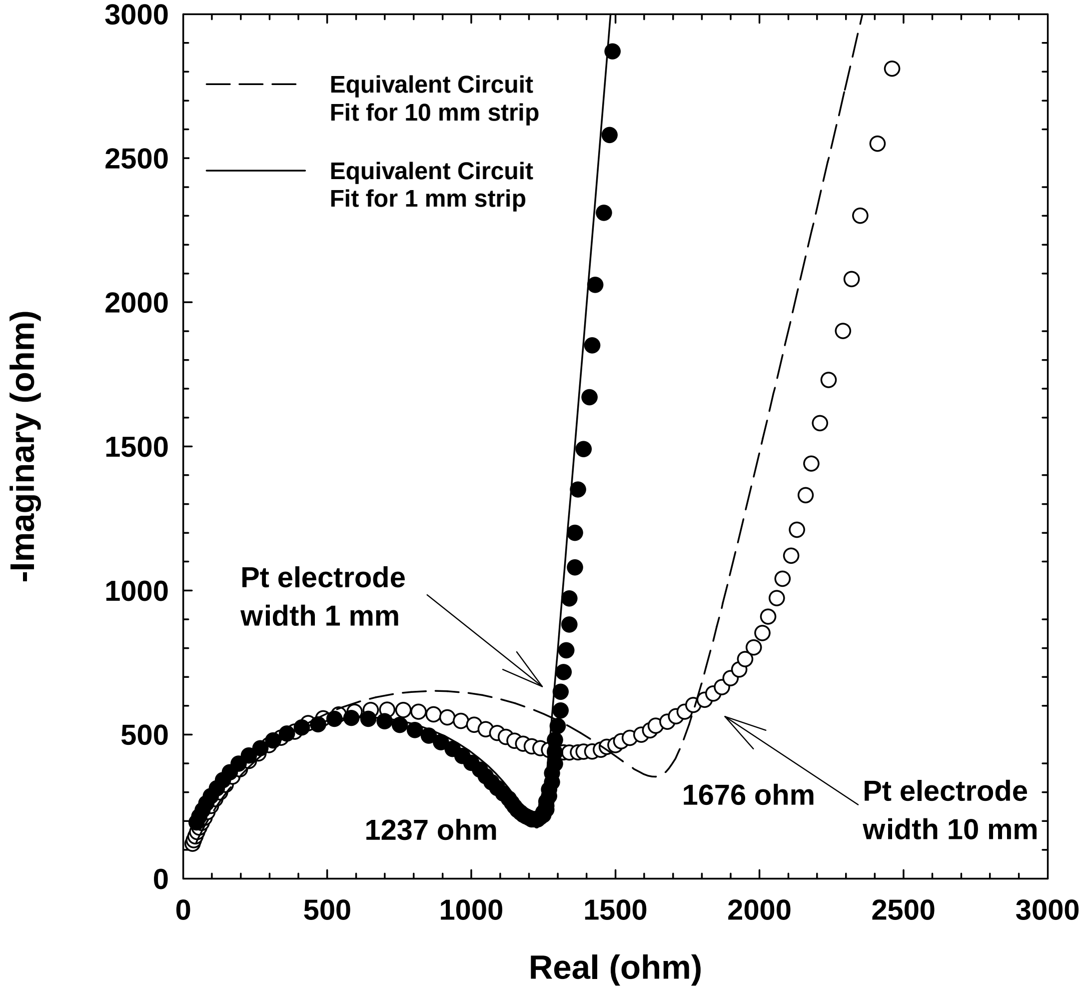

Figure 3.5. Impedance spectra for 1- and 10-mm wide Pt-strip electrodes of identical length. Impedance was recorded at 25 °C and relative humidity of 100% in the frequency range of 1 MHz-1Hz.

Figure 3.5 shows the impedance spectra of Nafion 117 using the two-probe EIS technique with 10-mm wide electrode. Distortion in impedance spectra in low frequency range is evident and is attributed to non-uniform current distribution. From Figure 3.5, extrapolation of semi-circle arc or linear region to the X-axis in order to obtain ionic resistance can be challenging to interpret. At 25 °C and 100% relative humidity, equivalent circuit $(R_1Q_1)(R_2Q_2)$ fit to the impedance data gave ionic resistance of 1237 ohm for 1-mm wide electrode and 1676 ohm for 10-mm wide electrode that is higher by 26% from 1-mm wide electrode. Reduction in Pt strip width from 10 to 1 mm attenuates the distortion in impedance spectra (Figure 3.5). Comparison of impedance spectra from Figure 3.5 shows that use of 1-mm wide Pt electrode in the two-probe method is preferred.

The equivalent circuit $(R_1Q_1)(R_2Q_2)$ was found to fit well with EIS data. At 25 °C and 100% relative humidity, 1-mm wide electrode produced ionic conductivity of 67 mS cm^{-1}. However, 10-mm wide electrode produced ionic conductivity of 50 mS cm^{-1} under identical conditions that is lower by 26% from that of 1-mm wide electrode. In our study for Nafion 117 conductivity, Pt strip of 1 mm width was employed as electrodes in all the six conductivity cells.

3.6. Capacitive Behavior of Polymer Electrolyte Membranes

Polymer electrolyte membranes exhibit capacitive as well as ionic behavior because of water-uptake, and interaction between ionic groups and water. PEMs under dry condition, such as Nafion 117 displays very low conductivity and have very low dielectric constant.[19-20] However, water-uptake in PEMs transforms their ionic and dielectric properties. The EIS technique has been employed mostly to study ionic conductivity of PEMs. However, impedance data from the EIS technique can be interpreted to extract effective capacitance. Equation (3.6.1) shows the expression for impedance of constant phase element and Equation (3.6.2) shows the expression for capacitance.[31-33]

$$Z(\omega)_{CPE} = \frac{1}{Q^0 (j\omega)^n} \tag{3.6.1}$$

$$C_{Membrane} = \left[(Q^0)^{1/n} R^{\frac{1-n}{n}} \sin(\frac{n\pi}{2}) \right] \text{at } \omega_{\max} \tag{3.6.2}$$

where ω_{max} is frequency at which imaginary value of PEM impedance reaches maximum. If frequency-independent parameters Q^0 and n are known by fitting an equivalent circuit, Equation 3.6.2 can be applied to obtain the capacitance of PEM.[33]

Table 3.6 Values of Parameters for Figure 3.6.2		
Parameters	**Liquid Water**	**RH 100%**
R_1 (ohm)	8.43×10^{2}	1.24×10^{3}
$Q^0{}_1$ (S s^n)	2.61×10^{-9}	2.27×10^{-9}
n_1	9.29×10^{-1}	9.31×10^{-1}
R_2 (ohm)	8.34×10^{4}	2.77×10^{7}
$Q^0{}_2$ (S s^n)	1.05×10^{-6}	3.58×10^{-7}
n_2	8.60×10^{-1}	9.48×10^{-1}
ω_{max} (Hz)	1.99×10^{5}	1.59×10^{5}
L (cm)	1.10×10^{0}	1.00×10^{0}
w (cm)	6.00×10^{-1}	6.00×10^{-1}
t (cm)	2.05×10^{-2}	2.00×10^{-2}
σ (S cm^{-1})	1.06×10^{-1}	6.74×10^{-2}
C_{PEM} (pF) (Eq.3.6.2)	9.63×10^{2}	8.78×10^{2}

Figure 3.6.1 shows the results of capacitance (C_{PEM}) that was calculated from Equation (3.6.2). Table 3.6 shows the values of parameters corresponding to Figure 3.6.2. Increase in water-uptake in Nafion 117 from 100% relative humidity to liquid water increases the C_{PEM} by 10% (Table 3.6). This increase in capacitance is consistent with increase in dielectric constant of Nafion 117 due to change in water uptake from water vapor to liquid water as reported by Paddison *et al*.[19]

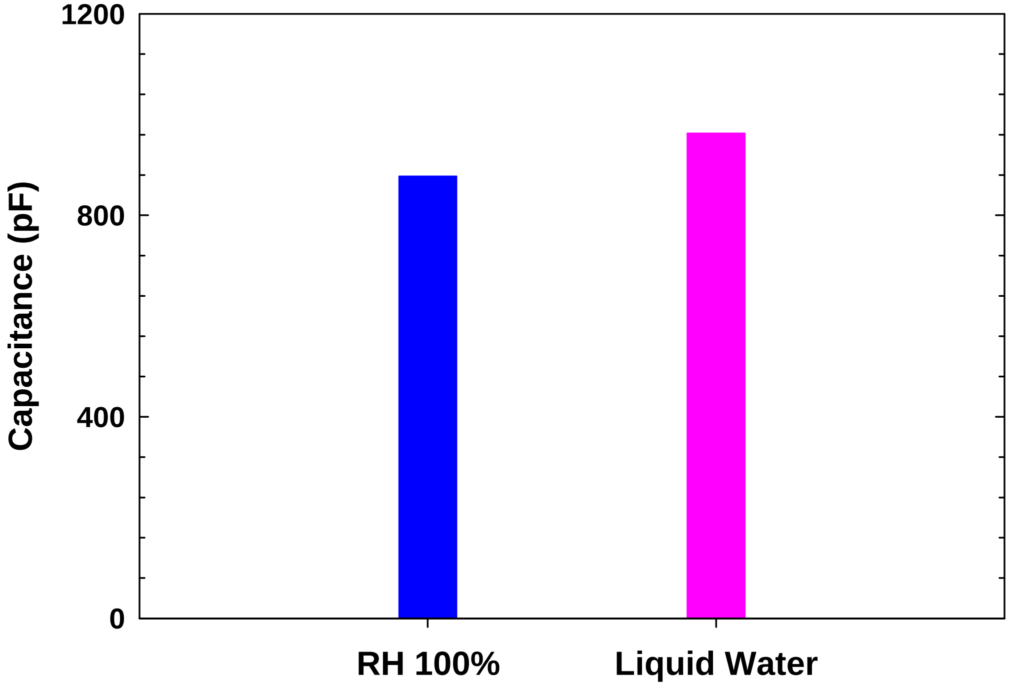

Figure 3.6.1. Capacitive behavior of Nafion 117 membrane with water vapor activity. Capacitance was calculated from Equation (3.6.2).

Figures 3.6.2 presents Nyquist plot of Nafion 117 membrane at RH 100% and in liquid water. PEM impedance varies with both ionic resistance and capacitance because of water-uptake. Figure 3.6.2 reflects the effect of change in ionic resistance and capacitance at high water content from liquid water and low water-content from water vapor at 100% relative humidity. For fixed dimensions of PEM, change in shape and size of impedance spectra is a sign of change in time-constant (*RC*). Imaginary impedance of Nafion 117 changed from 557 to 377 ohm due to change in water-content from water vapor at 100% relative humidity to liquid water (Figure 3.6.2). As shown in arc region of impedance spectra, change in imaginary part of PEM impedance is consistent with change in dielectric constant of Nafion membrane as reported by Paddison *et al*.[19] Figures 3.6.2 also shows the capability of a single equivalent circuit $(R_1Q_1)(R_2Q_2)$ to fit experimental impedance data at any measurement condition.

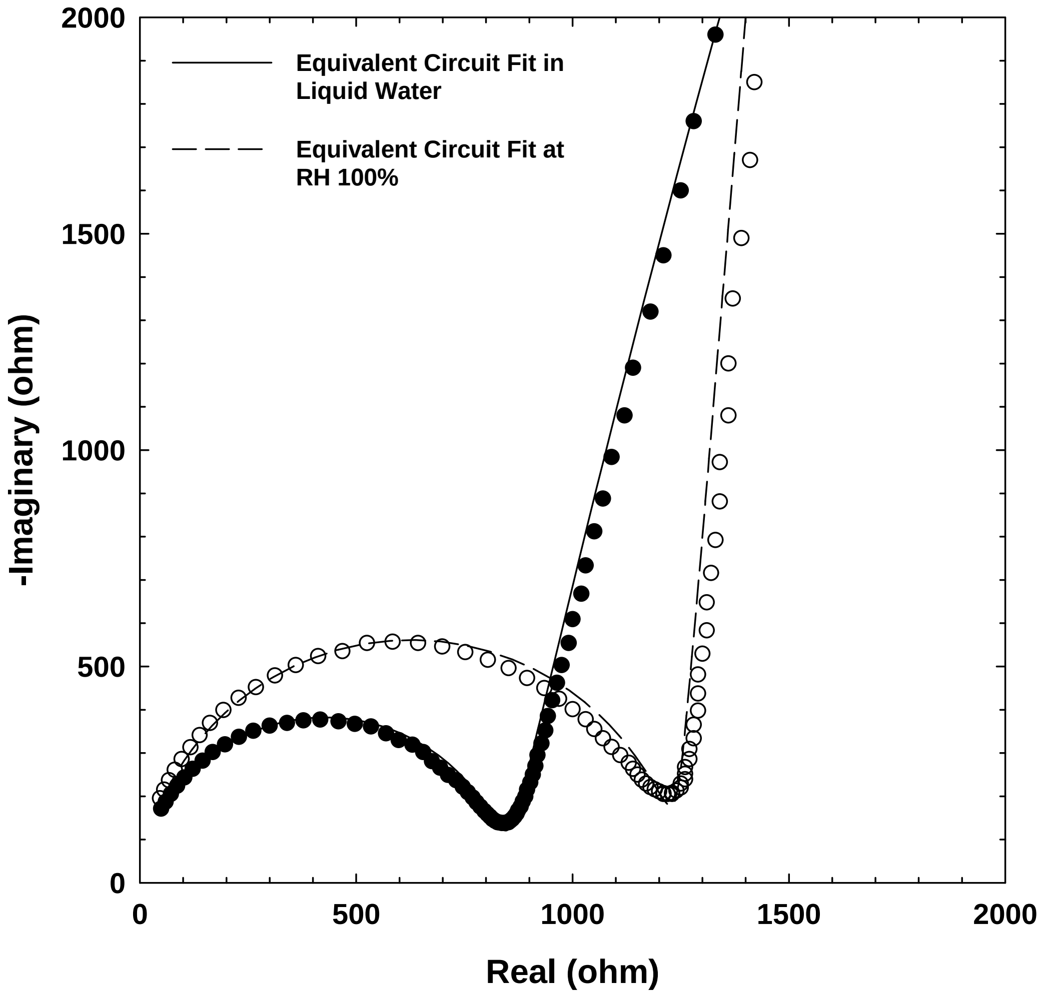

Figure 3.6.2. Impedance of Nafion 117 at 25 °C and in frequency range of 1 MHz-1Hz.

3.7. Two- and Four-probe Methods

The four-probe method can separate the interfacial impedance from the membrane impedance. Four-probe method offers advantage to study low-ionic resistance systems effectively. However, four-probe method requires more sophisticated equipment. In four-probe method, selecting a certain frequency range can be necessary to produce artifact-free impedance spectra that result from instrumental artifact. Two-probe method is relatively suitable to apply for systems with intermediate and high ionic impedances. Two-probe method also has relative advantages for system with interest in interfacial impedance. For system having multiple interfacial impedances such as PEM fuel cells, two-probe method can be applied to study impedance of MEA, bipolar plate, end plate, current collector, and interfaces.

Figure 3.7 shows the impedance spectra of Nafion 117 that was obtained from four-probe method using a BekkTech conductivity cell (BekkTech). Even in four-probe method, artifact and clustering of data occur as shown in Figure 3.7. Negative reactance in low frequency range (Figure 3.7) is due to instrumental artifact from interfacial contact of voltage-sensing electrodes and PEM. In fitting the equivalent circuit (*RQ*) for ionic conductivity calculation, we ignored the low frequency impedance data (< 60 Hz). In this work, Nafion 117 conductivity from a four-probe method (82 ± 1% mS cm^{-1}) and the two-probe method (79 ± 6% mS cm^{-1}) in water and at room temperature are essentially identical.

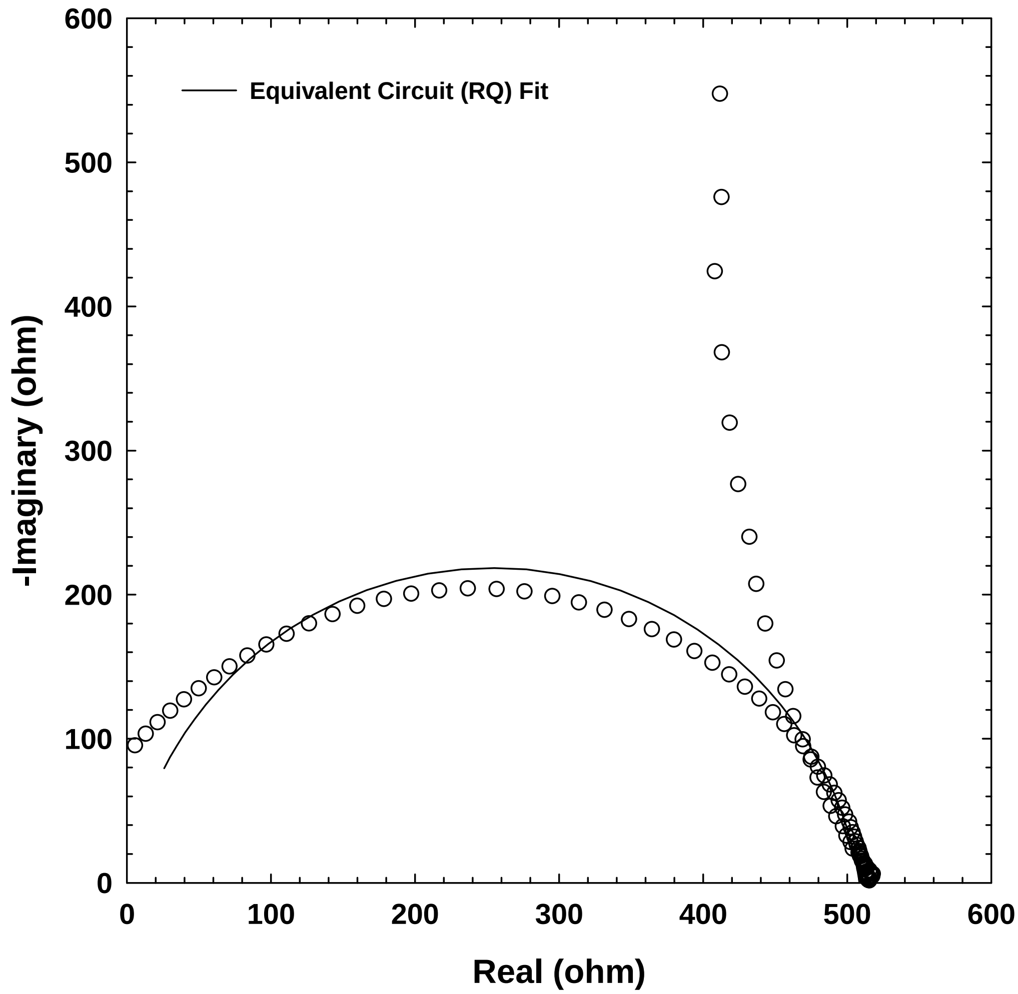

Figure 3.7. Nafion 117 impedance spectra by four-probe method in liquid water, at room temperature, and in frequency range of 1 MHz-1Hz.

3.8. Nafion 117 Conductivity

This work presents Nafion 117 conductivity results for comparative study of new PEM candidates. Nafion 117 conductivity was measured at various relative humidities (10-100%) and temperatures (25-80 °C) that encompass PEM fuel cells operating conditions. The two-probe EIS technique and in-plane configuration was employed to measure the ionic conductivity. Ionic conductivity increases with water-content and temperature. At fixed temperature, qualitative behavior of ionic conductivity at any relative humidity is similar. In case of fixed relative humidity, qualitative behavior of ionic conductivity at any temperature is also similar. Nafion 117 has reasonable conductivity at high relative humidity. However, Nafion 117 conductivity is severely low at dry condition that can have analogous effect on PEM fuel cells performance. This shortcoming in Nafion 117 has prompted the development of other PEMs.

Figure 3.8.1 illustrates the ionic conductivity behavior with relative humidity and temperature. At 25 °C, ionic conductivity increases from 0.33 to 68 mS cm^{-1} for relative humidity from 10 to 100%. At other temperatures, ionic conductivity displays similar qualitative trend. This increase in ionic conductivity from 10 to 100% relative humidity shows that water uptake has enormous effect on ionic conductivity. At any relative humidity, ionic conductivity increases by minimum two times for temperatures from 25 to 80 °C. However, ionic conductivity is influenced more by water-uptake than by temperature.

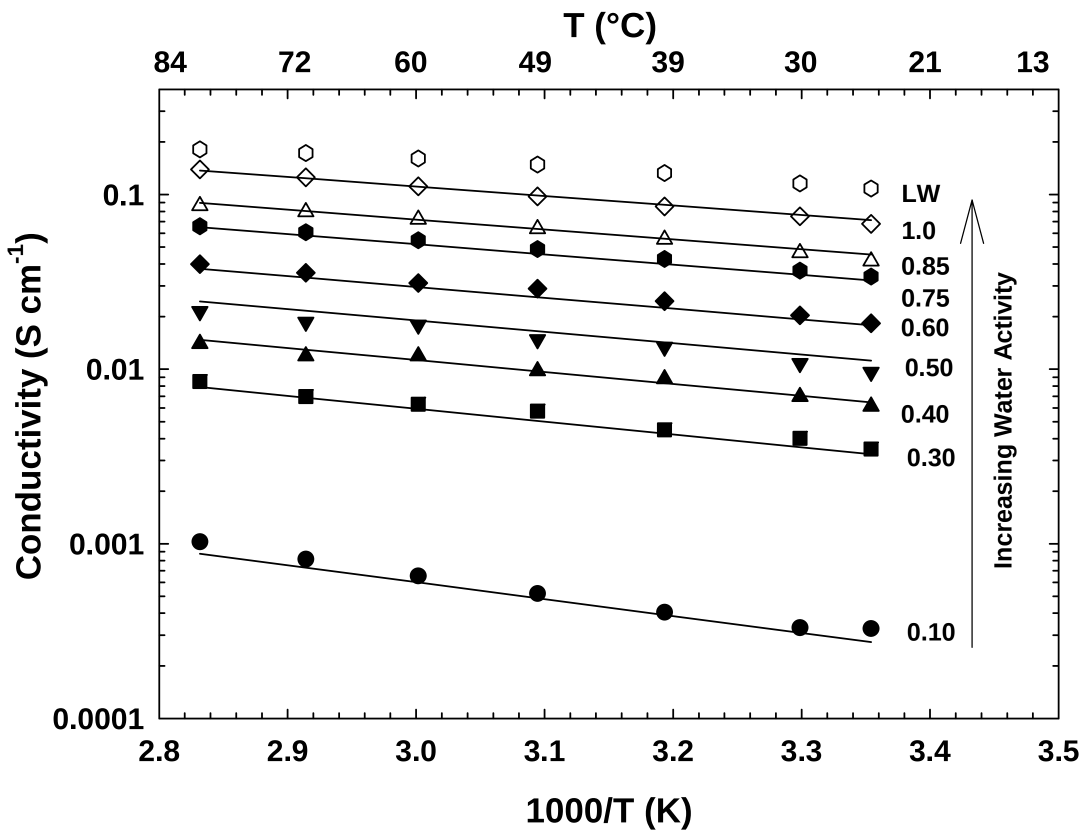

Figure 3.8.1. Nafion 117 conductivity as a function of temperatures from 25 to 80 °C. Symbols represent experimental results and solid lines represent results calculated from correlation (Equation 3.8). LW stands for liquid water.

Effect of relative humidity and temperature is more pronounced at low relative humidity and at low temperature. As a result, low-ionic conductivity has adverse effect on PEM fuel cells performance. Ionic conductivity in liquid water was about two times higher than that at 100% relative humidity.

Using the experimental data, a correlation for Nafion 117 conductivity was developed to calculate ionic conductivity as function of water vapor activity (0.1-1.0) and temperature (25-80 °C). The following expression shows the ionic conductivity correlation.

$$\sigma(a_w, T) = (0.6877 + a_w)^3 \exp(-\frac{10440}{RTa_w^{1/4}}) \quad (3.8)$$

$$E_a = \frac{10440}{a_w^{1/4}} \quad \text{kJ mol}^{-1}$$

where σ is ionic conductivity (S cm^{-1}), a_w is water vapor activity, and T is temperature in Kelvin and R is universal gas constant (8.314 J K^{-1} mol^{-1}). The correlation shows that proton activation energy is dependent on water vapor activity. Figure 3.8.1 shows that calculated values of ionic conductivity agree well with experimental results. The correlation captures the trend of ionic conductivity with temperature and relative humidity.

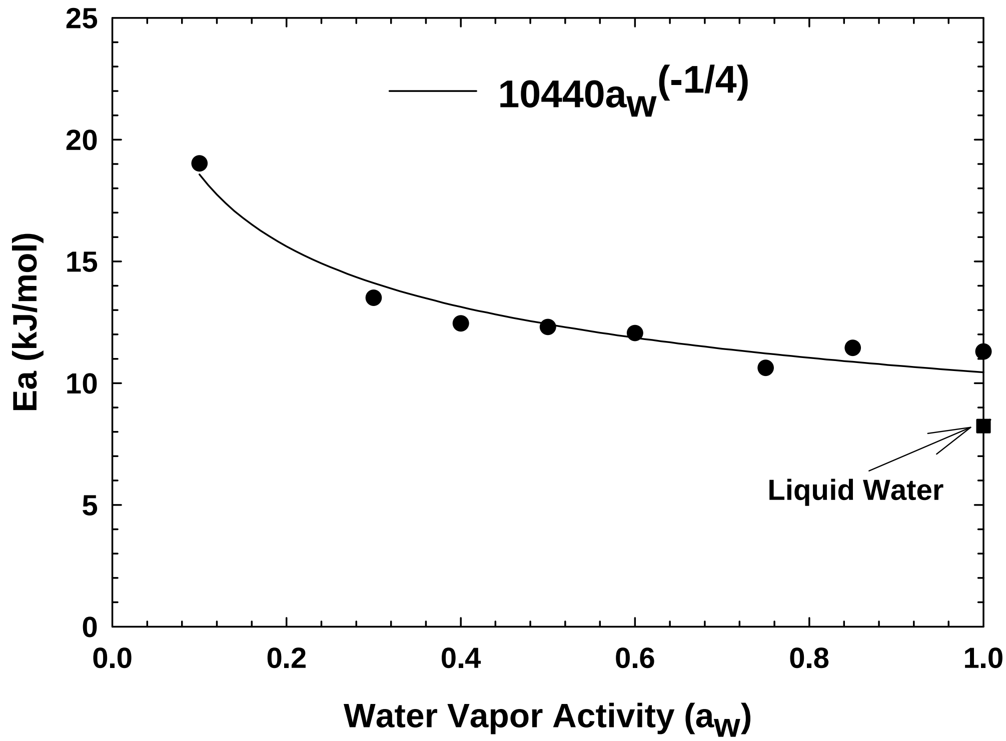

Figure 3.8.2. Proton activation energy behavior with relative humidity in Nafion 117 membrane. E_a represented by close symbols was obtained from Arrhenius plot of ionic conductivity against temperatures from 25-80 °C at fixed relative humidity.

Nafion 117 conductivity follows Arrhenius behavior with temperature as shown in Figure 3.8.1. At fixed relative humidity, activation energy for proton transport was constant with temperatures from 25 to 80 °C. However, Figure 3.8.2 reveals that activation energy varies with relative humidity. Activation energy decreased by 42% for relative humidities from 10 to 100% (19 to 11 kJ mol^{-1}). Activation energy further decreased by 27% for change in water-content from 100% relative humidity to liquid water. This decrease in activation energy with increase in water content suggests that high-water availability is favorable to proton transport.

3.9. Conclusions

An equivalent circuit is adequate to fit to impedance data of a PEM across a spectrum of temperature and RH condition. EIS technique can be effective for measurement of through-plane ionic conductivity by applying small-electrode area that yields measurable ionic resistance. In two-probe method, reduction in contact area at PEM-electrode interface improves current distribution resulting in distortion-free impedance spectra and in correct interpretation of ionic resistance. Water-uptake in PEM influences capacitance and time-constant leading to change in shape and size of PEM impedance spectra. Two- and four-probe methods produce comparable conductivity if artifact in impedance spectra is not considered. Nafion 117 conductivity is strongly related to water-content and temperature. Conductivity increases with both temperature and water-content. However, water-content has more influence than temperature on conductivity. The correlation for ionic conductivity calculates agreeable values at any water vapor activity and temperature. Activation energy of proton transport depends on water-uptake. High water-uptake reduces energy barrier for proton transport resulting in low-activation energy.

Acknowledgments: We gratefully acknowledge the financial support from Department of Energy (DOE) and National Science Foundation-Science and Technology Center (NSF-STC). The authors appreciate the generous contribution of Nafion 117 membrane from DuPont.

North Carolina State University, Raleigh assisted in meeting the publication cost of this article.

3.10. References

1. T. Soboleva, Z. Xie, Z. Shi , E. Tsang, T. Navessin, and S. Holdcroft, *J. Electroanal. Chem.* **2008**, *622*, 145-152.

2. J. Halim, F. N. Buchi, O. Haas, M. Stamm, and G. G. Scherer, *Electrochim. Acta* **1994**, *39*, 1303-1307.

3. A. V. Anantaraman and C. L. Gardner, *J. Electroanal. Chem.* **1996**, *414*, 115-120.

4. N. Walsby, S. Hietala, S. L. Maunu, F. Sundholm, T. Kallio, and G. Sundholm, *J. Appl. Polym. Sci.* **2002**, *86*, 33-42.

5. J. J. Sumner, S. E. Creager, J. J. Ma, and D. D. DesMarteau, *J. Electrochem. Soc.* **1998**, *145*, 107-110.

6. Y. Sone, P. Ekdunge, and D. Simsonsson, *J. Electrochem. Soc.* **1996**, *143*, 1254-1259.

7. M. Doyle, M. E. Lewittes, M. G. Roelofs, S. A. Perusich, and R. E. Lowrey, *J. Membr. Sci.* **2001**, *184*, 257-273.

8. R. F. Silva, M. DeFrancesco, and A. Pozio, *J. Power Sources* **2004**, *134*, 18-26.

9. P. C. Rieke and N. E. Vanderborgh, *J. Membr. Sci*. **1987**, *32*, 313-328.

10 M. J. Park, K. H. Downing, A. Jackson, E. D. Gomez, A. M. Minor, D. Cookson, A. Z. Weber, and N. P. Balsara, *Nano Lett.* **2007**, *7*, 3547-3552.

11. K. Miura, J. O. Hong, K. Yashiro, Y. Nigara, T. Kawada, and J. Mizusaki, *Trans. Mater. Res. Soc. Jpn*. **2001**, *26*, 1079-1082.

12. T. A. Zawodzinski, Jr., C. Derouin, S. Radzinski, R. J. Sherman, V. T. Smith, T. E. Springer, and S. Gottesfeld, *J. Electrochem. Soc*. **1993**, *140*, 1041-1047.

13. C. H. Lee, H. B. Park, Y. M. Lee, and R. D. Lee, *Ind. Eng. Chem. Res*. **2005**, *44*, 7617-7626.

14. S. Ma, Z. Siroma, and H. Tanaka, *J. Electrochem. Soc.* **2006**, *153*, A2274-A2281.

15. H. L. Lin, T. L. Yu, and F. H. Han, *J. Polym. Res*. **2006**, *13*, 379-385.

16. G. Alberti, M. Casciola, L. Massinelli, and B. Bauer, *J. Membr. Sci.* **2001**, *185*, 73-81.

17. T. A. Zawodzinski, T. E. Springer, J. Davey, R. Jestel, C. Lopez, J. Valerio, and S. Gottesfeld, *J. Electrochem. Soc.* **1993**, *140*, 1981-1985.

18. M. Merechal, J. L. Souquet, J. Guindet, and J. Y. Sanchez, *Electrochem. Commun*. **2007**, *9*, 1023-1028.

19. S. J. Paddison, D. W. Reagor, and T. A. Zawodzinski, Jr. *J. Electroanal. Chem*. **1998**, *459*, 91-97.

20. Z. Lu, G. Polizos, D. D. Macdonald, and E. Manias, *J. Electrochem. Soc.* **2008**, *155*, B163-B171.

21. T. A. Zawodzinski, Jr, M. Neeman, L. O. Sillerud, and S. Gottesfeld, *J. Phys. Chem*. **1991***, 95*, 6040-6044.

22. G. Blumenthal, M. Cappadonia, and M. Lehmann, *Ionics* **1996**, *2*, 102-106.

23. J. R. Atkins, C. R. Sides, S. E. Creager, J. L. Harris, W. T. Pennington, B. H. Thomas, and D. D. DesMarteau, *J. New Mater. Electrochem. Syst.* **2003**, *6*, 9-15-.

24. ASTM International, Designation E104-02, Standard Practice for Maintaining Constant Relative Humidity by Means of Aqueous Solutions, 1-3.

25. J. M. Prausnitz, R. N. Lichtenthaler, and E. G. de Azevedo, *Molecular Thermodynamics of Fluid Phase Equilibria*, 3rd ed., Chapter 9, p 512, Equations 9-11a, Prentice Hall PTR, New Jersey (**1999**).

26. J. F. Young, *J. Appl. Chem*. **1967**, *17*, 241-245.

27. P. H. Huang and J. R. Whetstone. Proc. Int. Symp. **1985**, 577-596, Publisher ISA, RTP, NC, USA.

28. L. Greenspan, J. Research National Bureau of Standards-A, Physics and Chemistry **1977**, *81*, 89-96.

29. H. F. Gibbard, Jr., and G. Scatchard, *J. Chem. Eng. Data* **1973**, *18*, 293-298.

30. H. F. Gibbard, Jr, G. Scatchard, R. A. Rousseau, and J. L. Creek, *J. Chem. Eng. Data* **1974**, *19*, 281-288.

31. M. E. Orazem and B. Tribollet, *Electrochemical Impedance Spectroscopy*, Chapter 13, p 234, John Wiley & Sons, New York, (**2008**).

32. X. Z. Yuan, C. Song, H. Wang, and J. Zhang, *Electrochemical Impedance Spectroscopy in PEM Fuel Cells*, Chapter 4, p 141-148, Springer London Dordrecht Heidelberg Limited, New York, (**2010**).

33. M. R. S. Abouzarri, F. Berkemeier, G. Schmitz, and D. Wilmer, *Solid State Ionics* **2009**, *180*, 922-927.

34. K. A. Mauritz and R. B. Moore, *Chem. Rev*. **2004**, *104*, 4535-4585.

CHAPTER 4

Chemically Crosslinked Polymer Electrolyte Membranes from Fluorinated Liquid Precursors for Application in Fuel Cells

Rameshwar Yadav[†], Douglas E. Betts[§], Peter S. Fedkiw[†], and Joseph M. DeSimone[†,§]

[†]North Carolina State University, Raleigh, NC, USA
[§]University of North Carolina, Chapel Hill, NC, USA

Abstract

Chemical crosslinking of liquid precursors for polymer electrolyte membranes (PEMs) has the ability to support variable acid content, to create the intricate barriers and tortuosity for reduced methanol crossover, and to reduce the cost via the ease of processing and mild reaction conditions. For direct methanol fuel cells (DMFCs), linear-chain PEMs suffer from drawbacks of methanol crossover from the anode to the cathode, limited conductivity, and high cost from processing steps and conditions. Chemically crosslinked PEMs have been prepared directly from photocurable liquid precursors under mild conditions without melt-processing or solvent-casting steps. Di-styrene end functionalized crosslinkers have been synthesized from perfluoropolyethers diols of variable molecular weights to vary the crosslink density in the membranes. Crosslinked PEMs have been prepared from the copolymerization of the fluorinated liquid crosslinkers and an ester of styrene sulfonate via UV-light initiated photopolymerization. Chemical crosslinking has allowed substantial increase in acid content, water-uptake, and ionic conductivity without compromising the

mechanical strength. For hydrogen-based fuel cells, the PEMs have exhibited remarkable water-uptake and conductivity that are three to four times higher than that of Nafion 117 membrane. For DMFCs, low-methanol permeability and reasonable ionic conductivity have been achieved due to the intricate crosslinked structure with a variable crosslink density. Under identical acid content, incorporation of low molecular weight crosslinker further reduces the methanol permeability by increasing the crosslink density. Depending on the molecular weight of the crosslinker and PEM composition, ionic conductivities from 10^{-4} to 10^{-1} S cm^{-1} and methanol permeabilities from 10^{-9} to 10^{-6} cm^2 sec^{-1} have been achieved. The selectivity, that is ratio of conductivity to permeability, is found to be two to three times higher than that of Nafion 117.

4.1. Introduction

Direct methanol fuel cells (DMFCs) can be competitive with and viable alternatives to batteries and other power generating devices because liquid fuel is directly converted into electricity efficiently.[1] DMFCs have promising attributes such as uninterrupted power supply from a liquid fuel source, simplicity in operation, high power-to-weight ratio, fast start-up times, high efficiency, and possible miniaturization for portability.[2,3] In DMFCs, electro-oxidation of methanol solution releases protons, electrons, and byproducts of carbon dioxide and water. The released protons migrate from the anode to the cathode through the PEM to combine with oxygen. The PEM is a critical and an integral component of the fuel cell stack in which PEM acts both as an electrolyte for proton transport and as a mechanical barrier for keeping the fuel separated from the oxygen. High-ionic conductivity, low-methanol permeability, low-swellability, low-oxidant crossover, acceptable thermal, mechanical, chemical and electrochemical stability, and affordable cost are essential properties of PEMs for early commercialization and widespread adaptability of DMFCs. Among all the associated challenges of DMFCs, methanol crossover is overriding because it deteriorates the DMFCs performance severely.

Benchmark PEM Nafion 117 is a linear-chain polymer that has application in hydrogen-, methanol- and other hydrocarbons-based PEM fuel cells because commercially available Nafion 117 has good chemical, thermal and mechanical stability.[4] However, high-methanol crossover from the anode to the cathode due to concentration gradient, electro-osmotic drag and facile electro-oxidation of methanol at the cathode is drawback of the

Nafion 117 membrane for its application in DMFCs.[5] Methanol crossover causes a reduction in the conductivity of PEM, swelling of the PEM, and mixed electrode potential at the cathode.[6,7] The resultant effect of methanol crossover in DMFCs is low-power density and low efficiency.[8,9] Delamination in the membrane electrode assembly (MEA) that stems from cyclic swelling and deswelling upon methanol uptake is another potential consequence of the methanol crossover. Nafion 117 exhibits higher swelling in methanol solution than in pure water as it lacks an intricate barrier to methanol crossover resulting from its linear-chain polymer structure.[10] Another disadvantage of the linear-chain polymer structure is lack of ability to support and sustain high ion-exchange capacity (IEC) above a value of 0.91 meq g^{-1} resulting in limited conductivity.

Nafion 117 is a copolymer of tetrafluoroethylene (TFE) and perfluoro(4-methyl-3,6-dioxa-7-octene-1-sulfonyl fluoride) (PSEPVE). TFE and PSEPVE are co-polymerized by free-radical initiated reaction in a solvent under pressure.[4] Following the synthesis of the co-polymer, the membrane is formed by the melt-extrusion of the polymer resin in the sulfonyl fluoride ($-SO_2F$) form. After melt-extrusion of the resin, hydrolysis in a base-alcohol mixture and ion-exchange in aqueous nitric acid converts the $-SO_2F$ groups into sulfonic acid ($-SO_3H$).[4] Despite having some attractive properties, Nafion 117 is expensive because of the many processing steps involved in its manufacture and suffers from shortcomings, such as limited IEC, high-methanol crossover, and poor conductivity under dry conditions.

For widespread adoption of DMFCs, alternative PEMs that have low-methanol crossover and reasonable conductivity are therefore highly sought. With a low-methanol crossover, DMFCs can be operated at concentrated methanol-water feed to enhance the performance. Preparing PEMs that have low-methanol permeability and reasonable conductivity is challenging because the transport mechanisms of water and methanol are similar. Water is integral to the operation of DMFCs because the electro-oxidation of methanol requires water to be present at the anode while the electro-oxidation of oxygen generates water at the cathode. The polarity of both water and methanol poses challenges to create PEMs with selective transport of water over methanol. This selective transport can lead to enhanced ionic conductivity and fuel cells performance. Many have reported that methanol crossover in PEMs can be reduced by incorporating inorganic fillers, such as silica, titania, zirconium phosphate, zirconia, montmorillonite, ormosil, alumina, mordenite, and clay.[11-24] However, these composite PEMs exhibit a reduction in methanol crossover at the expense of conductivity and membrane homogeneity. Besides the lack of intrinsic ionic conductivity in these fillers, the stability of the composite PEMs due to lack of interaction between the polymer host and the inorganic fillers is questionable.

There are some methanol-inhibiting compounds such as poly(vinyl alcohol), poly(vinyl pyridine), poly(vinyl aniline), poly(vinyl imidazole), poly(vinyl pyrrolidone) and poly(vinyl pyrrole) that have shown an increased barrier to methanol crossover through incorporation into PEMs.[18,19,25-36] However, adding these compounds typically results in a sacrifice in conductivity as these compounds lack intrinsic ionic conductivity. Furthermore, these organic compounds have inadequate chemical stability in the acidic environment of

PEM fuel cells. Developing PEMs that have low permeability and high conductivity without the addition of inorganic filler or other methanol-inhibiting compounds remains challenging.

Methanol permeation across PEMs occurs through combination of various phenomena, such as wetting of the upstream surface, sorption in PEMs, diffusion across PEMs, and consumption or pervaporation from the downstream surface. Tailoring of upstream surface that lacks favor to methanol can minimize the surface wetting and reduce the methanol crossover. Type and quantity of acid functional groups, type of polymer fluorocarbon *vs*. hydrocarbon, and solvent-host interaction influences the methanol sorption in PEMs. Structure of polymer such as linear, crosslinked or combination of the two structures plays important role in diffusion across the PEMs. The rate and type of methanol removal from the downstream surface such as electro-oxidation in DMFCs at cathode or pervaporation affects the methanol crossover. In this work, we have endeavored to control the methanol crossover through crosslinked polymer structure and through quantity of acid groups.

Crosslinked structure polymers instead of linear-chain polymers have the ability to provide an intricate barrier and tortuosity to methanol transport. These crosslinked structures support and sustain variable acid content that can be exploited to achieve reasonable ionic conductivity and low-methanol permeability. Unlike linear-chain PEMs that suffer from excessive swelling upon solvent uptake, crosslinked structure inhibits the swelling and expansion because crosslinking constrains the mobility of polymer chains and prevents dissolution of the polymer. Zhou *et al*. showed that chemical crosslinking of styrene-perfluoropolyethers (sPFPE) and styrene sulfonate ester (R_f-SSE) monomer allowed incorporation of high-acid content in PEMs that outperformed Nafion 117 membranes in hydrogen-based PEM fuel cells.[37] Water-uptake, conductivity, and power density of the crosslinked PEMs in hydrogen-based fuel cells exceeded that of Nafion 117 membrane.[37]

Here, we present an approach for preparing crosslinked PEMs from difunctional perfluoropolyethers (PFPE) and styrene sulfonic acid (SSA) in response to the shortcomings in the traditional PEMs. PFPEs are a unique class of fluoropolymers that are liquid at room temperature, possess high-chemical resistance, extremely low-surface energy, and low toxicity.[38] In the first step to prepare the crosslinked PEMs, commercially available liquid PFPE-diols were functionalized with styrene end groups to yield styrene-perfluoropolyether (sPFPE). The sPFPE is a difunctionalized, highly fluorinated, and curable liquid precursor. Crosslinkers of six different molecular weights (MWs) were synthesized to vary the crosslink density in the PEMs. For incorporating acid groups into the membrane, the styrene sulfonate ester comonomer (R_f-SSE) was synthesized from sodium *p*-styrene sulfonate. The liquid precursor sPFPE and R_f-SSE were then mixed to form a single-phase homogenous mixture. The mixture was converted into a solid acidic PEM by UV-initiated free-radical bulk polymerization, hydrolysis of the incorporated R_f-SSE group and subsequent ion-exchange. A series of crosslinked PEMs were synthesized to investigate the effect of composition, MW of the crosslinker sPFPE, and resulting crosslink density on the conductivity and methanol permeability of PEM.

Fourier Transform Infrared (FTIR) spectroscopy and Thermal Gravimetric Analysis (TGA) confirmed that the membranes were fully hydrolyzed and thermally stable, respectively. Measurement of IEC, water- and methanol solution-uptake, conductivity, and methanol permeability were performed to evaluate the crosslinked PEMs. The water- and methanol solution-uptake results were considered to investigate the effect of increasing acid content in the PEMs. Ionic conductivity was studied in liquid water and at room temperature. Methanol transport was investigated as function of PEM composition and MW of sPFPE. The IEC and crosslink density were varied to obtain a reasonable ionic conductivity and low-methanol permeability in comparison with Nafion 117. In one selected measurement in water vapor phase, it was noted that the crosslinked PEMs exhibited conductivity three to four times higher than that of Nafion 117. For DMFCs, low-methanol permeability and reasonable ionic conductivity were achieved from the crosslinked structure.

4.2. Experimental

4.2.1. Synthesis of Difunctional sPFPE Crosslinker

The synthesis of sPFPE and the R_f-SSE comonomer was based on earlier work done by Zhou *et al*.[37] Appendix C.1 provides the synthesis procedure in detail. The reaction involves the styrene-functionalization of PFPE diols with 4-vinylbenzyl chloride through a phase-transfer catalyzed reaction. Poly(tetrafluoroethylene oxide-co-difluoromethylene oxide α,ω-diol) (Fomblin ZDOL M_n = 3800, 2500, 2000 g mol^{-1}, CF_2CF_2O/CF_2O: 1/1 and Fluorolink Modifier M_n = 2000, 1500, 1000 g mol^{-1}, CF_2CF_2O/CF_2O: 4/1) were purchased from Solvay Solexis. Styrene linkages were incorporated onto both ends of the PFPE α, ω-diol by a base activated phase-transfer catalyzed reaction. For each MW of PFPE, proportional amount of 4-vinylbenzyl chloride was added to synthesize corresponding crosslinker. The final distyrene terminated perfluoropolyether (sPFPE) product was a transparent viscous liquid. ^{1}H-NMR confirmed that the PFPE diols were fully styrenated (Appendix C.1, Figure C.1.2). After styrene functionalization of PFPE diols with 4-vinylbenzyl chloride, the MW of each PFPE diol increases by 232 g mol^{-1}. Figure 4.2.3 shows the chemical structure of sPFPE.

4.2.2. Synthesis of Fluorinated Styrene Sulfonate Monomer

Sodium *p*-styrene sulfonate (MW = 205.5 g mol^{-1}) is immiscible with sPFPE. To improve the compatibility of the sodium *p*-styrene sulfonate monomer with sPFPE, a fluorinated ester that is compatible with sPFPE was synthesized using 4-vinylbenzene sulfonyl chloride and 3,3,4,4,5,5,6,6,7,7,8,8,8-tridecafluoro-1-octanol.[37,39] Appendix C.2 provides the synthesis procedure in detail. Fluorocarbon tail from 3,3,4,4,5,5,6,6,7,7,8,8,8-tridecafluoro-1-octanol was attached to the 4-vinylbenzne sulfonyl chloride (MW = 202.66 g mol^{-1}) in order to obtain 1-(3,3,4,4,5,5,6,6,7,7,8,8,9,9,9-pentadecafluoro-nonane-1-sulfonyl)-4-vinyl benzene, the precursor styrene sulfonate ester (R_f-SSE, MW = 529.61 g mol^{-1}), that is miscible with sPFPE.[37] The R_f-SSE product is a waxy and yellowish solid. ^{1}H-NMR spectroscopy showed that fluorinated tail was attached to the sulfonyl group ($-SO_2-$) (Appendix C.2, Figure C.2.2). Figure 4.2.3 shows the chemical structure of R_f-SSE.

4.2.3. Preparation of Chemically Crosslinked Membranes

Crosslinked membranes were fabricated through the UV-initiated free-radical bulk polymerization. Selected ratios of the liquid sPFPE difunctional crosslinker and the co-monomer R_f-SSE using 1 wt% α, α-diethoxyacetophenone photoinitiator were heated in a glass vial above 60 °C to obtain a homogeneous liquid phase. The heated liquid mixture was then poured onto a template and photo-chemically crosslinked upon exposure to UV-light radiation (λ = 365 nm) for 10 minutes under continuous nitrogen gas purge. After the photo polymerization of the liquid mixture, the crosslinked membrane in the ester form was peeled off gently from the template.

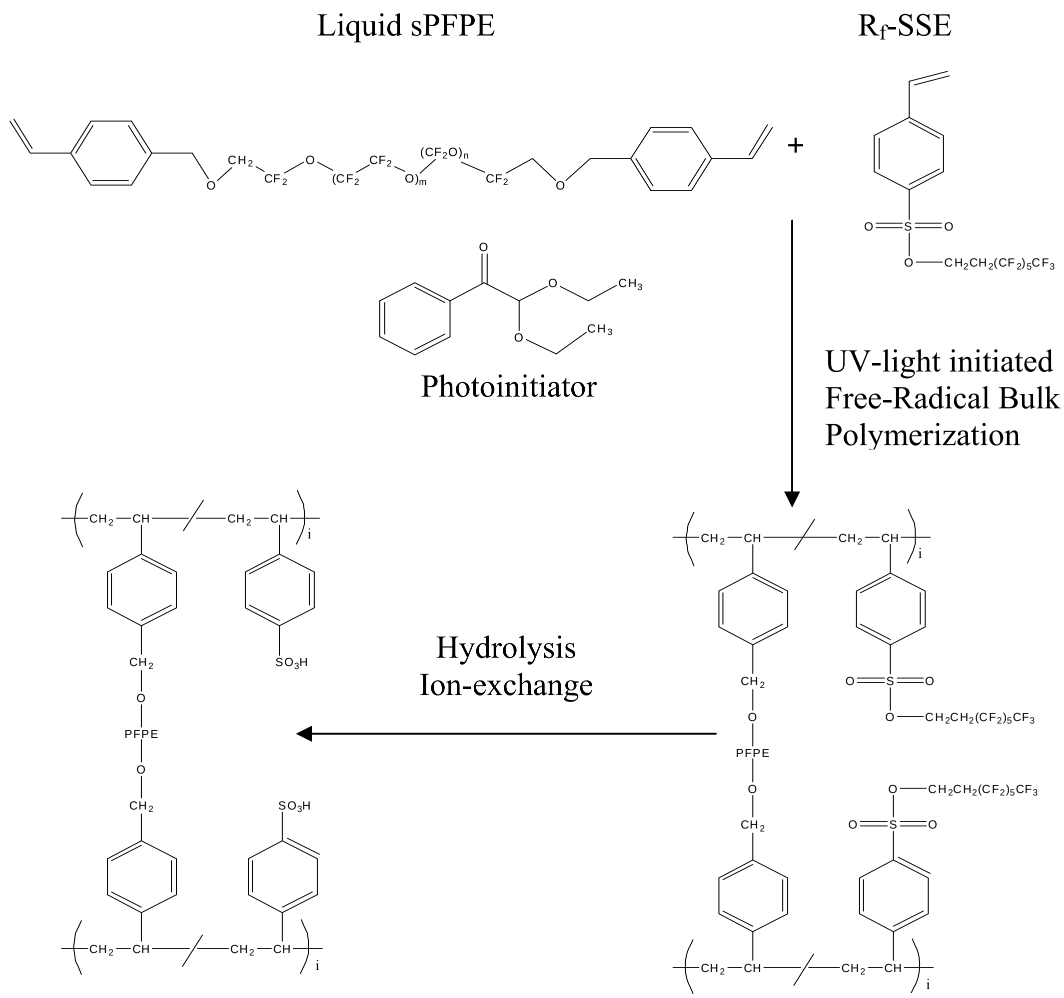

Figure 4.2.3. Chemical structure of chemically crosslinked copolymer from sPFEP/R_f-SSE.

Figure 4.2.3 shows the chemical structure of the sPFPE/R_f-SSE crosslinked membrane. Conversion of R_f-SSE ester into the acid form was accomplished by hydrolysis in aqueous base-methanol solution followed by acid treatment.[37] FTIR-ATR analysis of the membrane surface before hydrolysis (when the membrane was in ester form) and after hydrolysis (when the membrane was in Na^+-salt form) confirmed that the ester group in R_f-SSE was converted to corresponding sulfonic acid (-SO_3H). Figure C.3 in Appendix C.3 presents the FTIR-ATR spectra that confirm full hydrolysis of R_f-SSE. For a comparative study, a Nafion 117 membrane was treated by following Yadav *et al*.[40]

4.2.4. Measurement of Ion-Exchange Capacity

Ion-exchange capacity (IEC, meq g^{-1}) and equivalent weight (EW) were determined by elemental analysis of sulfur (Atlantic Microlab, Atlanta) and by stoichiometry from known weights of sPFPE and R_f-SSE in the membrane. For IEC from elemental and stoichiometry methods, we assumed that the sulfur and proton were from sulfonic acid (-SO_3H) only.

4.2.5. Analysis of Thermal Stability

The effect of MW on the thermal stability of PEM was studied by using a Perkin-Elmer Pyris 1 Thermogravimetric analyzer (TGA). In a typical TGA measurement, a piece of membrane sample in H^+ form was initially heated from 30 to 120 °C at 10 °C per min and held at 120 °C for 60 minutes to remove any moisture. In the second step, the sample was cooled down from 120 to 30 °C and held at 30 °C for 30 minutes to stabilize the temperature. In the third step, the sample was heated from 30 to 500 °C at 10 °C per minute. All the three steps were performed under continuous flow of 20 mL/min. The onset of rapid residual weight loss indicated the thermal degradation temperature.

4.2.6. Sorption of Water and Methanol Solution

The dry-weights of the membranes in acid form were measured after drying over P_2O_5 for two weeks. After the dry-weight measurement, membranes were soaked in deionized water for 24 hours and the weights of the water-soaked membranes were measured after blotting off the surface water. After water-uptake measurement, the membranes were dried overnight at room temperature and soaked in plenty of methanol solution (1 mol/L) for 24 hours in a sealed glass bottle. The weights of methanol solution-soaked membranes were measured after blotting off the surface. The methanol solution-uptake was obtained from the following expression:

$$\text{MeOH Solution Uptake} = \frac{W_{(Methanol)} - W_{dry}}{W_{dry}} \times 100$$

4.2.7. Measurement of Ionic Conductivity

Ionic conductivity of crosslinked PEMs was measured by the two-probe electrochemical impedance spectroscopy (EIS) technique described by Yadav *et al*.[40] Crosslinked PEMs were assembled in conductivity cells. The conductivity cells were then placed in a custom-made environment chamber to equilibrate the PEMs with water vapor and temperature.[40] Figure C.8 in Appendix C.8 shows the change in conductivity with time at fixed temperature in which crosslinked PEM attains equilibration with water vapor activity in 48 hours. For conductivity measurement in liquid water, PEMs were equilibrated with deionized water at room temperature. The bulk resistances of the PEMs were obtained from analysis of impedance data (Frequency range 1MHz-1Hz, AC voltage 10 mV).[40] Figure C.7 in Appendix C.7 shows the typical impedance spectra of a crosslinked PEM. Ionic conductivity was obtained from the method described by Yadav *et al*.[40]

4.2.8. Analysis of Methanol Permeability

Time-lag technique was followed to measure the methanol permeability across PEMs.[41-44] A two-compartment molecular diffusion cell was constructed to study the methanol permeability across PEMs at room temperature. The liquid heights in both compartments were maintained equal to eliminate any hydrostatic pressure-induced transport of methanol across the membrane. The volume of the transmitting-compartment (58 cm^3) relative to volume of the receiving-compartment (25 cm^3) was sufficiently large to keep the methanol concentration constant in the transmitting-compartment during the sampling from the receiving-compartment. The active surface area of the membrane for methanol diffusion was 3.56 cm^2. Appendix B.1 presents the photo of diffusion cell.

Molecular permeability, P, is defined as ($D \times K$) where D is the diffusivity and K is the partition coefficient. The mass-balance of methanol in the transmitting-compartment and receiving-compartment, using Fick's first law of molecular diffusion under pseudo-steady-state condition in the membrane is carried out to derive an expression for molecular permeability. Equations (4.2.8.1-3) provide the relationship between concentration, membrane dimensions, and membrane properties.[41-44]

$$Q_t = \frac{DKC_A}{L}\left[t - \frac{L^2}{6D}\right] - \frac{2LKC_A}{\pi^2}\sum_{n=1}^{n=\infty}\frac{(-1)^n}{n^2}\exp\left(\frac{-Dn^2\pi^2 t}{L^2}\right) \qquad (4.2.8.1)$$

$$C_B(t) = \frac{(DK)AC_A(t - t_0)}{V_B L} = \frac{PAC_A(t - t_0)}{V_B L} \qquad (4.2.8.2)$$

$$t_0 = \frac{L^2}{6D} \qquad (4.2.8.3)$$

where, Q_t is moles per unit area through the membrane at time t, P is permeability, D is diffusivity, K is partition coefficient, $C_B(t)$ is receiving-compartment concentration, C_A is transmitting-compartment concentration, A is active area of the membrane, L is membrane thickness, V_B is receiving-compartment volume, V_A is transmitting-compartment volume, t is time, and t_0 is lag-time ($L^2/6D$). For large time t, Equation (4.2.8.1) can be simplified into Equation (4.2.8.2) in which C_A is assumed to be constant and $C_A >> C_B$ from $V_A >> V_B$. Equation (4.2.8.2) can be used to determine the molecular permeability, P. Lag-time t_0 depends only on the membrane thickness and solvent diffusivity as shown in Equation (4.2.8.3).

In a typical permeability experiment, a water-soaked membrane was clamped between the two compartments. After assembling the membrane, the receiving-compartment was filled with deionized water and the transmitting-compartment was filled with 1 mol/L methanol solution. The methanol concentration in the receiving compartment was tracked with time and analyzed with a gas chromatograph (GC) that was equipped with a polar column. Appendix B.2 discusses procedure for methanol analysis and presents typical chromatograms of methanol concentration in the receiving-compartment.

Figures 4.2.8 a-b illustrate the typical behavior of change in the receiving-compartment concentration with time for a crosslinked PEM and a Nafion 117 and. A linear response is observed for change in concentration with time. Initially, various samples were analyzed and plotted against time to fit a linear curve. From the gradient of the linear fit, methanol permeability was calculated from Equation (4.2.8.2). Qualitative trend of the curve (Figures 4.2.8 a-b) confirms that the receiving-compartment concentration increases linearly with time.

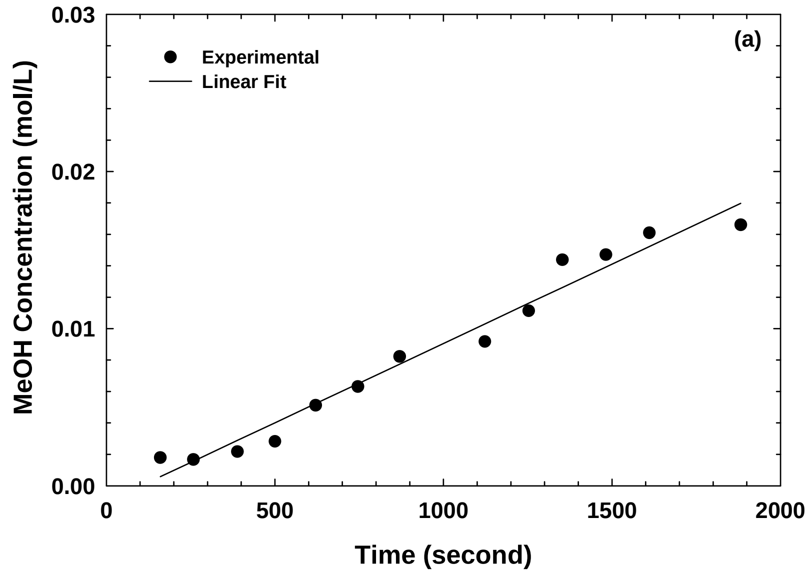

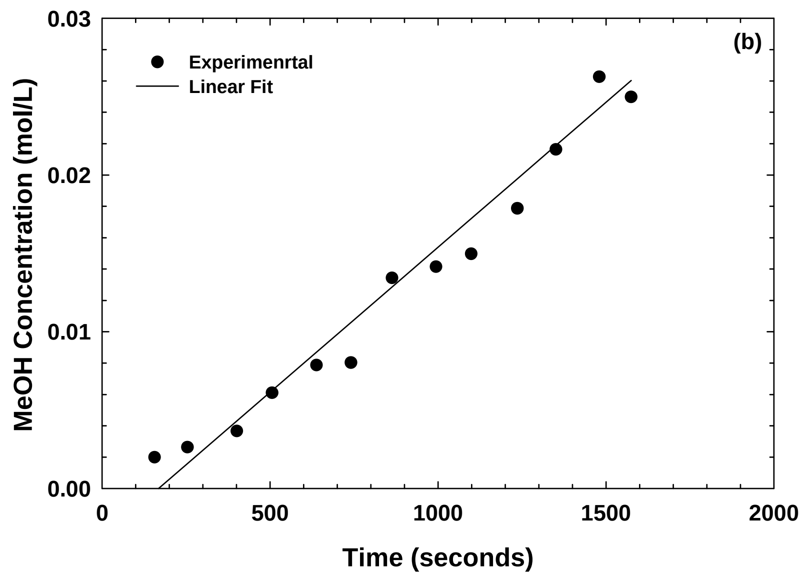

4.2.8. Change in receiving-compartment concentration with time for crosslinked PEM (Figure 4.2.8-a) and Nafion 117 membrane (Figure 4.2.8-b).

4.3. Results and Discussion

This section presents the results of crosslinked PEMs.

4.3.1. Difunctional sPFPE Crosslinker and Crosslinked PEMs

Liquid precursor sPFPE possesses promising credentials for developing novel fluoropolymers through easy and affordable processing steps. Two types of sPFPE crosslinker have been derived from Fomblin ZDOL and Fluorolink modifier PFPE diols (Fomblin ZDOL M_n = 2000, 2500, 3800, g mol^{-1}, CF_2CF_2O/CF_2O: 1/1; Fluorolink Modifier M_n = 1000, 1500, 2000 g mol^{-1}, CF_2CF_2O/CF_2O: 4/1). Because of different ratio of ether groups, crosslinking ability of Fomblin ZDOL sPFPE differs from that of Fluorolink Modifier sPFPE. Figure C.4 in Appendix C.4 shows the moles of sPFPE against MW of sPFPE in which it is believed that crosslinking can be increased with decreasing the MW. Liquid sPFPE crosslinkers are easily photocurable into novel fluoropolymers of any controllable shape and size because of styrene reactivity and low-surface energy (24 dyne cm^{-1}). Styrene functionality on fluorinated backbone confers sPPFE attractive features for developing novel fluoropolymers because styrene-based fluorinated liquid monomers are nearly non-existent. Even chemically synthesized styrene-based fluoropolymers are non-existent.

Combination of high flexibility from ether groups in PFPE and high-Young modulus and thermal stability from styrene yields mechanically and thermally robust materials for many applications. Low-surface energy and easy polymerization ability of sPFPE can be harnessed to create composite materials by imbibing liquid sPFPE in porous substrates, such as expanded PTFE. Appendix D discusses the synthesis and results of such composite PEMs based on liquid sPFPE crosslinker. Copolymerization of sPFPE with other monomers with similar reactivity can create other novel fluoromaterials as well. Easy and simple synthesis from commercially available PFPE diols and affordable processing condition such as photocuring are other advantages of sPFPE because synthesis of most fluoropolymers requires extreme reaction conditions, sophisticated equipment, and intensive cost.

For PEMs development, liquid precursor sPFPE has many advantages that allow high-acid content and variable crosslinking through easy processing steps to incorporate many properties favorable to fuel cells. MW and weight content of sPFPE provide opportunity to increase acid loading and adjust crosslink density to form intricate crosslinked structure in PEMs. For DMFCs, it is envisioned that crosslinked structures create intricate barrier and tortuosity to methanol transport in PEMs. In this work, liquid mixture of sPFPE/R_f-SSE have been converted into solid PEMs with varying acid loading and crosslink density, and sufficient mechanical and thermal stability for application in DMFCs.

Crosslinked PEMs were fabricated from the mixture of liquid precursor sPPFE and R_f-SSE. Figure C.5 in Appendix C.5 shows mole ratio of R_f-SSE to sPPFE against R_f-SSE weight-content in which the mole ratio increases non-linearly with R_f-SSE weight-content. The homogeneous mixture of sPFPE/R_f-SSE was photocured, hydrolyzed, and ion-exchanged to form PEMs without melt-processing or solvent-casting. Due to high reactivity of styrene in both sPFPE and R_f-SSE, the liquid mixture was fully converted into solid membrane. Covalent chemical crosslinking initiates and propagates uniformly from the styrene group at both ends of sPFPE and from styrene in R_f-SSE. Amount of any single or combination of any two liquid crosslinkers were varied from 20 to 60 wt% and R_f-SSE was varied from 20 to 60 wt% to fabricate a series of PEMs with variable acid loading and crosslink density. Acid loading depends on amount of R_f-SSE as well as on extent of copolymerization of sPFPE/R_f-SSE. Due to high and similar reactivity of styrene in both sPFPE and R_f-SSE, target acid loading was accomplished easily by the amount of R_f-SSE.

4.3.2. Ion-Exchange Capacity

Ion-exchange capacity (IEC) is a measure of acid content, acidity, and the ability of ion-transport in the membrane. Based on IEC measurement technique, IEC corresponds to the acid groups that exchange their protons readily with other ions. IEC of sulfonic acid based PEMs is expected to be higher than that of the other acids based PEMs because sulfonic acid is a stronger acid. As such, sulfonic acid is a generic acid and its acidity depends on the side group that is attached to $-SO_3H$. For example, acidity of fluorosulfonic acid (FSO_3H) and trifuorosulfonic acid (CF_3SO_3H) differs from that of methylsulfonic acid (CH_3SO_3H) and other hydrocarbons-based sulfonic acids.

Measurement of IEC by elemental analysis of sulfur or any other representative group assumes that all the sulfur containing acid groups or any other representative groups are fully and equally active. Accuracy of IEC by the elemental analysis method is compromised if other unknown sources of representative elements like S in sulfonic acid are present in

PEMs. In this work, IEC was studied by elemental analysis method. In addition, IEC was calculated stoichiometrically from known weights of sPFPE and R_f-SSE in the membrane. Figure 4.3.2 shows the IEC results as function of R_f-SSE weight content in crosslinked PEMs.

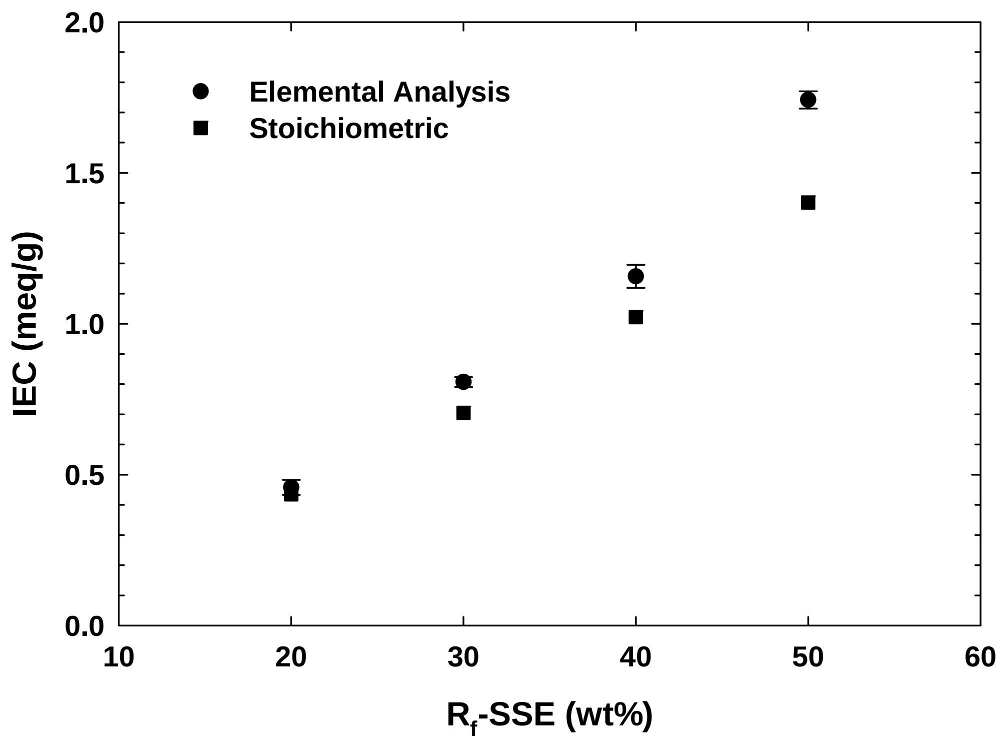

Figure 4.3.2. Ion-exchange capacity (IEC) by elemental analysis of sulfur and by stoichiometry. The remaining weight in the membrane was from sPFPE (4000 g mol^{-1}).

IEC of crosslinked PEMs increases almost linearly with the weight of R_f-SSE. As expected, IEC increased from 0.46 to 1.74 meq g^{-1} for R_f-SSE weight of 20 to 50%. This increase is remarkable and two times higher than that of Nafion 117 IEC of 0.91 meq g^{-1}. Such high IEC has been achieved because of covalent crosslinking ability of sPFPE and R_f-SSE. At high-acid loading, traditional linear-chain membranes like Nafion 117 lack the ability to retain their mechanically strength, and to constrain swelling especially at polar solvents uptake such as water and methanol. However, these crosslinked PEMs including PEMs with high IEC are mechanically intact and robust because crosslinking prevents their dissolution. The integrity of crosslinked structure confirms that these crosslinked PEMs sustain and support high-acid loading.

As shown in Figure 4.3.2, there is a good agreement between IEC results from elemental and stoichiometry methods. IEC from titration[37] and elemental methods also confirms that all the ester groups are fully converted into corresponding sulfonic acid after hydrolysis and ion-exchange. Because R_f-SSE is the only source of sulfur and sulfonic acid, we assumed that IEC is independent of MWs of crosslinker sPFPE. IEC shown in Figure 4.3.2 is representative IEC of crosslinked PEMs with other sPFPE MWs at corresponding weight of R_f-SSE.

4.3.3. Thermal Stability

Fluorinated backbone from PFPE and styrene impart sufficient thermal stability in these crosslinked PEMs at PEM fuel cells operating condition. In crosslinked PEMs, effect of sPFPE MWs on thermal stability has been investigated by TGA. Independent of crosslinker MWs, crosslinked PEMs exhibits initial thermal decomposition temperature of 160-260 °C that surpasses the requirement of PEM fuel cells. In selecting the composition of PEMs for TGA study, IEC was fixed at 1.16 meq g^{-1} because higher IECs are irrelevant from the methanol crossover perspective. Increasing the crosslinker MW enhances the thermal stability further because of flexibility from high MW. This enhanced thermal stability is expected because long and flexible chains from increased MW possess ability to withstand the temperature and overcome the initial thermal degradation.

Figure 4.3.3 shows the thermal behavior of crosslinked PEMs at various MWs of sPFPE. All the crosslinked PEMs are thermally stable up to 160-260 °C as shown by onset of thermal degradation (Figure 4.3.3). Thermal stability increases from 160 to 260 °C for increase in MW from 1000 to 4000. It was noted that combination of the low MW (1000 g mol^{-1}) crosslinker with the high MW (4000 g mol^{-1}) crosslinker exhibits improved thermal stability over single low-MW crosslinker. Under identical condition, one selected membrane in ester form (MW 2000 Fluorolink modifier) shows the highest thermal stability up to 300 °C as expected. Figure 4.3.3 illustrates that crosslinked PEMs have sufficient thermal stability to meet the challenges of hydrogen- and methanol-based fuel cells.

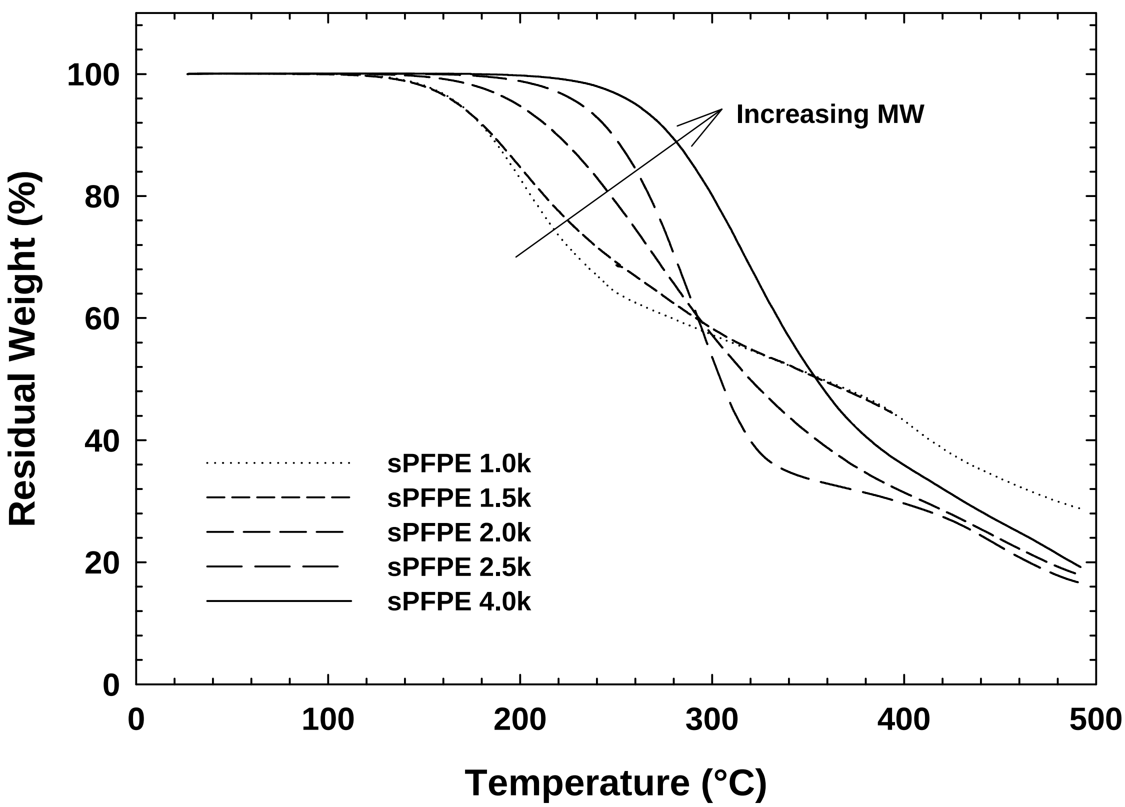

Figure 4.3.3. TGA of crosslinked PEMs in H^+ form at IEC of 1.16 meq g^{-1}. The first two crosslinkers (1.0 & 1.5k) are from Fluorolink Modifier and the last three crosslinkers (2.0, 2.5, and 4.0k) are from Fomblin Diols.

4.3.4. Water and Methanol Solution Uptake

Polar solvent uptake is determined to study the transport properties of PEMs because transport properties are profoundly dependent on solvent uptake. In PEM fuel cells, it is critical to retain water for fast and efficient proton conduction, and to reject methanol to reduce its crossover to the cathode. In this work, liquid water and methanol solution (1 mol/L) uptakes at room temperature have been studied in crosslinked PEMs. Concentration of methanol solution was fixed at 1 mol/L from the DMFCs perspective. As expected, liquid water and methanol solution uptakes increase with IEC. Independent of sPFPE MW, IEC shows strong effect on solvents uptake. High-solvent uptake is signature of strong ionic interaction that results from increased acid loading, hydrophilic-hydrophobic phase separation, and resulting nano-channel formations. Such high uptake has profound effect on PEMs performance in PEM fuel cells. Crosslink structures are expected to influence the polar solvents uptake because these structures have ability to prevent mobility in PEMs and hinder the ionic interaction, which contributes to solvent uptake. Furthermore, high-crosslink density from low-MW crosslinker retards the chain mobility, constrains the swelling and is responsible for creating more confining environment near ionic sites.

Figure 4.3.4 illustrates the methanol-solution uptake at room temperature in crosslinked PEMs and Nafion 117 membrane. For IEC increase of 0.46 to 1.16 meq/g, crosslinkers with both MWs 1000 and 4000 g mol^{-1} show almost equal methanol solution uptake (Figure 4.3.4). Under identical condition, Nafion 117 membrane exhibits methanol solution uptake of 31 wt% that is higher than that in crosslinked PEMs at corresponding IEC.

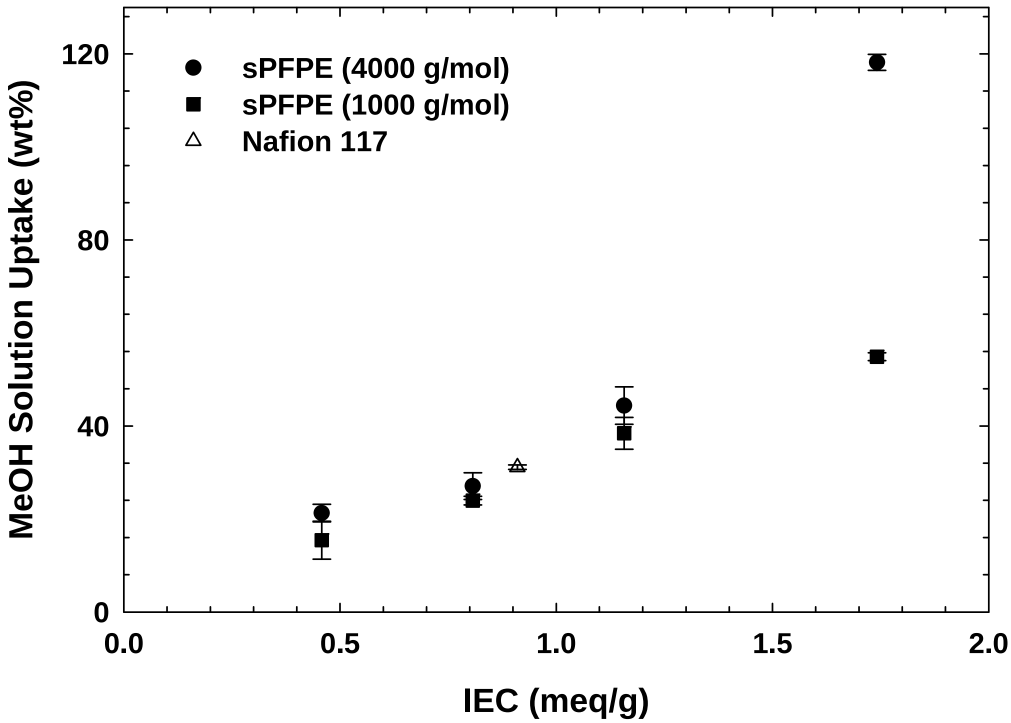

Figure 4.3.4. Methanol solution (1 mol/L) uptake at room temperature.

By incorporating high acid in crosslinked PEMs, solvent uptake is increased by three times higher than that of Nafion 117. Crosslinked PEMs and Nafion 117 show similar behavior with water uptake (results not shown). Due to low-acid loading at low IEC, there is lack of ionic interactions that appears in low-solvent uptake.

Increase in crosslink density from incorporating the low-MW sPFPE (1000 g mol^{-1}) shows negligible effect on solvent uptake at IEC of 0.46-1.16 meq/g. However, at 1.74 meq g^{-1}, incorporating low-MW crosslinker lowers the solvent uptake drastically from 118 to 55 wt% (Figure 4.3.4). The high-solvent uptake for high MW and low-solvent uptake for low MW confirm that crosslink density becomes effective and predominant at high-acid loading. Furthermore, this MW effect is evident in Figure C.6 in Appendix C.6, which shows methanol-solution uptake at IEC of 1.74 meq $g^{-1}$for three different MWs (4000, 2000, 1000 g mol^{-1}).

We expect that increased crosslinking display anomalous behavior on other properties of membrane. Based on water- and methanol solution-uptakes, we focused on investigating PEMs that are suitable for DMFCs. Water and methanol solution-uptakes were considered in selecting the MW of crosslinker and compostions of PEMs for ionic conductivity and methanol transport study.

4.3.5. Ionic Conductivity

Area specific resistance (ASR) is a critical property of PEMs that leads to ohmic losses in the performance of PEM fuel cells. Resistance across PEM has predominant effect on the ASR and ohmic losses because the other components of PEM fuel cells have relatively low resistances due to their respective intrinsic conductivities. In order to minimize the ohmic losses, reduction in ASR is achieved by both high-ionic conductivity and low-PEM thickness. Type of materials, processing methods and conditions applied in PEMs fabrication restricts the reduction in PEM thickness below certain values (20 μm for Nafion membranes).

For a given thickness of PEM, obviously, high-ionic conductivity reduces the ASR further. High-ionic conductivity is achieved by incorporating high-acid loading, by type of polymer materials, such as fluorocarbons *vs.* hydrocarbons, by type of acid group such as perfluoro sulfonic acid ($-CF_2-CF_2-SO_3H$) or hydrocarbon-based sulfonic acid ($-C_6H_4-SO_3H$), and by polymer structures such as linear, crosslinked or combination of the two. Our goal has been to exploit the ability of chemical crosslinking to incorporate variable-acid loading to achieve high-ionic conductivity for hydrogen-based PEM fuel cells and reasonable ionic conductivity at low permeability for methanol-based fuel cells.

In ionic conductivity study, goal of achieving low-methanol permeability determined the PEM composition, IEC, and crosslinked density from variable MW of the crosslinker sPFPE. Although, high-acid loading leads to remarkable conductivity in these crosslinked PEMs for hydrogen-based fuel cells, it was kept below 1.74 meq g^{-1} in permeability study because of unacceptable methanol crossover at higher IEC above 1.74 meq g^{-1}. In DMFCs, it is relevant to investigate conductivity in liquid water because of high-water availability in the PEMs. However, in one set of study, conductivity of crosslinked PEM (IEC = 1.85 meq g^{-1}) and Nafion 117 was studied as a function of temperature at 100% relative humidity from the perspective of humidified air at DMFCs cathode. In water vapor phase, crosslinked PEMs exhibit conductivity of three to four times higher than that of Nafion 117 because of high IEC. Figure 4.3.5 shows the conductivity results of crosslinked PEMs and Nafion 117.

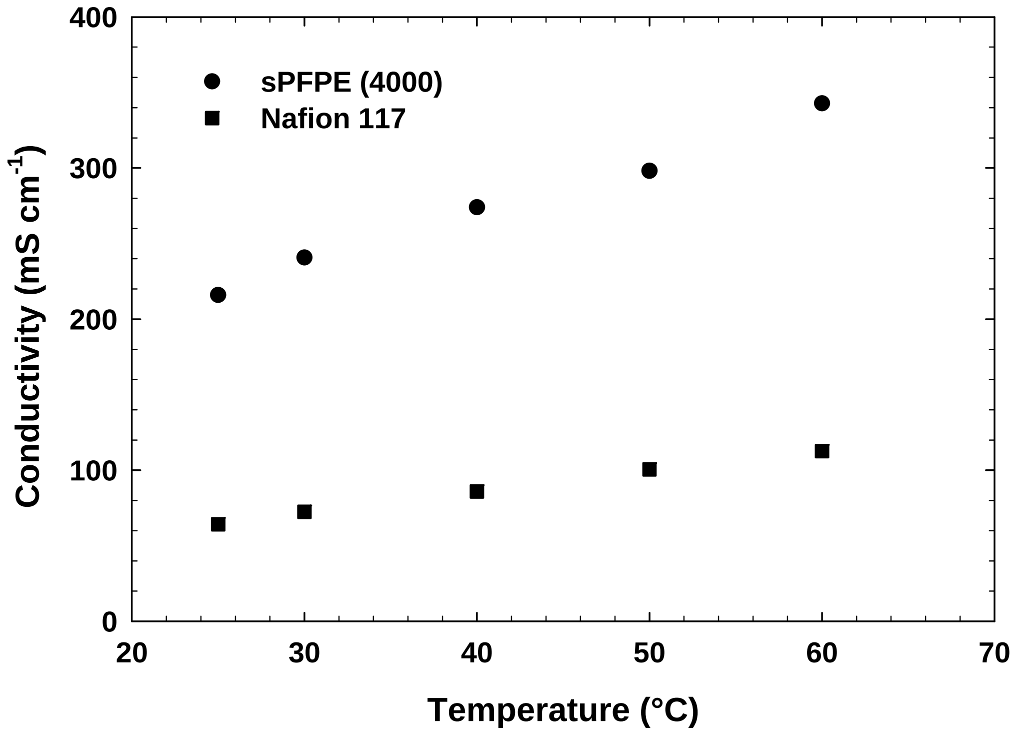

Figure 4.3.5. Conductivity at 100% relative humidity. The IEC of crosslinked PEM is 1.85 meq g^{-1} and that of Nafion 117 is 0.91 meq g^{-1}.

Ionic conductivity increases from 220 to 340 mS cm^{-1} for temperatures from 25 to 60 °C. This increase is startling in comparison with Nafion 117 conductivity of 62-140 mS cm^{-1} (Figure 4.3.5). Incorporating such high-acid loading in linear-chain PEMs such as Nafion 117 to achieve such high conductivity of 220-340 mS cm^{-1} can lead to dissolution of such PEMs.

Under identical IEC, other hydrocarbon- and aromatic-derived PEMs exhibit low conductivity because of lack of hydrophobic-hydrophilic phase separation. In these crosslinked PEMs, it is envisioned that fluorinated segment of PFPE contributes to microphase separation resulting in aggregation of nano-channels. High-acid loading and phase separation from highly fluorinated segment favor ionic interaction and growth that manifest into high-ionic conductivity.

Table 4.3.5 shows the conductivity of crosslinked PEMs in liquid water and at room temperature. Table C.9 in Appendix C.9 presents conductivity results of additional crosslinked PEMs with various compositions. Independent of crosslinker MW, ionic conductivity increases with IEC. Ionic conductivity is strongly dependent on acid loading because increase in IEC is expected to increase charge carrier concentration and its interaction. For the highest MW crosslinker (4000 g mol^{-1}), conductivity increases from 29 to 125 mS cm^{-1} for IEC of 0.81 to 1.74 meq g^{-1}. This increase in conductivity demonstrates the promising attributes of these membranes. In the intermediate MW crosslinker (2000 g mol^{-1}), conductivity increases from 34 to 117 mS cm^{-1} for IEC of 0.81 to 1.74 meq g^{-1} that is consistent with decrease in the MW.

Table 4.3.5 Crosslinked PEMs Properties in Liquid Water and at RT

Crosslinker MW ($g\ mol^{-1}$)	IEC ($meq\ g^{-1}$)	Conductivity ($mS\ cm^{-1}$)	Permeability ($10^{-6}\ cm^2\ sec^{-1}$)
2500	0.81	11.1 ± 11%	0.213
	1.16	57.9 ± 9%	1.07
2000	0.81	27.9 ± 3%	0.320
	1.16	73.0 ± 9%	0.819
2000	0.81	34.0 ± 1%	0.323
	1.74	117 ± 6%	-
1500	0.81	38.7 ± 3%	0.613
	1.16	84.7 ± 0.4%	0.624
	1.74	112 ± 2%	-
1000	1.16	72.9 ± 8%	1.48
	1.74	95.5 ± 7%	-
Nafion 117	0.91	104 ± 2%	2.19

For the lowest MW crosslinker (1000 g mol^{-1}), ionic conductivity increases from 22 to 96 mS cm^{-1} that shows the evidence of increased crosslink density from the low-MW crosslinker. The crosslinkers 2000 and 2500 that were derived from Fomblin ZDOL show conductivity increase of 28 to 73 and 11 to 58 mS cm^{-1}, respectively. At low IEC of 0.46-0.81 meq g^{-1}, miscibility of sPFPE with R_f-SSE is expected to increase with decrease in MW of the crosslinker. As a result, crosslinkers derived from Fluorolink Modifier lead to higher conductivity in PEM than that derived from Fomblin ZDOL. Figure 4.3.6.1 shows the graphical trend of conductivity for sPFPE (4000 g mol^{-1}) crosslinker. As shown in Figure 4.3.6.1, conductivity of crosslinked PEMs becomes higher than that of Nafion 117 at IEC of above 1.16 meq g^{-1}. For any given IEC, increase in the crosslinker MW enhances the conductivity due to reduction in crosslink density.

For example, at IEC of 1.74 meq g^{-1}, conductivity increases from 96 to 125 mS cm^{-1} for MW of 1000 to 4000 g mol^{-1}. Linear-chain PEM Nafion 117 has conductivity of 104 mS cm^{-1} in liquid water and at room temperature. Crosslinked PEMs with IEC of 1.74 meq g^{-1} show conductivity of 94-125 mS cm^{-1} that is comparatively better than that of Nafion 117 conductivity. We also confirmed that crosslinked PEMs with IEC above 1.74 meq g^{-1} demonstrate conductivity many times higher than that of Nafion 117 at any condition.

In another set of study, the high-MW crosslinker sPFPE (4000 g mol^{-1}) was combined with the low-MW crosslinker sPFPE (1000 g mol^{-1}) to improve the Young modulus in the membrane. Figure C.10 in Appendix C.10 shows the results of crosslinked PEMs conductivity in which the high and low MWs crosslinkers were combined. Independent of sPFPE (1000 g mol^{-1}) weight content, conductivity of such crosslinked PEMs increases with IEC and exhibits similar qualitative behavior as that of other PEMs shown in Table 4.3.5. However, at fixed IEC, conductivity increases almost linearly with decrease in the weight of sPFPE (1000 g mol^{-1}) due to enhanced crosslinking. It was observed that membranes with the low-MW crosslinker exhibit the smallest swelling, a beneficial feature for PEM fuel cells. On the other hand, membranes with the high-MW crosslinker exhibit the highest flexibility and reasonable swelling. The long chain in the high-MW crosslinker in combination with the short chain in the low-MW crosslinker yields membranes with sufficient flexibility, good stiffness and Young modulus that can meet the DMFCs challenges. Behavior of ionic conductivity from the combination of two crosslinkers assisted in selecting the composition for methanol permeability study.

4.3.6. Methanol Permeability and Selectivity

Crosslinked structures have distinct advantage over linear-chain structures in creating barrier to methanol transport across PEMs. For a given IEC, tortuous path and intricate barrier are expected to impede methanol crossover. Crosslinkable liquid precursor offers an excellent opportunity to fabricate membranes with variable acid loading and crosslink density from different MWs of the crosslinker. In DMFCs, the PEM must be a good conductor with reasonable ionic conductivity and a good barrier with low permeability. In liquid precursor approach, variable acid loading has been exploited to achieve reasonable conductivity as described in the previous section. The current section illustrates the results of crosslinked PEMs that are excellent barrier to methanol transport and have high selectivity (ratio of conductivity to permeability).

To the best of our knowledge, PEMs for DMFCs based on fluorinated and difunctional liquid precursors have rarely been reported. Conventionally, it has been challenging to develop PEMs that have both good conductivity and low permeability. In many examples, reduction in permeability across PEMs has been achieved with drastic reduction in conductivity resulting in limited improvement in DMFCs performance.

In our approach, acid loading and crosslink density were varied to fabricate PEMs with excellent barrier to methanol transport. Crosslinkers with six different MWs were incorporated to obtain variable crosslink density in order to reduce the methanol crossover. Methanol permeability was measured at room temperature with two-compartment diffusion cell at 1 mol/L methanol solution. At room temperature, we measured Nafion 117 conductivity of 104 mS cm^{-1} in liquid water and methanol permeability of 2.19×10^{-6} cm^2 sec^{-1}, which agree with literature.[45,46]

Due to crosslinking, any crosslinked PEM with IEC below 1.0 meq g^{-1} exhibits permeability lower than that of Nafion 117. The permeability increases slightly when IEC is increased from 1.0 to 1.74 meq g^{-1}. Despite increase in the permeability, these crosslinked PEMs demonstrate remarkable selectivity that is two to three times higher than that of Nafion 117. Selectivity that is ratio of conductivity to permeability was obtained from conductivity and permeability shown in Table (4.3.5). High selectivity (S cm^{-1}/cm^2 sec^{-1}) rather than only high conductivity or only low permeability is critical for PEMs to be effective in DMFCs.

For any MW of the crosslinker, the methanol permeability of crosslinked PEMs follows with IEC. For sPFPE 1000, permeability decreases from 1.48×10^{-6} to 4.07×10^{-7} cm^2 sec^{-1} because of decrease in IEC from 1.16 to 0.81 meq g^{-1}. This decrease in the permeability is remarkable and promising. Crosslinkers with other MWs reveal similar trend of decrease in permeability due to both crosslinking effect and acid loading (Table 4.3.6). Figure 4.3.6.1 shows the typical trend of conductivity and permeability against IEC in crosslinked PEMs for sPFPE (4000 g mol^{-1}). As expected, both conductivity and permeability increase with IEC due to increased charge-carrier concentration and its interaction. It is clear from Figure 4.3.6.1 that IEC can be adjusted to form membranes with target ionic conductivity and methanol permeability. Figure 4.3.6.1 also illustrates that membrane incorporating IEC higher than that of Nafion 117 can be obtained in which crosslinking creates structure that reduces permeability much lower than that of Nafion 117.

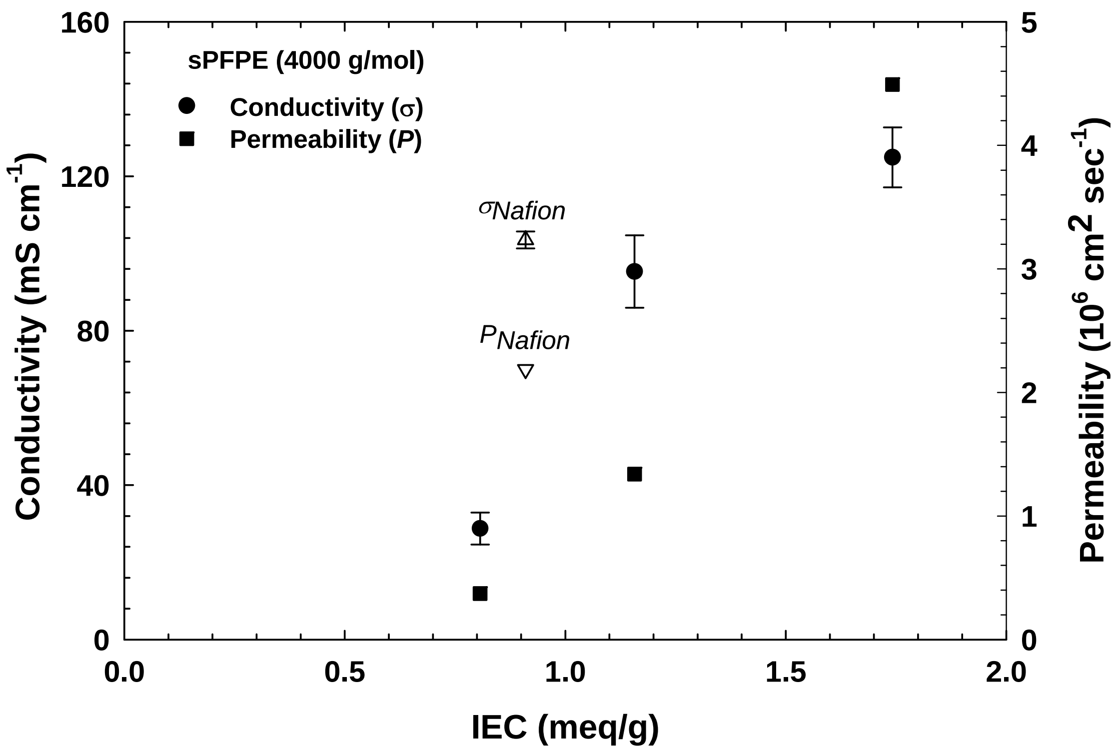

Figure 4.3.6.1. Crosslinked PEMs conductivity and permeability in liquid water and at room temperature.

In one set of study, effect of combination of two crosslinkers sPFPE (4000 g mol^{-1}) and (1000 g mol^{-1}) was studied on methanol permeability. It was found that crosslinking effect becomes more pronounced when the lowest MW crosslinker is combined with the highest MW crosslinker. At low IEC, methanol permeability decreases with increase in the weight of the lowest MW crosslinker due to strong crosslinking effect. At IEC of below 1.16 meq g^{-1}, crosslinked PEMs with combination of the two crosslinkers sPFPE (4000 g mol^{-1}) and (1000 g mol^{-1}) exhibit methanol permeability lower than that of Nafion 117. It is expected that these crosslinked PEMs would produce analogous effect on DMFCs performance. Another advantage of combination of two crosslinkers is reasonable flexibility from high MW and high Young modulus from low MW in the membrane. This combination provides good mechanical stability in these PEMs to meet the DMFCs challenges.

Figure 4.3.6.2 illustrates the selectivity of crosslinked PEMs and Nafion 117 membrane. It is obvious that the crosslinked PEMs have selectivity two to three times higher than that of Nafion 117. For example, selectivity increases from 7.12×10^4 to 1.05×10^5 to 1.36×10^5 S cm^{-1}/cm^2 sec^{-1} due to reduced permeabilities from increase in crosslink density from decreasing the MW from 4000 to 2000 to 1500 g mol^{-1}. Figure C.11 in Appendix C.11 shows the selectivities of additional crosslinked PEMs that are higher than that of Nafion 117. It is expected that this high selectivity in crosslinked PEMs can exhibit analogous effect on DMFCs performance.

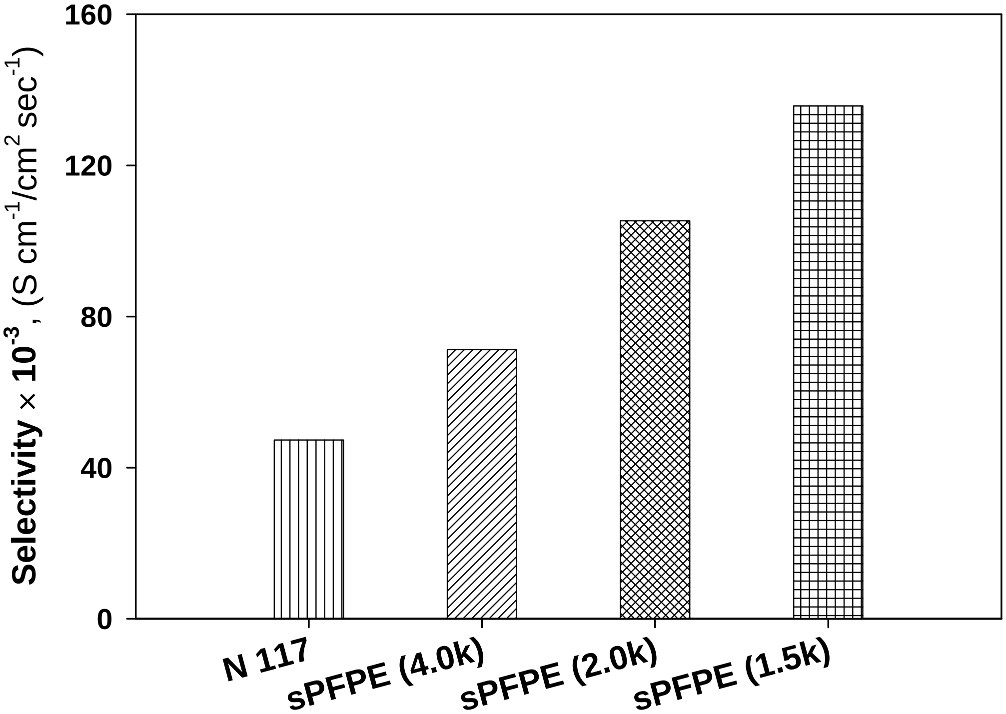

Figure 4.3.6.2. Crosslinked PEMs selectivity in liquid water and at room temperature.

Independent of PEMs composition, Figure 4.3.6.3 illustrates that increase in the conductivity is accompanied by increase in the permeability. For Figure 4.3.6.3, Table 4.3.5 provides the compositions of PEMs corresponding to conductivity and permeability. Ionic conductivity shows almost linear-variation with permeability. This trend suggests that methanol and ion-transport occur through common mechanism in which it is challenging to prefer ion transport to methanol transport. However, structure of the membrane plays critical role in ion-transport and solvent transport. From Figure 4.3.6.3, most of the crosslinked PEMs have lower permeability than that of Nafion 117. Due to their reasonable conductivities, these PEMs show promise to perform better than Nafion 117 because of their high selectivity. Although high selectivity is achieved with any conductivity and permeability, a good PEM must have both good conductivity at low permeability in order to perform better than Nafion 117 in DMFCs. Methanol permeability and conductivity results suggest that crosslinking approach has afforded such PEMs that can outperform Nafion 117.

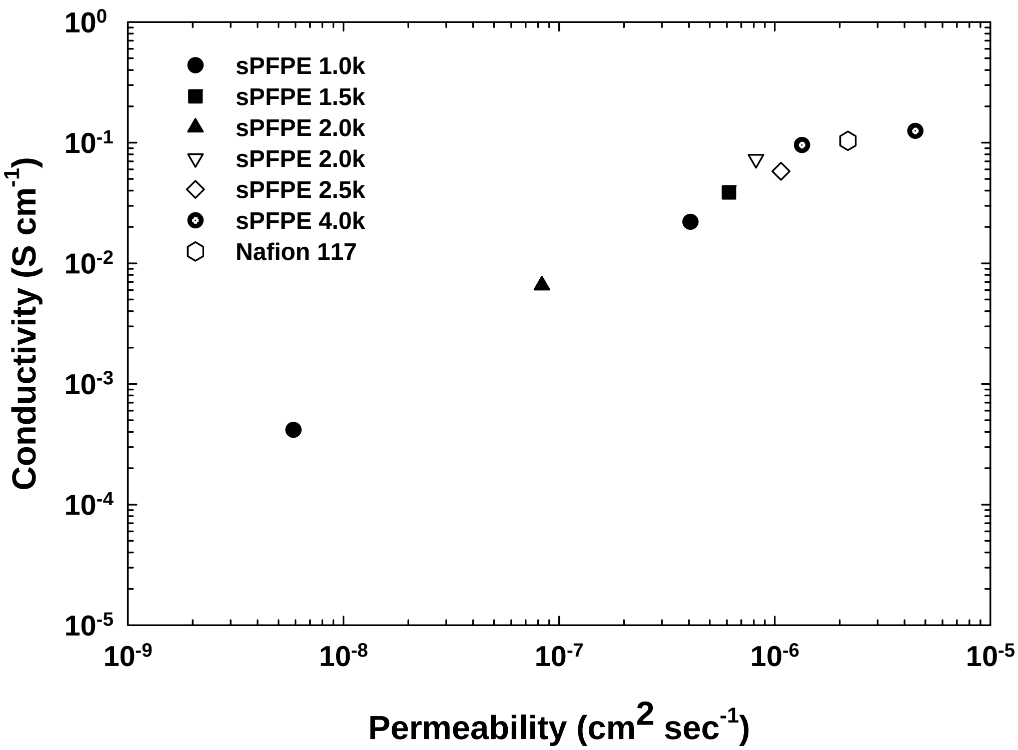

Figure 4.3.6.3. Crosslinked PEMs conductivity and permeability in liquid water and at room temperature. Table 4.3.5 provides the compositions of PEMs.

4.4. Summary

Novel fluoropolymers can be derived from commercially available PFPE diols by converting these diols into difunctional styrenyl-PFPE liquid precursors. Without use of solvent, possibilities exist to form many co-polymers of fluorocarbon and hydrocarbon by photocuring of liquid sPFPE in combination with other compatible co-monomers. For PEM fuel cells, crosslinker sPFPE and a comonomer R_f-SSE are chemically crosslinked to develop PEMs with variable acid content and crosslinked structures. In contrast to linear-chain structure, chemical crosslinking sustains and supports variable acid loading and crosslink density. Without chemical crosslinking, acid loading up to two times of Nafion 117 would result in hydrolytically unstable membrane.

For both hydrogen- and methanol-based fuel cells, acid loading and crosslinked structures from different sPFPE MWs can be adjusted to form PEMs with favorable properties. To improve the mechanical strength, combining low- and high-MW crosslinkers yields PEMs with reasonable flexural and compressive strengths. Acid loading and crosslink density can be tuned to achieve variable water uptake, ionic conductivity, and methanol permeability favorable to both hydrogen- and methanol-based fuel cells. For hydrogen-based fuel cells, crosslinked PEMs imbibe water two to three times more than that of Nafion 117 and exhibit conductivity three to four times higher than that of Nafion 117.

Chemical crosslinking provides the opportunity to develop PEMs with low-methanol permeability, reasonable conductivity and high selectivity. In comparison with linear-chain PEMs, difunctional crosslinker forms tortuous structure and intricate barrier that hinders methanol transport. It is envisioned that crosslink structure and intricate barrier disrupt the hydrophilic nano-channels formation and methanol crossover. At identical IEC, chemical crosslinking from liquid precursor has enables us to develop PEMs with selectivity higher, methanol permeability lower, and conductivity similar to that of Nafion 117. It is expected that high selectivity, low-methanol permeability and reasonable ionic conductivity can demonstrate an improved effect on the performance of DMFCs.

For a given IEC, incorporating low-MW crosslinker further reduces the methanol permeability without significant reduction in conductivity. Such low-methanol permeability without adding inorganic filler or methanol-inhibiting compounds are unrealistic. By chemical crosslinking, possibilities exist to incorporate high-acid loading and other methanol-inhibiting compounds to accomplish low permeability and high conductivity. In liquid precursor strategy, there are opportunities to prepare crosslinked PEMs directly in ionic form that can replace the traditional binder such as Nafion dispersion and hot-pressing step applied in MEA fabrication. Currently, MEA fabrication and performance evaluation of crosslinked PEMs in DMFCs are under investigation.

Acknowledgments: We gratefully acknowledge the financial support from Department of Energy (DOE) and National Science Foundation-Science and Technology Center (NSF-STC). Thanks are due to Dr. Keith Beck (Textile Engineering, Chemistry & Science, North Carolina State University, Raleigh, NC) for his assistance on methanol permeability experiment. We appreciate the generous contribution of Nafion membranes from DuPont.

North Carolina State University, Raleigh and UNC, Chapel Hill assisted in meeting the publication cost of this article.

4.5. References

1. X. Ren, M. S. Wilson, and S. Gottesfeld, *J. Electrochem. Soc.* **1996**, *143*, L12-L15.

2. S. J. C. Cleghorn, X. Ren, T. E. Springer, M. S. Wilson, C. Zawodzinski, T. A. Zawodzinski, and S. Gottesfeld, *Int. J. Hydrogen Energy* **1997**, *22*, 1137-1144.

3. F. Barbir and T. Gomez, *Int. J. Hydrogen Energy* **1996**, *21*, 891-901.

4. W. Grot, *Fluorinated Ionomers, PDL Fluorocarbon Series, William Andrew Publishing, New York*, **2008**.

5. M. W. Verbrugge, *J. Electrochem. Soc*. **1989**, *136*, 417-423.

6. K. Scott, W. M. Taama, P. Argyropoulos, and K. Sundmacher, *J. Power Sources* **1999**, *83*, 204-216.

7. S. Surampudi, S. R. Narayanan, E. Vamos, H. Frank, G. Halpert, A. LaConti, J. Kosek, G. K. Surya Prakash, and G. A. Olah. *J. Power Sources* **1994**, *47*, 377-385.

8. M. K. Ravikumar and A. K. Shukla, *J. Electrochem. Soc*. **1996**, *143*, 2601-2606.

9. S. P. Nunes, B. Ruffmann, E. Rikowski, S. Vetter, and K. Richau, *J. Membr. Sci*. **2002**, *203*, 215-225.

10. R. S. Yeo, *J. Appl. Polym. Sci*. **1986**, *32*, 5733-5741.

11. D. S. Kim, B. Liu, and M. D. Guiver, *Polymer* **2006**, *47*, 7871-7880.

12. K. Sasajima, H. Munakata, and K. Kanamura, *J. Electrochem. Soc*. **2008**, *155*, B143-B147.

13. M. K. Song, S. B. Park, Y. T. Kim, K. H. Kim, S. K. Min, and H. W. Rhee, *Electrochim. Acta* **2004**, *50*, 639-643.

14. M. K. Song, Y. M. Kim, Y. T. Kim, H. W. Rhee, A. Smirnova, N. M. Sammes, and J. M. Fenton, *J. Electrochem. Soc*. **2006**, *153*, A2239-A2244.

15. N. Miyake, J. S. Wainright, and R. F. Savinell, *J. Electrochem. Soc.* **2001**, *148*, A898-A904.

16. N. Miyake, J. S. Wainright, and R. F. Savinell, *J. Electrochem. Soc*. **2001**, *148*, A905-A909.

17. S. Panero, P. Fiorenza, M. A. Navarra, J. Romanowska, and B. Scrosati, *J. Electrochem. Soc*. **2005**, *152*, A2400-A2405.

18. W. Xu, C. Liu., X. Xue, Y. Su, Y. Lv, W. Xing, and T. Lu, *Solid State Ionics* **2004**, *171*, 121-127.

19. A. K. Sahu, G. Selvarani, S. Pitchumani, P. Sridhar, and A. K. Shukla, *J. Electrochem. Soc*. **2007**, *154*, B686-B695.

20. V. Baglio, A. S. Arico, A. D. Blasi, V. Antonucci, P. L. Antonucci, S. Licoccia, E. Traversa, and F. S. Fiory, *Electrochim. Acta* **2005**, *50*, 1241-1246.

21. Z. Liu, B. Guo, J. Huang, L. Hong, M. Han, and L. M. Gan. *Journal of Power Sources* **2006**, *157*, 207-211.

22. H. C. Kuan, C. S. Wu, C. Y. Chen, Z. Z. Yu, A. Dasari, and Y. W. Maib, *Electrochem. Solid State Letters* **2006**, *9*, A76-A79.

23. A. DEpifanio, B. Mecheri, E. Fabbri, A. Rainer, E. Traversa, and S. Licoccia, *J. Electrochem. Soc.* **2007**, *154*, B1148-B1151.

24. B. Libby, W. H. Smyrl, and E. L. Cussler, *Electrochem. Solid State Letters* **2001**, *4*, A197-A199.

25. C. W. Walker, Jr., *J. Electrochem. Soc*. **2004**, *151*, A1797-A1803.

26. C. S. Wu, F. Y. Lin, C. Y. Chen, and P. P. Chu, *J. Power Sources* **2006**, *160*, 1204-1210.

27. D. S. Kim, H. B. Park, J. W. Rhim, and Y. M. Lee, *Solid State Ionics* **2005**, *176*, 117-126.

28. D. S. Kim, H. B. Park, J. W. Rhim, and Y. M. Lee, *J. Membr. Sci.* **2004**, *240*, 37-48.

29. D. S. Kim, M. D. Guiver, S. Y. Nam, T. Yun, M. Y. Seo, S. J. Kim, H. S. Hwang, and J. W. Rhim, *J. Membr. Sci.* **2006**, *281*, 156-162.

30. G. G. Kumar, P. Uthirakumar, K. S. Nahma, and R. N. Elizabeth, *Solid State Ionics* **2009**, *180*, 282-287.

31. J. W. Rhim, H. B. Park, C. S. Lee, J. H. Jun, D. S. Kim, and Y. M. Lee, *J. Membr. Sci.* **2004**, *238*, 143-151.

32. J. C. Woong, S. Venkataramani, and S. C. Kim, *Polym. Int*. **2006**, *55*, 491-499.

33. C. H. Wang, C. C. Chen, H. C. Hsu, H. Y. Du, C. P. Chen, J. Y. Hwang, L. C. Chen, H. C. Shih, J. Stejskal, and K. H. Chen, *J. Power Sources* **2009**, *190*, 279-284.

34. B. Bae, H. Y. Ha, and D. Kim, *J. Electrochem. Soc*. **2005**, *152*, A1366-A1372.

35. Y. F. Huang, L. C. Chuang., A. M. Kannan, and C.W. Lin, *J. Power Sources* **2009**, *186*, 22-28.

36. S. Moravcova and K. Bouzek, *J. Electrochem. Soc*. **2005**, *152*, A2080-A2088.

37. Z. Zhou, R. N. Dominey, J. P. Rolland, B. W. Maynor, A. P. Pandya, and J. M. DeSimone, *J. Am. Chem. Soc*. **2006**, *128*, 12963-12972.

38. J. P. Rolland, R. M. V. Dam, D. A. Schorzman, S. R. Quake, and J. M. DeSimone, *J. Am. Chem. Soc*. **2004**, *126*, 2322-2323.

39. T. Ishizone, J. Tsuchiya, A. Hirao, and S. Nakahama, *Macromolecules* **1992**, *25*, 4840-4847.

40. R. Yadav and P. S. Fedkiw, *J. Electrochem. Soc*. **2010**, publication in progress.

41. J. Crank, *Clarendon Press, Oxford* **1975**, Second Edition, Chapter 4, p 51.

42. W. R. Vieth, *Oxford University Press, New York* **1991**, Chapter 2, p 21.

43. J. Comyn, *Elsevier Applied Science Publishers, New York* **1985**, Chapter 1, p 4.

44. P. Neogi, *Marcel Dekker, New York* **1996**, Chapter 4, p 175.

45. T. A. Zawodzinski, C. Derouin, S. Radzinski, R. J. Sherman, V. T. Smith, T. E. Springer, and S. Gottesfeld, *J. Electrochem. Soc*. **1993***, 140*, 1041-1047.

46. B. S. Pivovar, Y. Wang and E. L. Cussler, *J. Membr. Sci*. **1999**, *154*, 155-162.

CHAPTER 5

Chemically Crosslinked Anion Exchange Membranes from Photocuring of Fluorinated Liquid Precursor and Ionic Comonomer

Rameshwar Yadav[†], Peter S. Fedkiw[†], and Joseph M. DeSimone[†, §]

[†]North Carolina State University, Raleigh, NC, USA
[§]University of North Carolina, Chapel Hill, NC, USA

Abstract

Attractive features of alkaline fuel cells (AFCs) such as better water management and use of inexpensive non-noble metals electrocatalysts relative to traditional polymer electrolyte membrane (PEM) fuel cells have attracted interest in developing anion exchange membranes (AEMs) that have many advantages over liquid alkaline electrolytes. To date, lack of suitable AEMs analogous to traditional PEMs exists for AFCs. In response to lack of such AEMs, we have developed crosslinked AEMs directly in ionic form from chemical crosslinking of styrene-perfluoropolyethers (sPFPE) and 4-vinylbenzyl trimethyl chloride solution through UV-light initiated free-radical bulk polymerization at mild conditions. Crosslinked AEMs conductivity of 45 mS cm^{-1} in liquid water and at room temperature exemplifies the promising potentials of these AEMs for future AFCs. Success of our chemical crosslinking approach for PEMs reaffirms that the chemical crosslinking of sPFPE and 4-vinylbenzyl trimethyl chloride can produce AEMs with unprecedented level of anionic ion exchnage capacity, high conductivity and low-methanol permeability for the next generation AFCs.

5.1. Alkaline Fuel Cells

Alkaline fuel cells (AFCs) are electrochemical power devices that convert chemical energy of fuels directly into electricity efficiently. Like traditional polymer electrolyte membrane (PEM) fuel cells, the thermodynamic reversible potential of an oxygen-hydrogen AFC is 1.23 V and theoretical conversion efficiency is 83% at 25 °C.[1] Attractive features of AFCs have revived interest in a basic development of solid polymer electrolytes that have several distinct advantages over its liquid counterparts.[2] In AFCs, the electrochemical half-cell reactions involve electro-oxidization of fuels at the anode and electro-reduction of oxygen at the cathode. AFCs are low-temperature fuel cells (< 200 °C) in which hydroxyl ion (OH^-) is the charge carrier that migrates from the cathode to the anode through an alkaline electrolyte.[1,3]

Both AFCs and traditional PEM fuel cells have many features in common such as current collector, bipolar plate, gas diffusion layer, reactants supply systems, and other peripheral components. Due to relatively mild corrosion of bipolar plates in alkaline media, cheaper metals such as nickel can be used in bipolar plates and current collector.[4,5] The gas diffusion layer prevents the leakage of electrolytes in case of liquid electrolytes while distributing the reactants to the electrodes.[5]

Due to the alkaline electrolyte that is maintained at high pH, electro-reduction of oxygen is facile allowing the use of inexpensive non-noble metals and metal oxides electrocatalysts such as Ni at the anode and Ag at the cathode.[4,6-10] Both Ni and Ag are more stable in alkaline media than in acidic media.[11] Use of these electrocatalysts produces performances comparable to Pt/C electrocatalyst in PEM fuel cells.[5] Electrocatalytic study has shown that cathode containing 4 mg cm^{-2} of Ag/C produces equivalent performance of 0.5 mg cm^{-2} of Pt/C in alkaline fuel cells.[8] However, in AFCs, oxygen reduction rate is still less facile than the hydrogen oxidation rate. AFCs can operate on hydrogen as well as on liquid fuels, such as methanol, ethanol, ethylene glycol, and glycerol. Electro-oxidation of methanol is more facile, and electro-kinetically faster in alkaline media than in acidic media due to favorable condition.[3,4,7,12-16]

AFCs have distinct advantages in water management through water migration from the anode where electro-oxidation of fuels generates water to the cathode where electro-reduction consumes water.[4,7,17] This water migration reduces the water flooding at the cathode that commonly occurs in PEM fuel cells. Efficient water transport maintains sufficient hydration without external humidification and enhances the conductivity in the AFC electrolyte.[18]

Traditionally, AFCs operate on liquid KOH solution electrolyte that suffers from several challenges that have restricted AFCs application mostly in space research efforts. However, research opportunity exists to combine the beneficial features of both AFCs and PEM fuel cells to develop the next generation power devices using anion exchange membranes.

5.2. Anion Exchange Membrane

The challenges associated with liquid alkaline electrolyte have led to the development of anion exchange membranes (AEMs) that have gained fundamental importance because of enhanced performance in AFCs. For comparative performance of AFCs, it is critical to develop AEMs with properties equivalent to PEMs. Conventionally, AFCs operate on liquid alkaline electrolytes that are circulatory or KOH solution (30-40 wt%) stabilized in a porous matrix (hazardous asbestos).[1,2,5,19] Circulatory electrolytes give advantage of good thermal and water management, easy replacement and CO_2 removal.[2] Liquid electrolytes poses water management challenge at the electrodes and long-term electrode durability in highly caustic environment.[5]

These liquid alkaline electrolytes often deteriorate due to carbonate/bicarbonate (CO_3^{2-}/HCO_3^-) formation from acidic CO_2 uptake in alkaline media. Liquid AFCs operating on organic fuels face severe and acute carbonate formation problem. Mobile metal carbonate (K_2CO_3) crystals fill the support pores and diminish the electrolyte conductivity.[7,20] At the cathode, carbonate precipitation creates mass transfer limitations.[1,4,7,21] Reduction in ionic conductivity and cathode blockage gradually degrade the AFC performance.[21] Degradation of binder used in electrode fabrication causes electrolyte weeping.

In methanol-based AFCs, CO_2 generation from electro-oxidation of methanol augments the carbonate precipitation leading to a more severe problem in liquid electrolyte. CO_2 that is acidic reduces pH of the electrolyte leading to decrease in electro-chemical reactivity of methanol.[14] Liquid alkaline electrolytes are corrosive, have limited conductivity, are difficult to handle, are cumbersome to maintain, and exhibit poor performance in AFCs.

AEMs possess several distinct advantages over liquid alkaline electrolytes. These membranes have fixed cationic charges, which permit efficient anion transport. In AEMs, low CO_2 solubility and immobilized cations diminish the carbonate precipitation relative to free carbonates in liquid alkaline electrolyte. AEMs have good conductivity, chemical resistance, and mechanical strength to serve as a separator between the fuel and the oxidant. Simplicity in selection and design because of polymeric materials offers many variables to maximize the AEM properties. Ability to control the thicknesses of membrane allows membrane electrode assembly (MEA) fabrication with optimum properties that is not feasible with liquid alkaline electrolytes. Unlike liquid electrolyte in which electrolyte weeping and corrosion occurs aggressively, AEMs can minimize such challenges due to solid nature. AEM have shown to prolong the performance of AFC. Table 5.2 shows the key differences between solid polymer and liquid alkaline electrolytes. Ionic conductivity of AEMs are expected to be lower than that of PEMs because protons (H^+) have two times higher mobility than the hydroxyl ions ($H^+ = 3.625 \times 10^{-3}$, $OH^- = 2.05 \times 10^{-3}$ $cm^2\ sec^{-1}\ V^{-1}$).[22,23] In addition, protons have two times higher diffusion coefficient than hydroxyl ions.

Table 5.2 Comparison of Solid Polymer and Liquid Alkaline Electrolytes	
Solid Polymer Electrolytes	**Liquid Electrolytes**
Immobile cation	Mobile cation
No carbonate precipitation at the cathode	Carbonate precipitation at the cathode
Selectivity of polymer materials	No selectivity
Good mechanical separator	Poor separator due to support requirement
Easy to maintain	Cumbersome to maintain
Light weight	Heavy weight
Choice of thickness in MEA fabrication	Limited choice
Low corrosion	Severe corrosion
No electrolyte weeping	Electrolyte weeping

Due to the low solubility of methanol in AEMs[7,22] and an electro-osmotic drag in the opposite direction to the methanol flux[4,17], AEMs are intrinsically better barriers than the traditional PEMs to the methanol transport with 30% lower methanol crossover. Polar solvent uptake study has shown that AEMs have lower solvent uptake and permeabilities relative to Nafion 115 membrane.[22] This methanol crossover can enable a membrane electrode assembly (MEA) with low-membrane thickness resulting in low-ohmic losses. One more advantage of AEM is that these membranes are also suitable for carbonate fuel cells in which O_2 is electro-reduced with CO_2 at the cathode.[24]

The widely perceived problem with AEM is low conductivity. Most of reported AEMs have exhibited conductivity lower than of traditional PEMs.[7] Lack of a suitable binder has curtailed the fabrication of MEA that can produce optimum performance. Generally, KOH solution is added in the fuel stream to serve as ionic interface at the electrode. However, it is essential that no metal cations are present where CO_2 is generated or present in fuel and oxidant such as air otherwise traditional KOH problem will persist.[25]

5.3. Existing Anion Exchange Membranes

AEMs have been reported by others are those of radiation-grafting of vinylbenzyl chloride onto base films such as poly(vinylidene fluoride) (PVDF) and fluorinated poly(tetrafluoroethylene-*co*-hexafluoropropylene) (FEP) and poly(ethylene-*co*-tetrafluoroethylene) (ETPE). These membranes lack mechanical strength and ionic conductivity that are comparable with acidic membranes. The lack of anionic dispersion for MEA fabrication also compromises the full benefits of these AEMs.

Radiation-grafting is an economical way to produce affordable AEMs because preformed films are inexpensive and can be customized to suit the application. The grafting of reactive vinylbenzyl chloride (VBC) onto fluoropolymers films such as FEP, PVDF, and ETFE followed by amination in aqueous trimethylamine and ion-exchnage with aqueous KOH yields affordable membranes with good properties. Figure 5.3 shows the synthesis steps of such radiation-grafted AEMs.

Danks *et al*. prepared AEM from radiation-grafting of PVDF with vinylbenzyl chloride (VBC).[26] After amination with aqueous trimethyl amine and ion-exchange with KOH, PVDF-derived AEM turned dark brown indicating chemical degradation of the membrane and had lower IEC than expected from 54% of degree of grafting. It was observed that backbone degradation had occurred due to high grafting and alkali immersion exaggerated this degradation. It was concluded that PVDF-derived membrane lacks chemical resistance due to amination and ion-exchange with hydroxide.

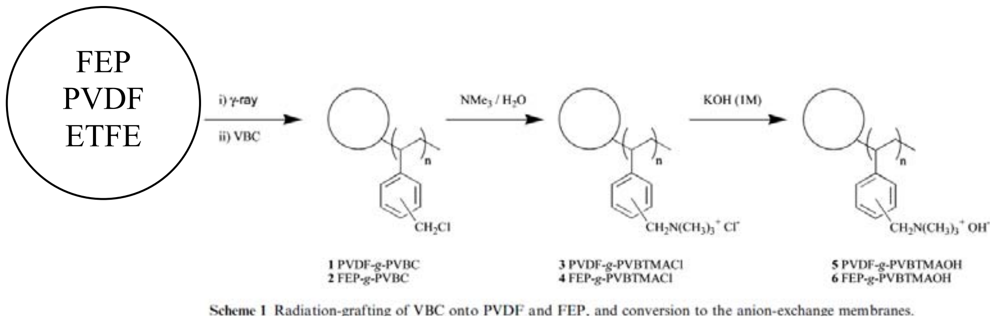

(a)

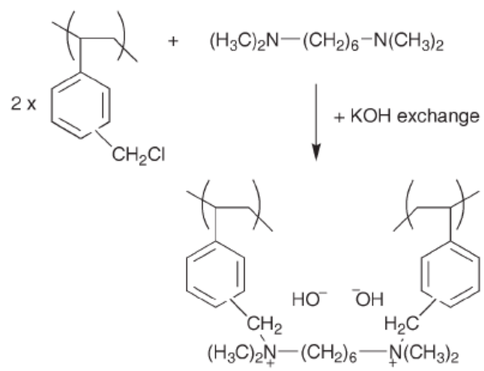

(b)

Figure 5.3. (a) Radiation-grafting of vinylbenzyl chloride onto FEP, PVDF, and ETFE followed by amination and ion-exchange into AEMs.[17] (b) Electrode binder.[27]

Slade *et al*. demonstrated AEM derived from radiation-grafting of FEP with vinyl benzyl chloride followed by amination and ion-exchange, These membranes showed conductivity of 23 mS cm^{-1} in liquid water and at 50 °C.[3] They also reported OH^- activation energy of 12.6 ± 0.6 kJ mol^{-1} that is twice the value of proton conduction in Nafion 115. It was found that OH^- migration has stronger temperature-dependence than H^+. Radiation-grafting of FEP produced more stable polymer than PVDF because of C-H backbone in PVDF is vulnerable to chemical degradation due to dehydrofluorination. For 20-26% degree of grafting, IEC of 0.92 to 1.10 meq/g was obtained in these AEMs. Ionic conductivity was 23 mS cm^{-1} in liquid water and at 50 °C that was 20% of Nafion 115 conductivity. However, the hydration number in AEM was 28 that was higher than that of Nafion 115 (22).

Varcoe *et al*. reported AEMs derived from radiation-grafting of poly(ethylene-*co*-tetrafluoroethylene) (ETFE) followed by amination in 50 wt% aqueous trimethylamine (Figure 5.3.2).[17] The optimum grafting level was disclosed to be 24% because any grafting level below 20% led to low-ionic conductivity and above 30% rendered the membrane brittle. These AEMs showed conductivity of 34 mS cm^{-1} in liquid water at 50 °C.[17] Conductivity from 25 to 55 °C was essentially independent of temperature in these AEMs. In contrast, Nafion 115 showed increasing trend of conductivity with temperature. Conversion of AEMs from OH^- to CO_3^{2-} increased the activation energy from 6.2 ± 2.4 to 16.1 ± 0.4 kJ mol^{-1}. Pure methanol and water uptake study showed that AEM absorbed less methanol (30 wt%) than water (40 wt%), where as Nafion 115 absorbed more methanol (71 wt%) than water (36 wt%). Consistently, methanol permeability across AEM was lower ($5.4 \pm 2.8 \times 10^{-7}$ cm^2 sec^{-1}) than that of Nafion 115 ($19 \pm 9 \times 10^{-7}$ cm^2 sec^{-1}).

Electrode binders are required to be insoluble in aqueous media and in polar fuel such as methanol. In addition, the binder must be a good ion conductor such as OH^- conductor for AFCs. Varcoe *et al*. obtained a binder that was based on crosslinking of poly(vinylbenzyl chloride) with a diamine.[27] Figure 5.3 (b) shows the chemical structure of this binder. To date, there is a lack of Nafion dispersion analog that can serve as an electrode binder to fabricate and produce high performance MEA for AFCs. Aqueous KOH is added to fuel stream to improve the ion transport at the electrode. However, free K^+ cation leads to the carbonate formation and lowers the AFC performance.

5.4. Chemically Crosslinked Anion Exchange Membranes

An AEM that can be formed from fluorinated liquids and an ionic co-monomer using simple photocuring methods could be an ideal candidate for future MEA fabrication without using traditional binder like Nafion dispersion. This work presents a novel approach to prepare crosslinked AEMs in response to various drawbacks and poor performance of liquid alkaline electrolytes. Through simple synthesis steps, the mixture of a di-functional crosslinker and an ionic comonomer have been converted into solid AEMs through photo-polymerization at mild conditions. This approach has benefits of reducing the processing steps and time to a minimum. Membrane fabrication directly in the ionic form is another advantage of this approach. It is known that OH^- has lower diffusion coefficient than that of H^+.[28] In order to achieve high ionic conductivity, it is essential to maximize the loading of anionic IEC.[4] Crosslinking can enable such high IEC loading as it has already been demonstrated in crosslinked acidic PEMs (Chapter 4).

5.4.1. Synthesis of Chemically Crosslinked AEMs

Crosslinked anion exchange membranes were formed from a fluorinated liquid crosslinker and 4-vinylbenzyl trimethyl ammonium chloride through UV-light initiated free-radical bulk polymerization. The reaction involves styrene-functionalization of PFPE diols with 4-vinylbenzyl chloride to yield a styrene-functionalized perfluoropolyether (sPFPE) that is a difunctionalized, highly fluorinated, and curable. The sPFPE is a fluorinated liquid with low-surface energy (24 dyne/cm at 20 °C), which assists in the easy fabrication of membranes. The comonomer 4-vinylbenzyl trimethyl ammonium chloride is immiscible with sPFPE because the comonomer is a hydrocarbon and ionic, and sPFPE is fluorinated and non-ionic. To form a crosslinked membrane, both sPFPE and 4-vinylbenzyl trimethyl ammonium chloride along with 1 wt% α,α-diethoxyacetophenone photoinitiator were dissolved in the solvent 3,3,4,4,5,5,6,6,7,7,8,8,8-Tridecafluoro-1-octanol at 70 °C in order to obtain a clear, homogeneous and transparent solution. The comonomer 4-vinylbenzyl trimethyl ammonium chloride was selected due to its good stability in alkaline media.[4,29]

Photocuring of the solution with UV-light exposure (λ = 365 nm) for 10 minutes under continuous N_2 gas purge produced crosslinked AEMs in chloride ion (Cl^{-1}) form. Residual solvent was removed from the crosslinked AEMs under vacuum-drying. After solvent removal, clear and transparent membranes were peeled off gently from the template. Ion-exchange with 1 mol/L KOH solution at room temperature converted immobilized benzyl trimethyl ammonium chloride to corresponding hydroxide. Figure 5.4.1 shows the preparation steps and structure of crosslinked AEMs.

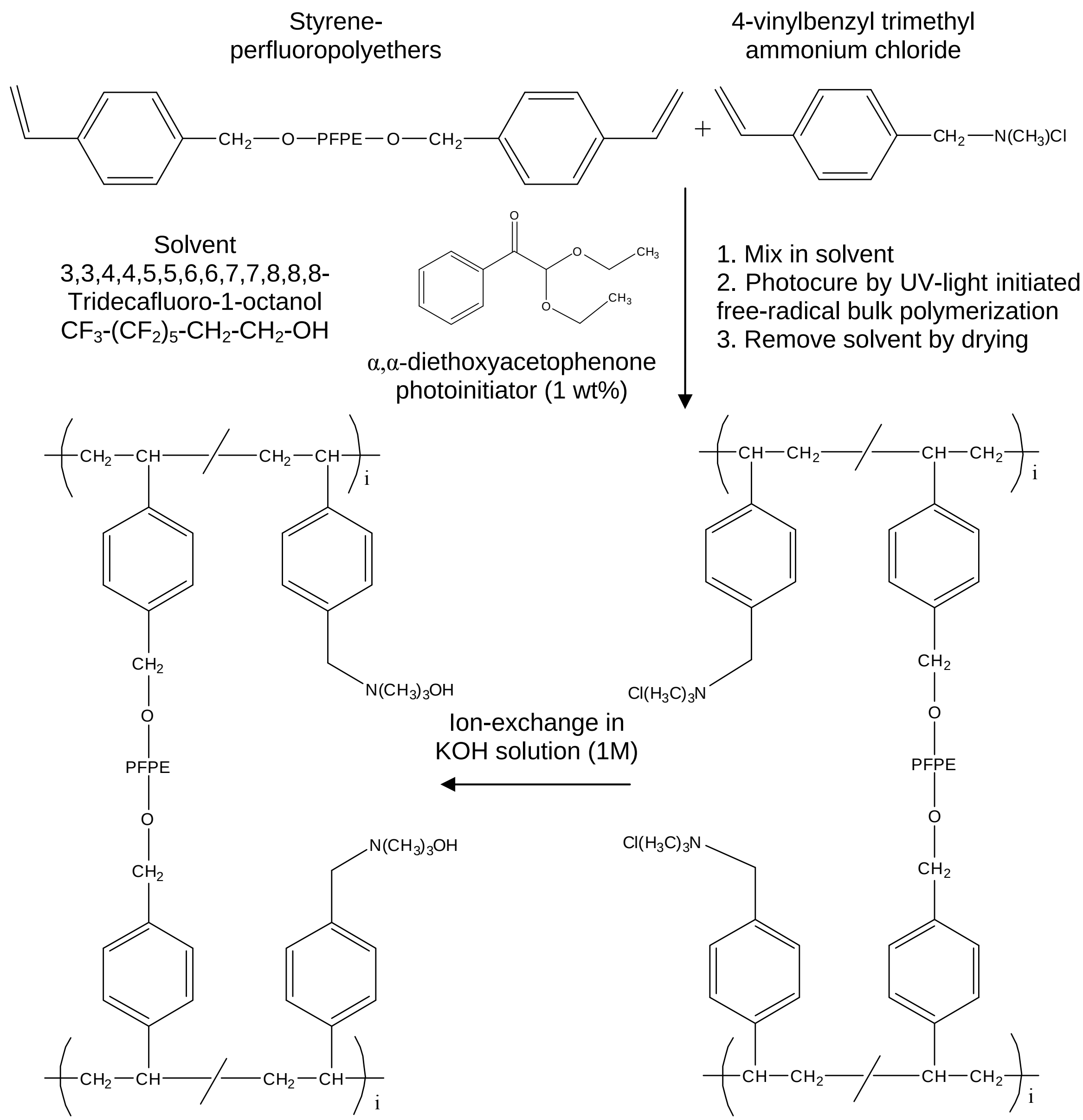

Figure 5.4.1. Synthesis steps of chemically crosslinked anion exchange membrane.

Initially, PFPE diols with MW (4000 g mol^{-1}) was used to synthesize sPFPE and fabricate crosslinked AEMs. Another liquid comonomer *N, N*-dimethyl vinylbenzyl diamine can also be copolymerized to form AEMs following protocols shown in Figure 5.4.1. This liquid comonomer is expected to be miscible with sPFPE at low solvent.

Analogous to acidic crosslinked PEMs that have acid loading from 0.46 to 1.84 meq g^{-1}, it is expected that these crosslinked AEMs can contain high anionic IEC due to crosslinked structure. Figure 5.4.2 shows IEC as function of 4-vinylbenzyl trimethyl ammonium chloride weight. IEC shown in Figure 5.4.2 was obtained from stoichiometry and composition of AEMs. Depending on the mechanical stability, IEC in crosslinked AEMs can exceed that of other reported AEMs. To accomplish maximum IEC, it would be necessary to optimize the concentration of the sPFPE/4-vinylbenzyl trimethyl ammonium chloride solution.

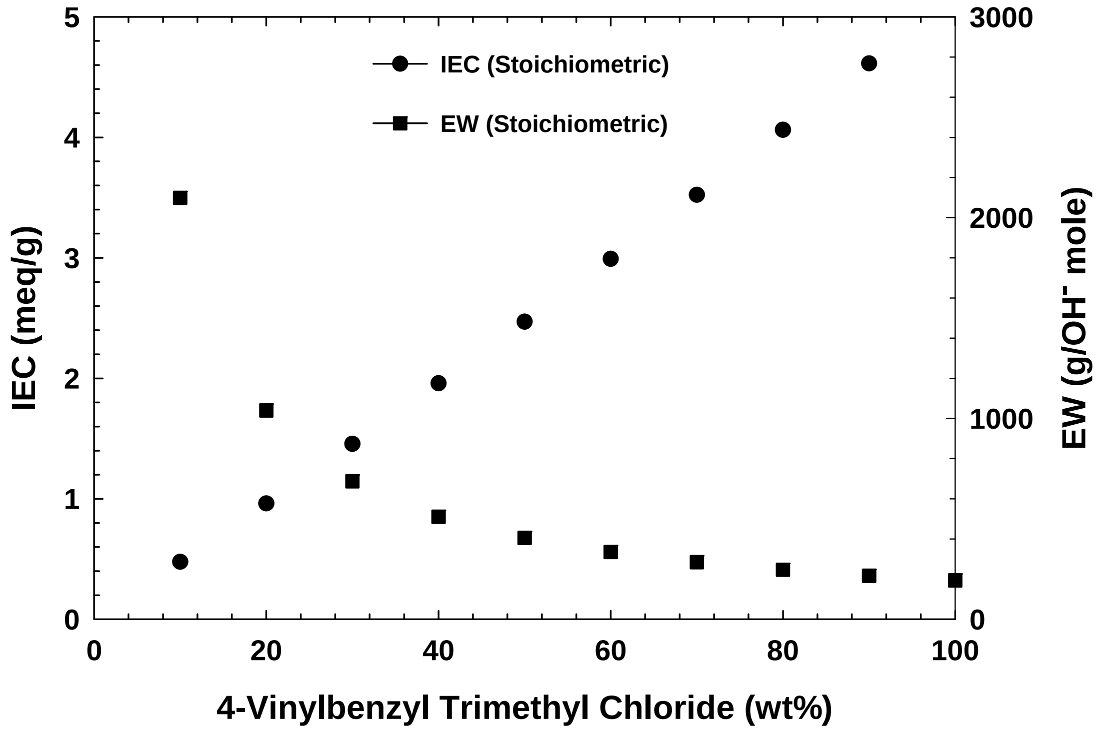

Figure 5.4.2. Crosslinked AEMs IEC and EW as function of 4-vinylbenzyl trimethyl chloride weight.

5.5. Advantages of Crosslinked AEMs

Crosslinked AEMs have immobilized cations that reduce the mobile carbonate precipitation. Immobilized cations promote efficient transport of anions across the AEM. Due to fluorinated segment in PFPE, these crosslinked AEMs are expected to have good chemical resistance in alkaline media. Such chemical resistance is necessary for durability of AEMs. In addition to offering chemical resistance, fluorinated segment in PFPE is expected to contribute hydrophilic-hydrophobic phase separation that is essential for efficient ion transport. Chemical crosslinking prevents dissolution of the membrane and can enable substantial amount of anionic IEC leading to many favorable properties in these AEMs. Unprecedented level of IEC, water uptake and conductivity can be realized in these crosslinked AEMs. Variable crosslink density from different MWs of sPFPE can impart good mechanical strength to these AEMs. Due to crosslink structure and fluorine content, these AEMs can meet the thermal stability requirement of AFCs as acidic crosslinked PEMs based on PFPE have demonstrated (Chapter 4).

This section provides initial results of crosslinked AEMs without any optimization in composition and synthesis condition. Initially, crosslinked AEMs have been fabricated to confirm the miscibility and subsequent photocuring of 4-vinylbenzyl trimethyl ammonium chloride with sPFPE. Both sPFPE and ionic comonomer are miscible in partly fluorinated solvent and form a clear solution. Preliminary result on ionic conductivity (45 mS cm^{-1} in liquid water and at room temperature at IEC of 1.43 meq g^{-1}) suggests that these AEM have good and promising properties. Such high-ionic conductivity is comparable with traditional

PEMs. To achieve the full benefits of crosslinking in AEM, anionic IEC needs to be increased, solvent concentration and polymerization condition needs to be optimized, and dimensions of AEM needs to be controlled in order to obtain the target AEM.

Currently, there is a lack of ionomer dispersion analogous to traditional Nafion dispersion for MEA fabrication.[4] Crosslinking of ionic sPFPE/4-vinylbenzyl trimethyl chloride solution circumvents the requirement of an ionomer dispersion and hot-processing. Scheme 1 shows the steps to fabricate MEA without such requirements. Due to fabrication of the membrane directly in ionic form, MEA fabrication by thermal polymerization of the sPFPE/4-vinylbenzyl trimethyl chloride solution that can be sandwiched between the anode and cathode containing gas diffusion layers (GDLs) eliminates the requirement of traditional dispersion and hot-pressing while retaining the integrity of AEMs. It is hoped that MEA fabrication by Scheme 1 can transform the whole construction of AFC and address the associated challenges.

In Scheme 1, solvent removal after thermal polymerization could be challenging. However, porous electrode/GDL system can allow solvent removal upon heating. The other route to form MEA can be photocuring of sPFPE/4-vinylbenzyl trimethyl chloride solution on top of the one electrode/GDL and subsequent bonding of the other electrode/GDL.

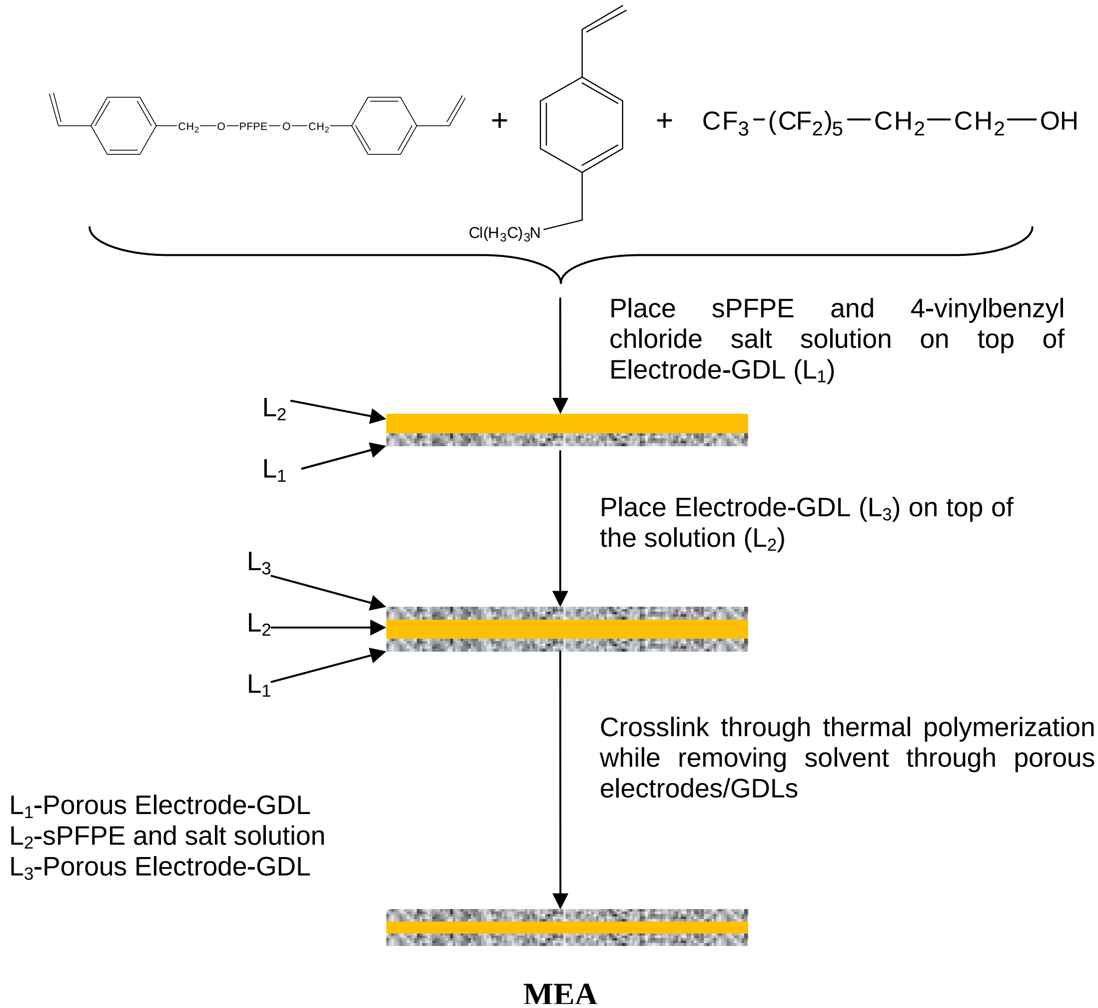

Scheme 1. Alkaline MEA fabrication directly in ionic form without using any dispersion.

Photocuring can also enable MEA fabrication from catalyst dispersion in which electrocatalysts can be mixed with sPFPE/4-vinylbenzyl trimethyl chloride solution to form a dispersion. Layer-by-layer approach in which Layer 1 is catalyst dispersion for one electrode/GDL, Layer 2 is sufficient sPFPE/4-vinylbenzyl trimethyl chloride solution for the membrane, and Layer 3 is the catalyst dispersion for the other electrode/GDL followed by photocuring of all the three layers L1-L2-L3 together can produce MEA without any binder and hot-processing.

Scheme 2 illustrates an approach to fabricate hybrid membranes for self-humidification of MEA. Hybrid membranes are another type of electrolyte in which acidic membrane and alkaline membranes are bonded together to create junction for water generation. It is envisioned that photocuring of liquid precursor with acidic comonomer and alkaline comonomer through layer-by-layer method can yield hybrid membrane. This hybrid approach can produce gradient of pH in the MEA that is favorable to electrokinetics in fuel cells.

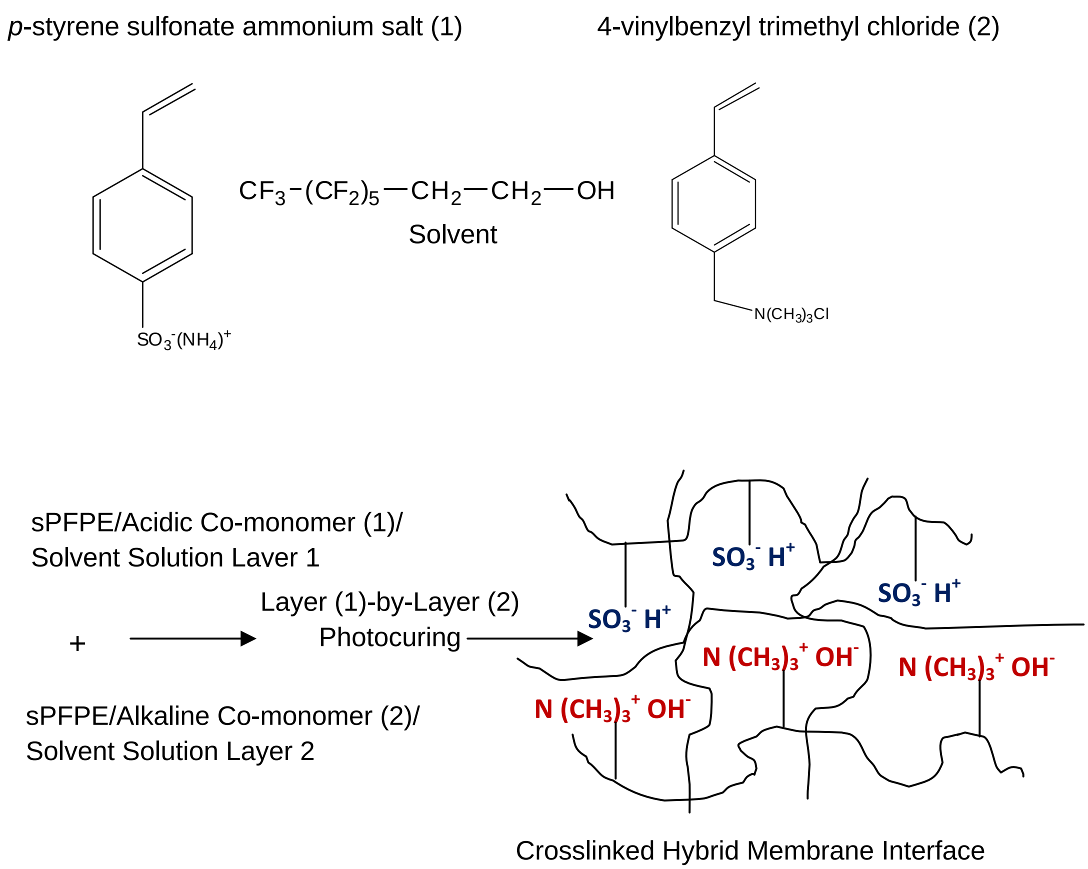

Scheme 2. Hybrid crosslinked membrane fabrication.

Scheme 3 shows the application of electric field during polymerization of sPFPE and 4-vinylbenzyl trimethyl ammonium chloride to induce chaining in through-plane direction in order to improve the conductivity for a given IEC. Membrane fabrication from the solution of styrene-perfluoropolyether (sPFPE) and 4-vinylbenzyl trimethyl chloride offers another opportunity to improve the ionic conductivity for a given IEC by aligning the ionic domain in through-plane direction with polymerization under electric field.

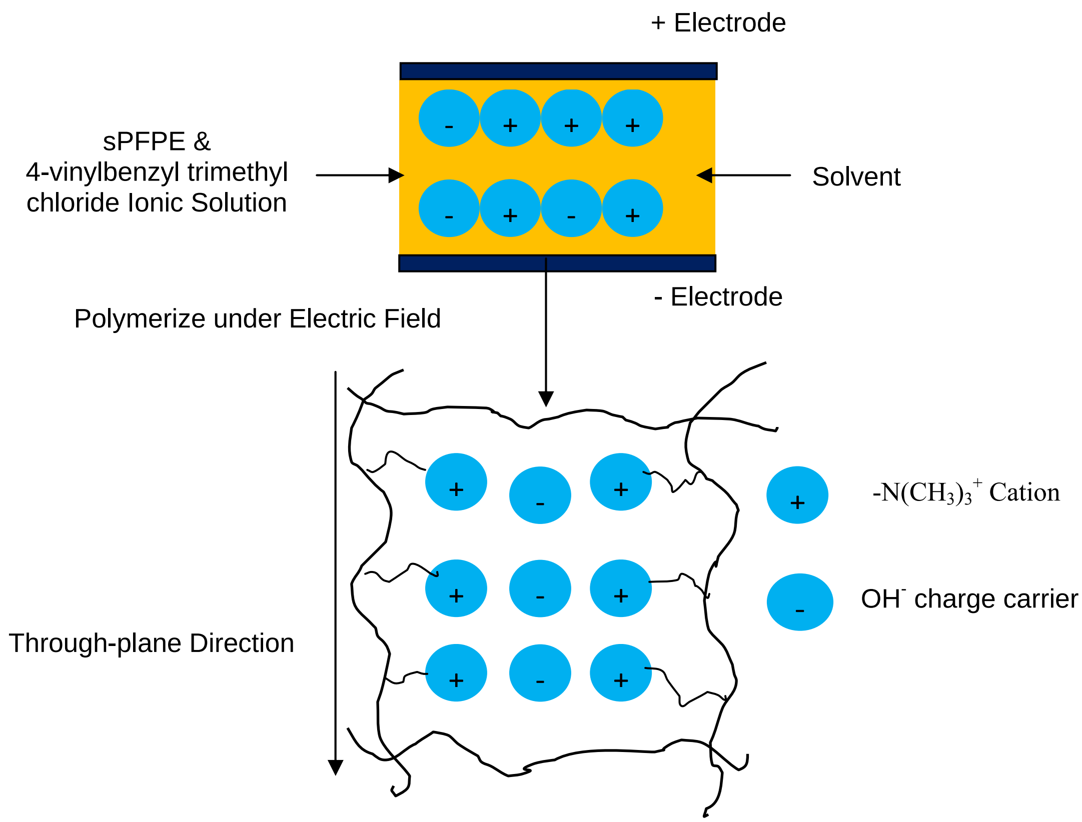

Scheme 3. Electric field aligned crosslinked anion exchange membrane.

5.6. Summary

A novel approach has been presented to fabricate crosslinked AEMs in ionic form from fluorinated liquid crosslinker sPFPE and 4-vinylbenzyl trimethyl ammonium chloride. Conductivity results have shown that these AEMs can be potentially competitive with traditional PEMs. We envision that these crosslinked AEMs can sustain and support unprecedented level of anionic IEC and conductivity that can potentially transform the AFC performance. Methanol crossover rate is expected to be low due to alkaline media and crosslinked structure in AEM.

5.7. References

1. E. Gulzow, *J. Power Sources* **1996**, *61*, 99-104.

2. K. Kordesch, V. Hacker, J. Gsellmann, M. Cifrain, G. Faleschini, P. Enzinger, R. Fankhauser, M. Ortner, M. Muhr, and R. R. Aronson, *J. Power Sources* **2000**, *86*, 162–165.

3. R. C. T. Slade and J. R. Varcoe, *Solid State Ionics* **2005**, *176*, 585-597.

4. J. R. Varcoe and R. C. T. Slade, *Fuel Cells* **2005**, *5*, 187-200.

5. F. Bidault, D. J. L. Brett, P. H. Middleton, and N. P. Brandona *J. Power Sources*, **2009**, *187*, 39-48.

6. C. Coutanceau, L. Demarconnay, C. Lamy, and J. M. Leger, *J. Power Sources* **2006**, *156*, 14-19.

7. E. Antolini and E. R. Gonzalez, *J. Power Sources* **2010**, *195*, 3431–3450.

8. J. R. Varcoe, R. C. T. Slade, G. L. Wright, and Y. Chen *J. Phys. Chem. B*, **2006**, *110*, 21041-21049.

9. K. Kinoshita, Electrochemical Oxygen Technology, *John Wiley & Sons Inc.* **1992**, Chapter 2.

10. N. Wagner, M. Schultze and E. Gülzow, *J. Power Sources* **2004**, *127*, 264–272.

11. L. Li and Y. Wang, *J. Membr. Sci.*, **2005** *262*, 1-4.

12. E. H. Yu and K. Scott, *J. Power Sources* **2004**, *137*, 248-256.

13. R. Parsons and T. VanderNoot, *J. Electroanal. Chem.* **1988**, *257*, 9-45.

14. K. Matsuoka, Y. Iriyama, T. Abe, M. Matsuoka, and Z. Ogumi, *J. Power Sources* **2005**, *150*, 27-31.

15. K. Asazawa, T. Sakamoto, S. Yamaguchi, K. Yamada, H. Fujikawa, H. Tanaka, and K. Oguro, *J. Electrochem. Soc.* **2009**, *156*, B509-B512.

16. A. V. Tripkovic, K. D. Popovic, B. N. Grgur, B. Blizanac, P. N. Ross, and N. M. Markovic, *Electrochim. Acta*, **2002**, *47*, 3707-3714.

17. J. R. Varcoe, R. C. T. Slade, E. L. H. Yee, S. D. Poynton, D. J. Driscoll, and D. C. Apperley, *Chem. Mater.*, **2007**, *19*, 2686-2693.

18. E. Gulzow, M. Schultze, and U. Gerke, *J. Power Sources*, **2006**, *156*, 1-7.

19. P. Gouérec, L. Poletto, J. Denizot, E. S. Cortezon, and J. H. Miners, *J. Power Sources*, **2004**, *129*, 193–204.

20. F. R. Brushett, W. P. Zhou, R. S. Jayashree, and P. J. A. Kenis, *J. Electrochem. Soc.*, **2009**, *156*, B565-B571.

21. G. F. McLean, T. Niet, S. Prince-Richard, and N. Djilali, *Int. J. Hydrogen Energy*, **2002**, *27*, 507-526.

22. J. R. Varcoe, R. C. T. Slade, E. L. H. Yee, S. D. Poynton, and D. J. Driscoll, *J. Power Sources*, **2007**, *173*, 194-199.

23. D. Stoica, F. Alloin, S. Marais, D. Langevin, C. Chappey, and P. Judeinstein, *J. Phys. Chem. B*, **2008**, *112*, 12338–12346.

24. C. M. Lang, K. Kim, and P. A. Kohl, *Electrochem. Solid State Letters*, **2006**, *9*, A545-A548.

25. E. Gulzow and M. Schultze, *J. Power Sources*, **2004**, *127*, 243-251.

26. T. N. Danks, R. C. T. Slade, and J. R. Varcoe, *J. Mater. Chem.*, **2002**, *12*, 3371-3373.

27. J. R. Varcoe and R. C. T. Slade, *Electrochem. Commun.*, **2006**, *8*, 839–843.

28. E. Agel, J. Bouet, and J. F. Fauvarque, *J. Power Sources*, **2001**, *101*, 267-274.

29. T. Sata, M. Tsujimoto, T. Yamaguchi, and K. Matsusaki, *J. Membr. Sci.*, **1996**, *112*, 161-170.

CHAPTER 6

SUMMARY AND RECOMMENDATIONS

6.1. Summary

Styrene functionalization of commercially available PFPE diols yields di-functional liquid precursors that have promising attributes to form ionic membranes. These liquid precursors and a compatible comonomer yield novel crosslinked polymer materials that are fluorinated, robust and mechanically stable. Combination of PFPE chains with styrene provides a good balance of mechanical and thermal properties in these crosslinked materials. Both PFPE and styrene functional groups confer good mechanical strength and thermal stability in these membranes that meet the requirement of PEM fuel cells. Synthesis of traditional fluoropolymers is costly and requires sophisticated process and stringent reaction condition. In our approach, photocuring converts the liquid precursor mixtures into solid membrane without involving any melt-processing or solvent-casting steps.

The different MWs and weight contents of PFPE diols enable the variable crosslink density that leads to a wide range of acid loading in the crosslinked PEMs. These crosslinked PEMs sustain and support acid loading from 0.50 to 1.85 meq g^{-1} without any dissolution. The higher end of IEC is two times that of benchmark Nafion membrane. This acid loading results in proportional increase in many favorable properties in these membranes. At high IEC, ionic conductivity of three times higher than that of Nafion membrane is a remarkable achievement in these crosslinked PEMs.

Crosslinked structure has distinct advantage over linear-chain structure in suppressing the methanol crossover. Crosslinking forms intricate barriers and tortuous networks that are effective in retarding methanol transport. Permeability study confirms that crosslinking reduces the methanol crossover substantially while maintaining good conductivity. The combined effect of low-methanol crossover and reasonable conductivity results in high selectivity (ratio of conductivity to permeability) that is favorable to DMFCs. Furthermore, combining the low and high MWs crosslinkers produces PEMs with improved mechanical properties.

Crosslinking of liquid precursor sPFPE with 4-vinylbenzyl trimethyl ammonium chloride produces novel anion exchange membranes (AEMs) that have several distinct advantages over their liquid counterparts. Without any optimization, initial conductivity results suggest that these crosslinked AEMs are competitive with acidic PEMs. The synthesis strategy applied for these AEMs also promises MEA construction without any traditional ionomer binder by forming the crosslinked AEM in a pre-assembled template of electrodes.

6.2. Contributions from This Research Effort

a) Development of crosslinkers with six different MWs offers excellent opportunity to obtain variable crosslink density that can be exploited to obtain many favorable properties in the fluoropolymers.

b) Crosslinking of polymer is effective in reducing the methanol crossover in crosslinked PEMs that have promising potentials for DMFCs. This reduction has been achieved while retaining good conductivity in these crosslinked PEMs. Due to this approach, these crosslinked PEMs have shown 3-fold higher selectivity than that of Nafion membrane.

c) From the liquid precursor and 4-vinylbenzyl trimethyl ammonium chloride, fabrication of membranes directly in ionic form has enormous benefits for the next generation AEMs. Initial results have shown that these alkaline crosslinked membranes can be competitive with traditional PEMs.

d) The universal correlation for conductivity of Nafion membrane yields satisfactory results in comparison with experimental data. The correlation captures the behavior of conductivity in the wide range of temperature and water vapor activity encompassing the operating condition of PEM fuel cells.

6.3. Recommendations for Future Direction

The following recommendations are to promote the use of liquid precursor sPFPE for the next generation membranes in PEM fuel cells.

6.3.1. Crosslinked Interpenetrating Polymer Network in Nafion Membrane

Crosslinked interpenetrating polymer network from sPFPE/R_f-SSE mixture can supplement the ion-exchange capacity (IEC) in Nafion membrane where sPFPE is styrene-perfluoropolyethers and R_f-SSE is styrene sulfonate ester (Chapter 4, Experimental Section). Nafion is a copolymer of tetrafluoroethylene (TFE) and perfluoro-2-(2-fluoro sulfonyl ethoxy) propyl vinyl ether (PSEPVE). Both monomers TFE (57 wt%) and PSEPVE (43 wt%) are mixed in approximately 6:1 molar ratio and then copolymerized to obtain equivalent weight (EW) of 1100 g/H^+ mol (0.91 meq g^{-1}). Any increase in PSEPVE to increase the IEC above 0.91 meq g^{-1} leads to β-scission in Nafion polymer.[1] Therefore, polymer degradation at lower EW than 1100 g/H^+ mol has restricted Nafion IEC to 0.91 meq g^{-1}.

To the best of our knowledge, no improvement in IEC of Nafion membrane has been reported in which Nafion membrane has been modified through crosslinking to incorporate additional acid loading. Here, we present a novel approach to incorporate a crosslinked interpenetrating polymer network (IPN) in Nafion membrane through copolymerization of sPFPE/R_f-SSE. The crosslinker sPFPE is a liquid monomer with low surface energy (22 dyne cm^{-1} at 20 °C) that readily percolates into porous polymer structure. In our study, we have demonstrated that the sPFPE/R_f-SSE mixture imbibes into porous expanded-PTFE film ensuring complete pore filling. Photocuring of this mixture-filled ePTFE produces composite membrane with crosslinked network and $–SO_3H$ functional group for ion-transport. Based on our experience with sPFPE/R_f-SSE mixture, we hypothesize that this sPFPE/R_f-SSE mixture can imbibe into swollen structure of Nafion membrane because sPFPE/R_f-SSE is fluorinated and has low-surface energy. After photocuring of Nafion membrane that is filled with sPFPE/R_f-SSE mixture, we envision a crosslinked network in Nafion polymer with additional sulfonic acid ($-SO_3H$) functional group.

Nafion, a random copolymer, has partly amorphous and disordered morphology. Nafion membrane can swell and even dissolve in solvent such as perfluorohydrophenanthrene (Flutec).[2] Both amorphous morphology and $-SO_2F$ functional group lead to significant solvent uptake.[2,3] The sPFPE/R_f-SSE mixture is miscible with solvent 3,3,4,4,5,5,6,6,7,7,8,8,8-tridecafluoro-1-octanol in all composition. Moreover, this solvent is partly fluorinated due to fluorinated tail ($F-(CF_2)6-$) and has good polarity due to hydroxyl group ($-CH_2CH_2-OH$). Soaking the Nafion polymer in this solvent for sufficient time can swell and open up the structure due to fluorinated and polar nature of the solvent.

This solvent will provide a favorable route to incorporate sPFPE/R_f-SSE mixture into Nafion polymer because of solvent uptake in Nafion polymer and solvent miscibility with sPFPE/R_f-SSE. The sPFPE/R_f-SSE mixture will penetrate into and occupy the expanded portion of Nafion polymer structure. After photocuring, hydrolysis and ion-exchnage of sPFPE/R_f-SSE filled Nafion membrane, the sPFPE/R_f-SSE will form a crosslinked structure that will provide additional sulfonic acid group and IEC above that of current IEC of 0.91

meq g^{-1}. Crosslinked structure will serve as an IPN that will be mechanically stable and robust to overcome any delamination and dissolution.

In addition, sPFPE/R_f-SSE will be compatible with Nafion polymer and participate in hydrophobic-hydrophillic phase separation due to PFPE backbone in crosslinked IPN. This IPN will also contribute to reducing swelling in Nafion polymer because of crosslinking. Figure 6.3.1 illustrates synthesis step to incorporate crosslinked IPN in Nafion polymer and a schematic of crosslinked Nafion membrane. Initially, this approach will require study of solvent, 3,3,4,4,5,5,6,6,7,7,8,8,8-tridecafluoro-1-octanol, uptake in Nafion polymer. This solvent is slightly viscous at room condition. Soaking of Nafion polymer in this solvent at elevated temperature will enhance the uptake.

Chapter 4 (Experimental section) describes the synthesis of sPFPE with various molecular weights and comonomer R_f-SSE. For target IEC through crosslinked IPN, initially, selected ratio of sPFPE and R_f-SSE can be prepared in the solvent. After soaking the Nafion polymer in sPFPE/R_f-SSE mixture for sufficient time, blotting off unfilled sPFPE/R_f-SSE from the Nafion polymer surface will eliminate any crosslinked layer formation on the surface of Nafion membrane. Weight measurements of Nafion polymer before soaking in the solvent and after photocuring of sPFPE/R_f-SSE in the polymer can provide the estimate of sPFPE/R_f-SSE uptake and IEC. Duration for complete photocuring of sPFPE/R_f-SSE in Nafion polymer may vary from standard photocuring time of sPFPE/R_f-SSE that is about 10 minutes.

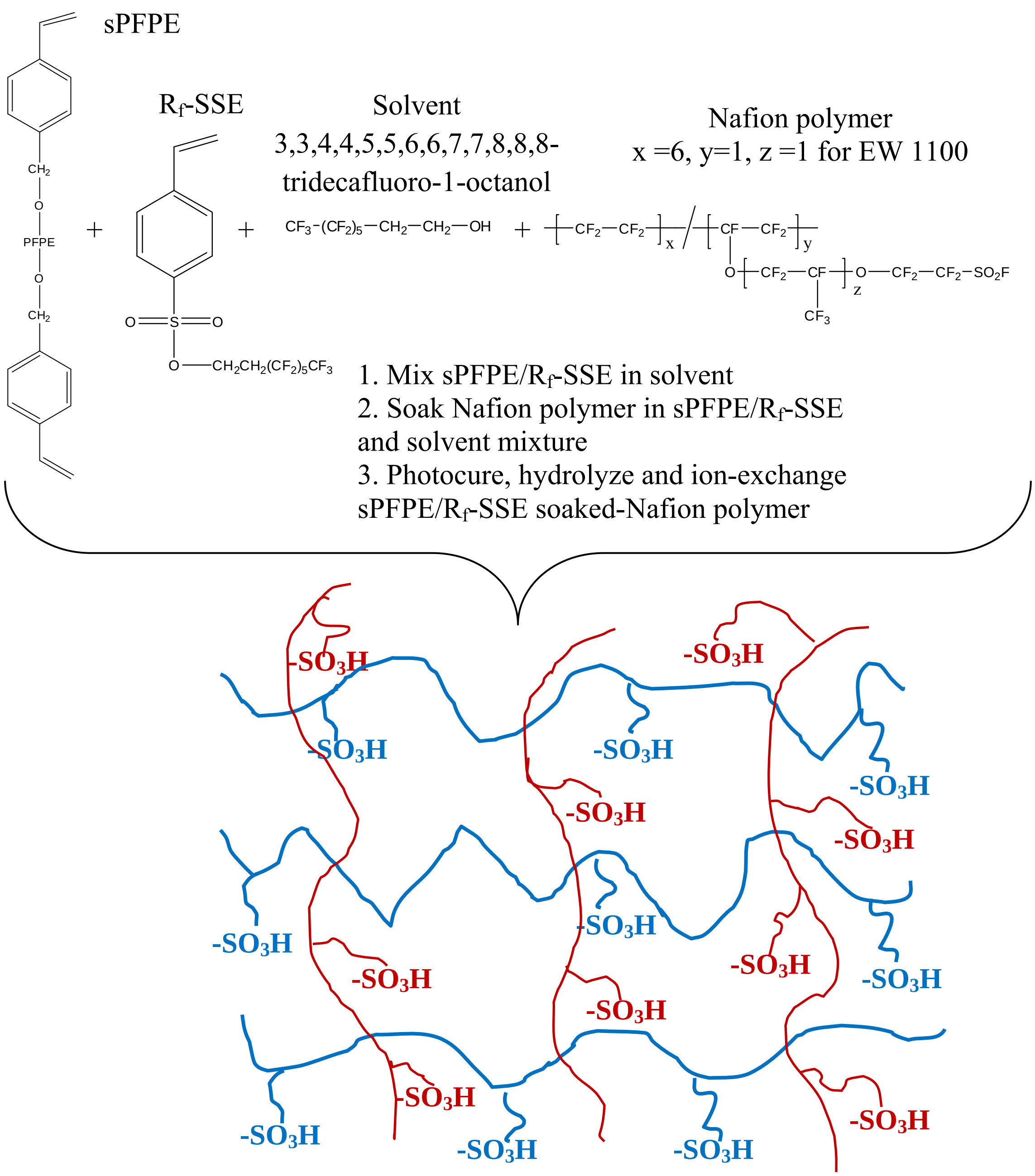

Figure 6.3.1. Crosslinked Nafion membrane. Light red represents crosslinked interpenetrating polymer network from sPFPE/R_f-SSE and light blue represents Nafion polymer parent chain.

After photocuring for sufficient time, typical hydrolysis in base/alcohol solution and ion-exchnage in acid solution can convert both R_f-SSE and $–SO_2F$ groups into corresponding sulfonic acid. Characterization techniques, such as IEC, polar solvent uptake, thermal stability, tensile strength and ionic conductivity will elucidate the effect of crosslinked IPN on Nafion membrane properties. Depending on behavior of crosslinked Nafion membrane, acid loading can be increased through judicious selection of sPFPE/R_f-SSE ratio. Furthermore, different MWs of sPFPE provide opportunity to enhance the crosslink density, acid loading and other associated properties in Nafion membrane containing crosslinked IPN.

6.3.2. Crosslinked PEMs in Sulfonimide Form

Crosslinked PEMs in proton form can be converted into sulfonimide form (-SO_2-NH-SO_2-CF_3) through trifluoromethane sulfonimide/acetonitrile (NH_2-SO_2-CF_3/CH_3CN) treatment. Sulfonimides are strong and stable acids that become proton conductor in presence of water.[4,5] In our study, we have demonstrated the performance of crosslinked PEM in proton form (Chapter 4). Following the R_f-SSE synthesis pathway as described in Chapter 4, immobilized sulfonic acid in crosslinked PEM can readily be converted into corresponding sulfonyl chloride (-SO_2Cl) upon treatment with thionyl chloride or sulfuryl chloride in anhydrous DMF. In aqueous environment, sulfonimides dissociate to form a stable anion and a proton. It is thought that proton forms a hydronium ion (H_3O^+) that transports across the membrane in presence of water.[4,6] The schematic below illustrates the ionized form of sulfonimide that has an immobilized anion and a free proton.[7]

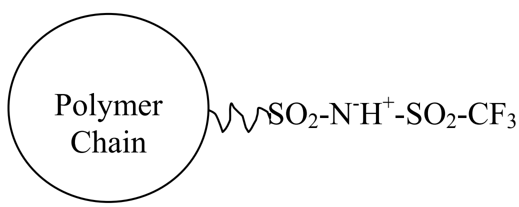

Sulfonimides have free energy of dissociation comparable with that of perfluoro sulfonic acid.[8] Sulfonimide-based polymer membranes have improved thermal stability over sulfonic acid-based membranes.[9] These sulfonimide-based membranes have shown to maintain hydration at temperature where traditional sulfonic acid-based membranes lose water.[6,10] It has also been mentioned that sulfonimide-based ionomers enhance the oxygen reduction kinetics in PEM fuel cells.[6,9,10]

It is proposed that soaking of crosslinked PEMs in thionyl chloride will convert immobilized -SO_3H group to corresponding -SO_2Cl.[11,12] Figure 6.3.2 shows the synthesis steps to obtain sulfonyl chloride group into crosslinked PEM. For full conversion of -SO_3H to -SO_2Cl, it will be critical to maintain anhydrous reaction environment because water will lead to hydrolysis of SO_2Cl. Crosslinked PEMs in Na^+ salt instead of H^+ form can be preferred for good control on anhydrous environment. Due to ionic group in crosslinked PEMs, thionyl chloride and DMF can easily penetrate into membrane because they are polar. After obtaining crosslinked PEMs in –SO_2Cl form, it will be essential to preserve the membrane in an anhydrous environment until the treatment with NH_2-SO_2-CF_3/CH_3CN because water will lead to hydrolysis of –SO_2Cl. For sulfonimide functional group in crosslinked PEM, one-step treatment with NH_2-SO_2-CF_3/CH_3CN in $N(C_2H_5)_3$ can convert –SO_2Cl to corresponding –$SO_2NHSO_2CF_3$ group with release of HCl acid.[4,11-13]

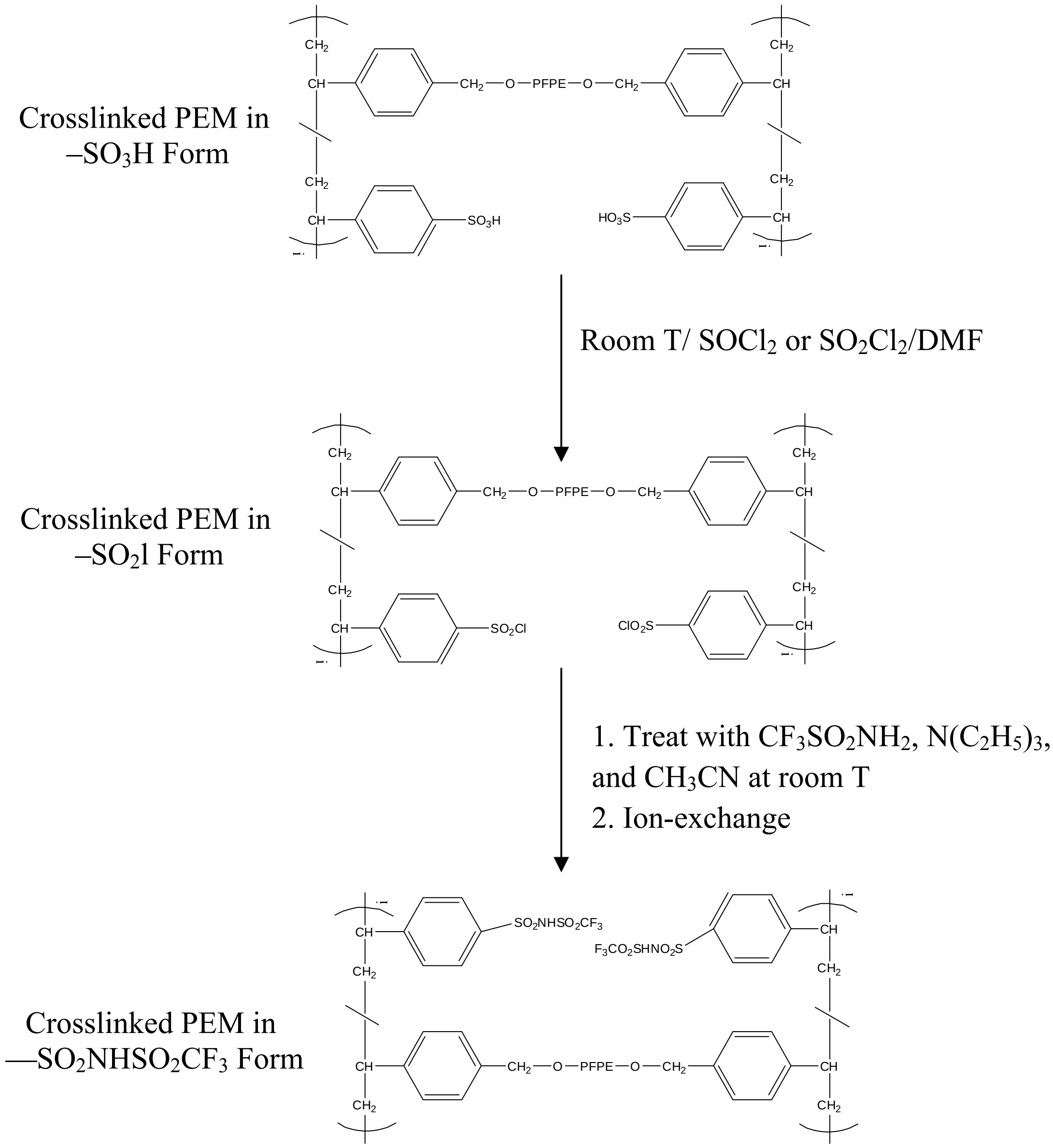

Figure 6.3.2. Crosslinked PEM in sulfonimide ($-SO_2NHSO_2CF_3$) form.

Initially, it will be important to optimize the reaction condition and time for converting the membrane to $–SO_2Cl$ form and then to $–SO_2NHSO_2CF_3$. Emerson *et al*. have shown other environmental friendly routes to obtain $–SO_2Cl$ functional group in polymers from corresponding sulfonic acid.[14] Depending on the requirement, crosslinked PEM in proton form can fully or partly be converted into sulfonimide. Figure 6.3.2 illustrates the chemical structure of crosslinked PEM that is full sulfonimide form. Due to sulfonimide group, these crosslinked PEMs can be good proton conductor and barrier to methanol transport. It is well known that proton conduction and methanol transport are proportional. However, sulfonimide has advantage of retaining proton conductivity while providing methanol barrier property. With retarding effect of crosslinking on methanol transport, sulfonimides in these crosslinked polymer materials can further produce PEMs with excellent proton conductivity and methanol barrier property. Application of crosslinked PEM in sulfonamide form will also enhance the oxygen reduction kinetics as reported by others.[6,9,10]

6.3.3. Crosslinked PEMs Photocured Directly in Ionic Form

Photocuring of liquid crosslinker sPFFE and an ammonium salt of styrene sulfonic acid (SSA) can convert the sPFPE and salt solution into solid ionic membrane without employing any esterfication (R_f-SSE) and hydrolysis. Fabrication of polymer electrolyte membranes (PEMs) directly in ionic form has distinct advantage in reducing the post-fabrication treatment steps as well as eliminating the requirement for a traditional ionomer binder for membrane electrode assembly (MEA) construction. Chemical synthesis of PEMs involves several processing steps that impose constraints on MEA construction. Traditionally, Nafion dispersion serves as a binder between the electrode and PEM in MEA assembly. Besides providing the structural support to the electrode, this binder has important role to play in proton transport around catalytic surface.

The new PEMs that are alternative to Nafion membrane must be compatible with Nafion binder in order to achieve the full benefit of these new PEMs. Use of Nafion binder can compromise the advantages of new PEMs because Nafion binder suffers from challenges associated with Nafion membrane. MEA based on new PEMs that have promises to outperform Nafion membrane must be accomplished without the use of traditional Nafion binder.

One novel way of MEA construction is to form the membrane directly in ionic form in a pre-assembled template of electrodes. This approach will eliminate the several synthesis steps that prevent membrane fabrication and MEA construction together. In our current approach for membrane fabrication (Chapter 4), crosslinked PEMs were formed from photocuring, hydrolysis, and ion exchange. The hydrolysis step requires heating of membrane in base/methanol solution at high temperature to convert the ester into acid group. Because of hydrolysis condition, MEA construction from crosslinked PEMs requires Nafion binder that may compromise the promising advantages of these crosslinked PEMs. Initially, we attempted to mix SSA-Na^+ salt with liquid crosslinker sPFPE. This salt is immiscible with sPFPE because of strong polarity.

From our experience, only few solvents can fully dissolve SSA-Na^+ salt. We found that this salt is fully miscible in formamide, ethylene glycol, and glycerol. In case of glycerol, heating above the room temperature was essential to form a clear solution. High dielectric constant of formamide (80), ethylene glycol (32), and glycerol (43) as well as intrinsic nature of these solvents may be responsible for their miscibility with this SSA-Na^+ salt. However, these solvents are immiscible with sPFPE and could not be used to realize a homogeneous solution of sPFPE and SSA-Na^+ salt.

Ammonium salts of *p*-styrene sulfonic acid broaden the range of solvents that can be miscible with both sPFPE and the ammonium salt of *p*-styrene sulfonic acid. We have observed that standard SSA-NH_4^+ salts as well as other derivatives SSA-NR_4^+ (R-CH_3, C_2H_5, C_3H_7, C_4H_9) can be miscible with 3,3,4,4,5,5,6,6,7,7,8,8,8-tridecafluoro-1-octanol solvent. This solvent can dissolve both sPFPE and ammonium salts of *p*-styrene sulfonic acid.

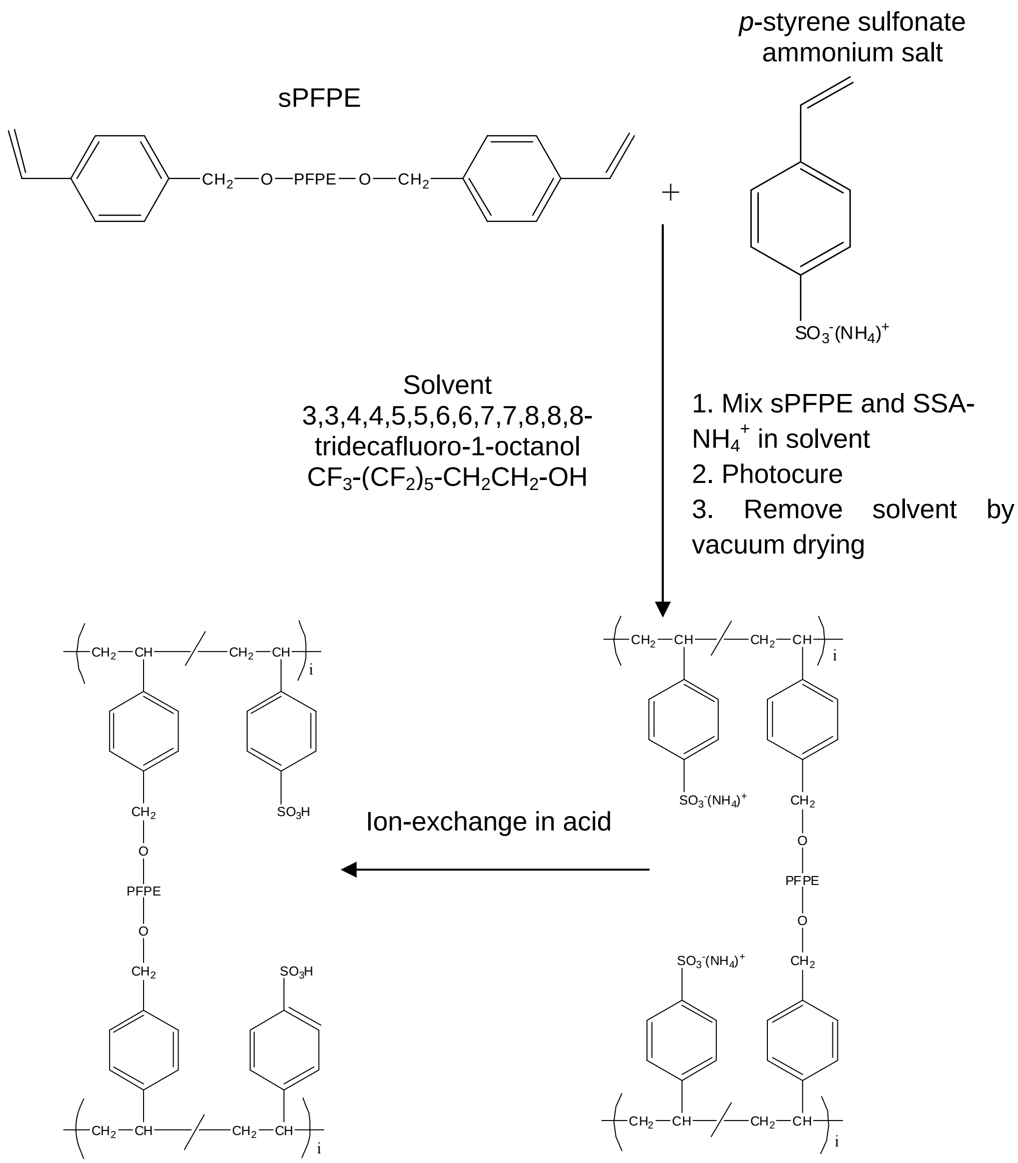

Figure 6.3.3. Crosslinked PEMs photocured directly in ionic form

Figure 6.3.3 illustrates the synthesis steps of fabricating crosslinked PEM directly in ionic form. After photocuring of the sPFPE/SSA-NH_4^+ solution, single step of ion-exchange with acid solution can produce PEMs in proton form. This approach eliminates the hydrolysis step, a major advantage for MEA construction. Depending on the MEA construction strategy, this membrane fabrication directly in ionic form can also eliminate the requirement of Nafion dispersion as binder. For efficient proton transport, good adhesion at electrode-PEM interface can be achieved, depending on the success of this approach.

Initially, synthesis steps shown in Figure 6.3.3 will require optimization of concentration in sPFPE/SSA-NH_4^+ and solvent solution. We have already demonstrated (Chapter 5) that sPFPE is miscible with solvent 3,3,4,4,5,5,6,6,7,7,8,8,8-tridecafluoro-1-octanol. In case of any challenge with sPFPE and SSA-NH_4^+, other analogous ammonium salts such as SSA-$N(CH_3)_4^+$, SSA-$N(C_2H_5)_4^+$, SSA-$N(C_3H_7)_4^+$ and SSA-$N(C_4H_9)_4^+$ are proposed that may be favorable to mix with sPFPE in the solvent. We also found that incorporating a fluorinated tail between styrene and sulfonic group, such as CH_2=CH-C_6H_4-O-CF_2-CF_2-SO_3^- Na^+ produces ionic co-monomer that is miscible with sPFPE in the solvent 3,3,4,4,5,5,6,6,7,7,8,8,8-tridecafluoro-1-octanol. Incorporating fluorinated tail (-CF_2-CF_2-) adjacent to -SO_3- in the comonomer has advantage of enhancing the acidity of sulfonic acid because perfluoro sulfonic acids are stronger than their hydrocarbon counterparts.

The solvent-based PEM synthesis approach (Figure 6.3.3) also requires minimum loss of solvent during polymerization of sPFPE and SSA-salt. After PEM fabrication in ionic form, it is essential to remove the solvent completely. The solvent removal could be challenging in a situation where solution of sPFPE and SSA-NH_4^+ salt is sandwiched between the two electrodes. Prolonged drying after polymerization step can remove the solvent through the porous electrodes and gas diffusion layer assembly.

In case of solvent removal from MEA becoming challenging, the following strategy is recommended: photocure solution of sPFPE and SSA-NH_4^+ salt on the top of one electrode, remove the solvent, and then assemble the other electrode with the first electrode in order to obtain complete a MEA. If pre-formed electrode that are bonded onto gas diffusion layer poses serious challenge in MEA construction from sPFPE and SSA-NH_4^+ salt solution, the alternative approach can be the following: use Pt/C catalyst particles and sPFPE and SSA-NH_4^+ salt solution to form a dispersion, pour this catalyst dispersion onto a template (denote this as Layer 1), pour sufficient sPFPE and SSA-NH_4^+ salt solution on the top of the Layer 1 to achieve target thickness in the membrane (denote this as Layer 2), and then pour the catalyst dispersion same as in Layer 1 on the top of the Layer 2 (denote this as Layer 3) and finally photocure all the three Layers 1, 2, and 3 to construct MEA in one step. The recommended strategy in this section (Figure 6.3.3) has promising features to replace the traditional method of MEA construction that compromises the benefits of new PEMs.

6.3.4. Crosslinked PEMs Containing Methanol-Inhibiting Functional Groups

Crosslinked PEMs can contain methanol-inhibiting functional groups that suppress methanol crossover. Due to chemical crosslinking, high-acid loading in conjunction with methanol-inhibiting functional groups can yield PEMs with high conductivity and low-methanol permeability. This combination of high acid loading and methanol-inhibiting groups can improve the effectiveness of crosslinked PEMs in DMFCs. The methanol-inhibiting functional groups, such as poly(vinyl alcohol), poly(vinyl phenol), poly(vinyl aniline), poly(vinyl pyridine) and poly(vinyl pyrrolidinone) have shown to reduce the methanol permeability across the PEMs. It should be noted that these functional groups lack their own intrinsic ionic conductivity.

At fixed IEC, incorporation of these compounds reduces both ionic conductivity and methanol permeability. To retain the ionic conductivity, additional acid loading becomes important in order to realize the full benefit of these methanol-inhibiting compounds. Advantages of both variable IEC from crosslinking approach and methanol-inhibiting functional groups can be combined to produce PEMs with high conductivity and low permeability. Definitely, crosslinking has advantage over linear-chain PEMs in allowing favorable IEC for adding these methanol-inhibiting compounds. In crosslinking approach, we have demonstrated that PEMs can sustain IEC from 0.5 to 1.85 meq/g. Higher end of IEC has resulted in remarkable conductivity in crosslinked PEMs. It is thought that methanol permeability will be so high at these high ends of IEC that crosslinked PEMs may not be suitable for DMFCs. At these high IECs, methanol-inhibiting functional groups can be exploited to reduce the methanol permeability while retaining the high conductivity in crosslinked PEMs.

We propose to photocure sPFPE, R_f-SSE, and any one of the following monomers: vinyl perfluorooctanoate, 4-acetoxystyrene, 4-aminostyrene, 4-vinylpyridine, and 1-vinyl-2-pyrrolidinone to obtain crosslinked PEMs as shown in Figure 6.3.4. The liquid crosslinker sPFPE and R_f-SSE can be mixed with anyone of these methanol-inhibiting monomers in a solvent to form a homogeneous solution. The vinyl perfluorooctanoate is miscible with both sPFPE and R_f-SSE without any solvent. However, 4-acetoxystyrene, 4-aminostyrene and 4-vinylpyridine and 1-vinyl-2-pyrrolidinone require a solvent to mix with both sPFPE and R_f-SSE in order to form a homogeneous and transparent solution. Figure 6.3.4 illustrates the synthesis mechanism to produce crosslinked PEMs that have sulfonic acid as well as methanol-inhibiting functional groups. All the comonomers shown in Figure 6.3.4 have sufficient reactivity to copolymerize completely with the crosslinker sPFPE. After photocuring, hydrolysis of the membrane converts the following functional groups: R_f-SSE into sulfonic acid, vinyl perfluorooctanoate into vinyl alcohol and 4-acetoxystyrene into vinyl phenol. The other three comonomers 4-aminostyrene, 4-vinyl pyridine and 1-vinyl-2-pyrrolidinone retain their original chemical identity after hydrolysis and ion-exchange.

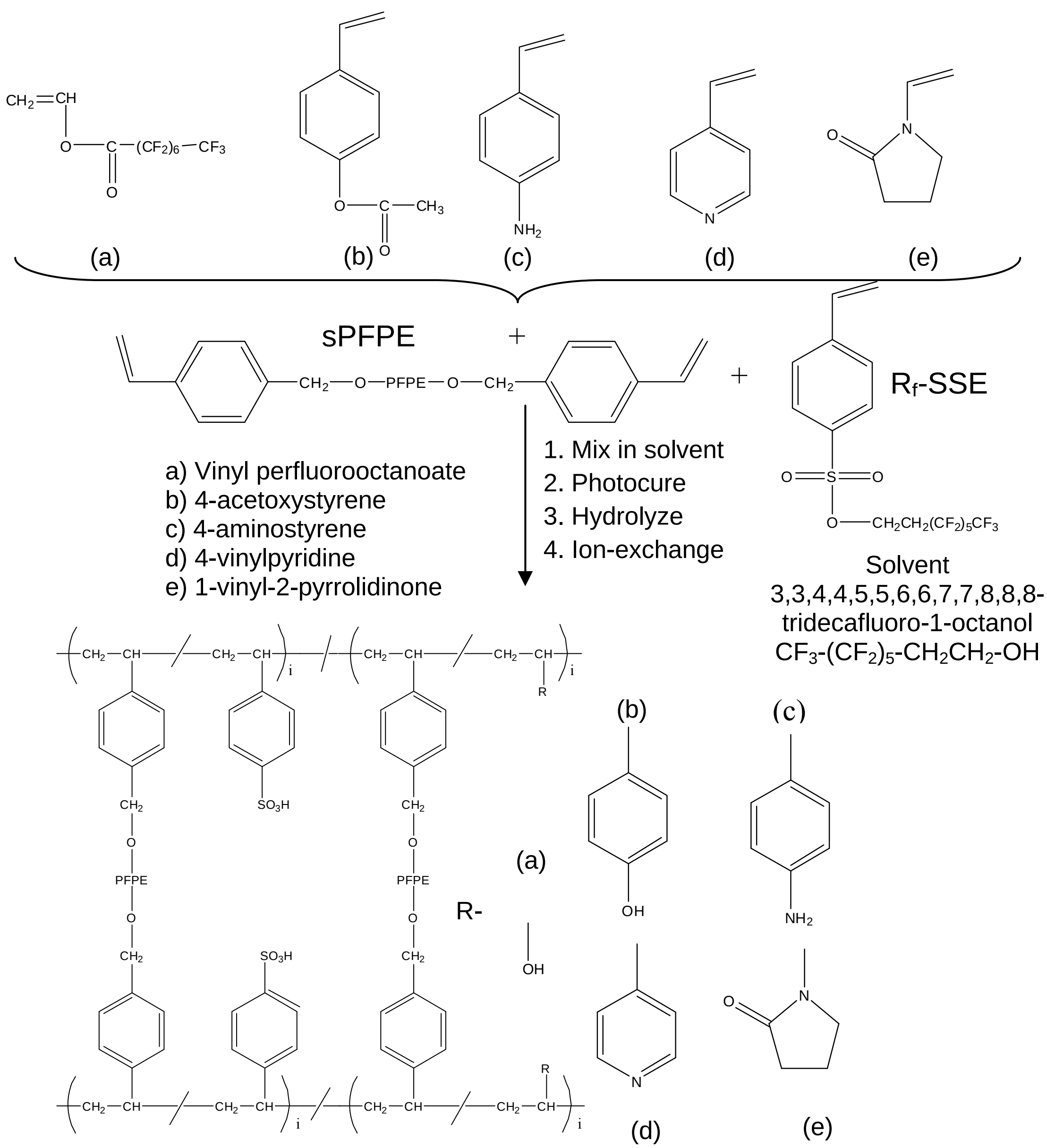

Figure 6.3.4. Crosslinked PEM containing methanol-inhibiting functional group.

It is also important to note that these methanol-inhibiting comonomers have lower polarity than the sodium salt of styrene sulfonic acid. This low polarity is an advantage for mixing these co-monomers with sPFPE and R_f-SSE in solvent 3,3,4,4,5,5,6,6,7,7,8,8,8-tridecafluoro-1-octanol. This solvent is partly polar and partly fluorinated. Initially, forming a homogeneous and transparent solution will be important to fully copolymerize all the three monomers. Amount of both R_f-SSE and methanol-inhibiting co-monomers will determine the conductivity and permeability in crosslinked PEMs.

Chapter 4 discusses the importance of crosslinking effect on methanol permeability at IEC below 1.5 meq g^{-1}. We have demonstrated that crosslinking is effective in reducing the methanol permeability. It is recommended that these methanol-inhibiting comonomers should be incorporated in crosslinked PEMs above 1.5 meq g^{-1} of IEC. At higher ends of IEC, these functional groups will inhibit methanol crossover while high-acid loading will yield high-ionic conductivity. The strategy recommended in Figure 6.3.4 has enormous potential to produce crosslinked PEMs that can be effective in DMFCs. This strategy shows a novel way to increase selectivity (ratio of conductivity to permeability) above that of traditional PEMs by exploiting crosslinking of liquid precursors in combination with methanol-inhibiting compounds.

6.3.5. Alternative Miscible Comonomers

The liquid precursor sPFPE can be photocured with styrene-based partly fluorinated co-monomers yielding PEMs with perfluoro sulfonic acid functional group instead of regular styrene sulfonic acid (SSA) functional group. The perfluoro sulfonic acids are stronger and more stable than that of their hydrocarbon counterparts. Nafion is a classic example of that perfluoro sulfonic acid. For example, trifluoromethyl sulfonic acid is stronger than methane sulfonic acid. In Chapter 4, we illustrate the synthesis scheme to obtain crosslinked PEMs based on SSA. Because styrene sulfonate salts are immiscible with the crosslinker sPFPE, an ester of SSA with a fluorinated tail (R_f-SSE) is necessary for its miscibility with sPFPE. The esterficiation requires attaching 3,3,4,4,5,5,6,6,7,7,8,8,8-tridecafluoro-1-octanol to SSA. The ester has a long fluorinated tail ($-(CF2)_6-$) that is cleaved during hydrolysis of the membrane.

Alternative styrene-based comonomers are proposed in Figure 6.3.5 that resemble perfluoro sulfonic acid of Nafion or related membranes. These proposed comonomers have fluorinated functional group ($-CF_2CF_2-$) attached to sulfonyl fluoride that assists in improving the acidity of corresponding sulfonic acid. Sulfonyl fluoride has lower polarity than the corresponding sulfonic acid. Because of fluorinated segment and relatively low polarity of sulfonyl fluoride, these comonomers will mix with the liquid crosslinker sPFPE.

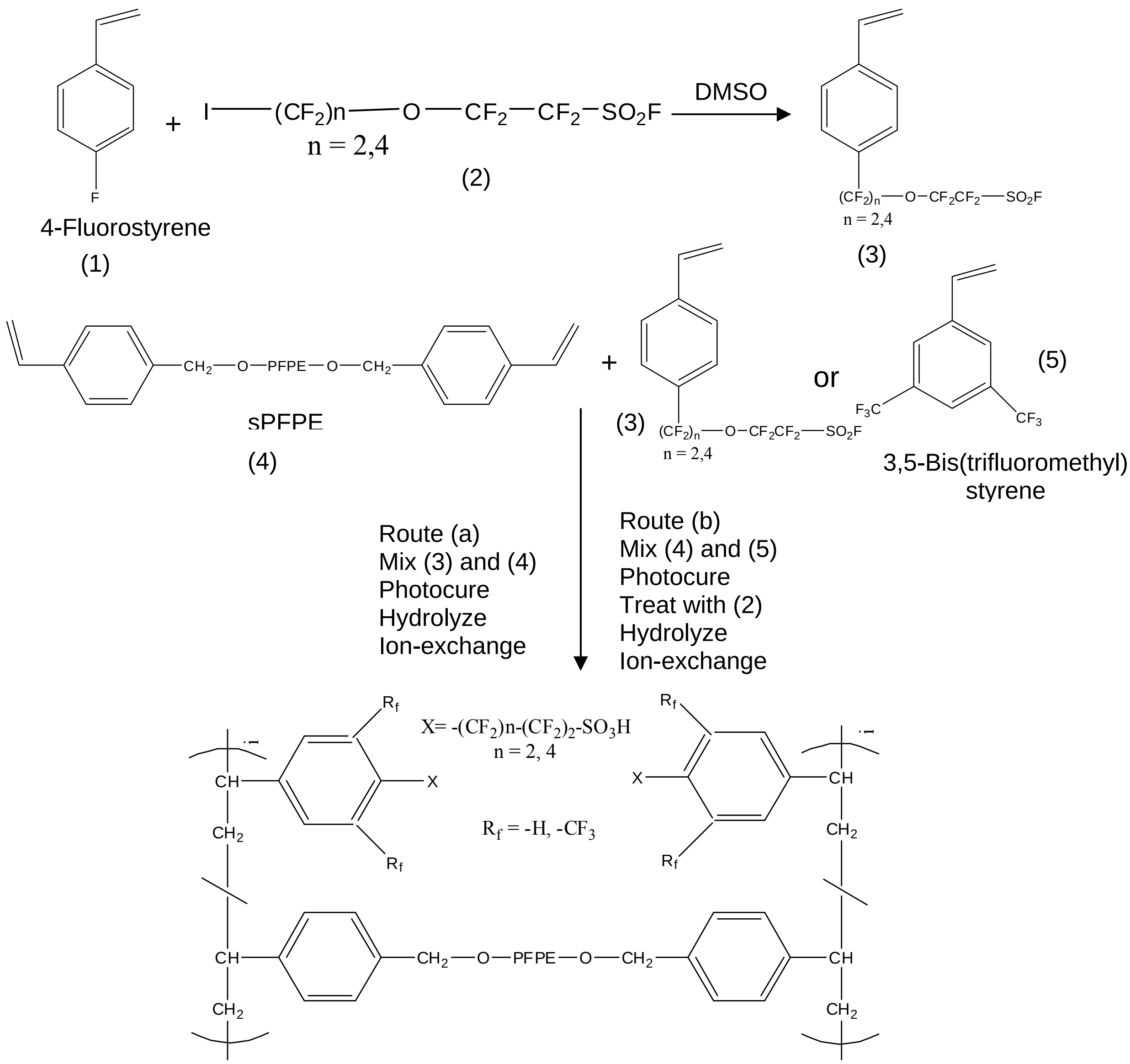

Figure 6.3.5. Crosslinked PEMs containing fluorinated sulfonic acid. Reagent (2) 5-iodooctafluoro-3-oxapentanesulfonyl fluoride (n = 2). Reagent (2) 7-iodoperfluoro-3-oxapentanesulfonyl fluoride (n = 4).

Unlike the current ester R_f-SSE (Chapter 4) that leads to loss of weight in the membrane after hydrolysis, these proposed comonomers have advantage of retaining the membrane weight after hydrolysis because there is no loss of any functional group. In these comonomers, hydrolysis will convert sulfonyl fluoride to corresponding sulfonic acid in the crosslinked PEMs. Figure 6.3.5 shows the reaction mechanism to obtain comonomer from 4-fluorostyrene and reagents 5-iodooctafluoro-3-oxapentanesulfonyl fluoride (n = 2) or 7-iodoperfluoro-3-oxapentanesulfonyl fluoride (n = 4) denoted as (2).

Treating aryl-based polymer with anyone of these reagents denoted as (2) in Figure 6.3.5 introduces the corresponding sulfonic acid in the polymer.[15] As shown in Figure 6.3.5, no solvent is involved in polymerization of sPFPE with these alternative comonomers. Initially, it will be necessary to selectively attach the reagent (2) with 4-fluorostyrene (1) at *para*-position to obtain a miscible co-monomer denoted as (3) in Figure 6.3.5. Yoshimura *et al*. have demonstrated that the reagent (2) can be substituted at *ortho*- and *meta*-positon of an aryl-based polymer.[15]

In addition to a miscible comonomer (3), 3,5-Bis(trifluoromethyl) styrene denoted as (5) is proposed that is miscible with the liquid crosslinker sPFPE. It was found that sPFPE (4000 g/mol) and comonomer 3,5-Bis(trifluoromethyl) styrene (5) formed a transparent solution after mixing and a clear membrane after photocuring. However, after photocuring, the crosslinked membrane from sPFPE (4k) and comonomer (5) needs chemical treatment with reagent (2) to incorporate sulfonic acid. Treating the membrane with reagent (2) at adequate condition can incorporate perfluoro sulfonic acid.[15] After chemical treatment with reagent (2), hydrolysis in base/alcohol can convert sulfonyl fluoride into corresponding sulfonic acid. It is hoped that both proposed schemes for crosslinked PEMs as shown in Figure 6.3.5 can improve the properties of crosslinked PEMs that are favorable to PEMs fuel cells.

6.3.6. Reduction of Oxygen, and Oxidation of Methanol and Hydrogen

The nature of interface between PEM and electrode strongly influences the kinetics of electrochemical reactions in the PEM fuel cells. It is important that the reactants diffuse rapidly from the bulk to the reaction site at the catalyst surface. In PEM fuel cells electrode, all the ingredients of electrode must contribute to reactants transport to the catalytic site. Both solubility and diffusivity of reactants through the ionic part of the electrode promote the electrochemical reactions. In addition, the electrocatalyst should have high roughness factor that is ratio of electrochemical active area to apparent geometric area. However, in real PEM fuel cells electrodes, some of the active area is diminished due to ionic binder that is applied in electrode fabrication.

Rotating disk electrode (RDE) experiment is a classic method to determine the diffusivity, activity of electrocatalyst with or without ionic film such as Nafion and charge transfer resistance that characterizes the interfacial behavior of membrane and electrode. In this experiment, rotation speed is a variable that provide means to vary the diffusion layer thickness with rotation speed. High rotation speed can eliminate diffusion layer thickness and enhance the kinetics. Deposition of polymer film is delicate task in this method. It is critical that polymer film adheres well with working electrode that rotates at high speed.

To determine the active area of electrocatalyst covered with or without polymer film, typical voltammetry can be performed in dilute sulfuric acid (0.5 M) that is saturated with argon. Working electrode covered with polymer film slows down the proton transport to the electrode. Extent of hydrogen adsorption/desorption is related with active area of the working electrode. Area analysis of hydrogen adsorption/desorption from the working electrode shows the electrochemical active area. The electrochemical reactions shown below describe the electro-reduction of oxygen and electro-oxidation of hydrogen and methanol occurring in actual PEM fuel cells at the cathode and the anode.

Oxygen reduction reaction	$O_2 + 4H^+ + 4e \rightarrow 2H_2O$	(6.3.6-a)
Hydrogen oxidation reaction	$H_2 \rightarrow 2H^+ + 2e$	(6.3.6-b)
Methanol oxidation reaction	$CH_3OH + H_2O \rightarrow CO_2 + 6\ H^+ + 6e$	(6.3.6-c)

Oxygen can be electro-reduced on platinum electrode covered with ionic films in presence of 1 M sulfuric acid.[16-18] After covering the electrode with polymer film, limiting current for oxygen reduction is lowered due to transport limitation of oxygen from the bulk to the electrode surface. RDE promotes the oxygen transport to the electrode. Hydrogen and methanol can be electro-oxidized in presence of 1 M sulfuric acid. Cyclic voltammetry under argon-saturated sulfuric acid can be performed to obtain electrode active area.[16,17] Voltammetry under oxygen-saturated sulfuric acid can be performed to obtain current *vs* potential at various rotation speeds.[16] The following equations (6.3.6.1-5) describe the relationship between relevant parameters for study of PEMs effect on kinetics of electrochemical reactions (6.3.6-a-c).[16,19,20] Equation (6.3.6.1) is modified Koutecky-Levich equation accounting film on the electrode surface.[16,18]

$$\frac{1}{i} = \frac{1}{i_K} + \frac{\delta_f}{nFAD_f C_f} + \frac{1}{0.62nFAD_b^{2/3}\omega^{1/2}\nu^{-1/6}C_b} \tag{6.3.6.1}$$

$$i_K = nFAk_f C_b \tag{6.3.6.2}$$

$$k_f = k^0 \exp[-\frac{\alpha nF}{RT}(E - E^{0'})] \tag{6.3.6.3}$$

$$i_0 = FAk^0 C_b \tag{6.3.6.4}$$

$$Rct = \frac{RT}{Fi_0} \tag{6.3.6.5}$$

where i is the current of electrochemical reactions shown in (6.3.6-a-c), i_K is kinetic current in absence of mass-transfer resistance, n is the number of electrons, F is Faraday constant, A is electrode area, δ_f is film thickness, D_f is diffusivity in film, C_f is concentration in film, D_b is diffusivity in bulk, C_b is concentration in bulk, ν is the kinematic viscosity, ω is the rotation rate, k_f is the potential-dependent rate constant, E is the potential, $E^{o'}$ is formal potential of an electrode, k^0 is standard rate constant, α is the charge-transfer coefficient, i_o exchange current, R_{ct} is the charge-transfer resistance, R is gas constant and T is the system temperature. Reactant permeability (D_fC_f) in film can be experimentally determined experimentally.[19]

The kinetics of the electro-reduction of oxygen and electro-oxidation of hydrogen and methanol on RDE covered by crosslinked PEMs films can be studied to determine the effect of these PEMs on electrochemical kinetics. Analysis of voltammogram data by plotting i vs $\omega^{-1/2}$ at various potentials E and by using Equations (6.3.6.1-5) can yield rate constant k_f, charge-transfer coefficient α, and standard rate constant k^0 from which exchange current i_o can be calculated.[16,19,20] Exchange-current of electrochemical reactions (6.3.6-a-c) on crosslinked PEMs film can be analyzed and results can be compared with that of Nafion 117 PEM. This study can give the information to what extent crosslinked PEMs promote the electrochemical kinetics in PEM fuel cells.

The apparatus for this study consists of potentiostat, rotator, 5-neck glass cell, working-, counter-, and reference-electrodes.[16] Working electrode consists of smooth platinum disc covered with ionic membrane film. Polymer film can be formed on the working electrode by depositing a known volume of solution. The working electrode covered with solution can be dried under dust-protected environment at room condition. Film thickness can be determined by using PEMs solution density, volume of deposited solution and electrode surface area.

6.3.7. Performance Evaluation of Crosslinked PEMs in DMFC

The performance evaluation of crosslinked PEMs in direct methanol fuel cells (DMFCs) can corroborate the methanol barrier properties and proton conductivity that these PEMs have exhibited (Chapter 4). These crosslinked PEMs have ability to retard methanol crossover through crosslinked network while retaining good conductivity. This low permeability at reasonable conductivity makes these PEMs an attractive candidate for DMFCs because these PEMs have demonstrated three-fold higher selectivity over that of Nafion 117 membrane. Selectivity (ratio of conductivity to permeability) is an effective measure of methanol barrier property in a PEM.

Crosslinked PEMs with IEC of 0.81-1.74 meq g^{-1} (R_f-SSE 30-50 wt%) have shown relatively low methanol permeability. Based on conductivity and permeability results as discussed in Chapter 4, these PEMs can demonstrate higher power density than that of Nafion 117 if permeability and conductivity dictate the DMFCs performance. Several factors influence DMFCs performance such as type of electrocatalysts, electrodes, MEA construction, various interfaces and operating condition. It is important to maintain the identical measurement conditions in order to extract the role of membrane on DMFCs performance.

In electrode fabrication, conventionally, Nafion dispersion is applied as a binder in catalyst ink formulation mainly to assist proton transport from electro-catalytic reaction sites. If used on a pre-fabricated electrode, Nafion dispersion improves the adhesion between the electrode and the membrane. It is important that Nafion dispersion must adhere well with new membranes during MEA construction. Strategy proposed in section 6.3.4 addresses the challenges associated with ionomer binder in MEA construction. This strategy eliminates the Nafion dispersion requirement as binder because crosslinked membrane can be formed directly in ionic form within the electrodes. Alloy of platinum and ruthenium (Pt-Ru) is more effective than pure Pt as electrocatalyst for methanol electro-oxidation. It is hoped that combining both low permeability and good conductivity of crosslinked PEMs with favorable electrocatalysts that promote methanol electro-oxidation and oxygen electro-reduction can address DMFCs challenges and promote their widescale commercialization.

6.4. References

1. T. J. Romack, J. M. DeSimone, and T. A. Treat, *Macromolecules* **1995**, *28*, 8429-8431.

2. A. J. Greso, R. B. Moore, K. M. Cable, W. L. Jarrett, and K. A. Mauritz, *Polymer* **1997**, *38*, 1345-1356.

3. G. Gebel, P. Aldebert, and M. Pineri, *Polymer* **1993**, *34*, 333-339.

4. A. J. Appleby, O. A. Velev, J. G. LeHelloco, A. Parthasarthy, S. Srinivasan, D. D. DesMarteau, M. S. Gillette, and J. K. Ghosh, *J. Electrochem. Soc.* **1993**, *140*, 109-111.

5. W. Grot, *Fluorinated Ionomers*, **2008**.

6. J. J. Sumner, S. E. Creager, J. J. Ma, and D. D. DesMarteau, *J. Electrochem. Soc.* **1998**, *145*, 107-110.

7. V. D. Z. Bermudez, C. Poinsignon, and M. B. Armand, *J. Mater. Chem.* **1997**, *7*, 1677-1692.

8. A. Oishi, H. Matsuoka, T. Yasuda, and M. Watanabe, *J. Mater. Chem.* **2009**, *19*, 514-521.

9. S. C. Savett, J. R. Atkins, C. R. Sides, J. L. Harris, B. H. Thomas, S. E. Creager, W. T. Pennington, and D. D. DesMarteau, *J. Electrochem. Soc.* **2002**, *149*, A1527-A1532.

10. M. K. Rahman, G. Aiba, M. A. B. H. Susan, Y. Sasaya, K. Ota, and M. Watanabe, *Macromolecules* **2004**, *37*, 5572-5577.

11. G. Chamoulaud and D. Belanger, *Langmuir* **2004**, *20*, 4989-4995.

12. C. G. Cho, Y. S. Kim, X. Yu, M. Hill, and J. E. McGrath, *J. Polym. Sci.: Part A: Polym. Chem.* **2006**, *44*, 6007-6014.

13. L. A. Ford, D. D. DesMarteau, and D. W. Smith Jr., *J. Fluorine Chem.* **2005**, *126*, 653-660.

14. D. W. Emerson and S. O. Ifalade, *Ind. Eng. Chem. Res.* **2005**, *44*, 7045-7048.

15. K. Yoshimura and K. Iwasaki, *Macromolecules* **2009**, *42*, 9302-9306.

16. A. Ayad, Y. Naimi, J. Bouet, and J. F. Fauvarque, *J. Power Sources* **2004**, *130*, 50-55.

17. F. A. Uribe, T. E. Springer, and S. Gottesfeld, *J. Electrochem. Soc.* **1992**, *139*, 765-773.

18. S. Gottesfeld, I. D. Raistrick, and S. Srinivasan, *J. Electrochem. Soc.* **1987**, *134*, 1455-1462.

19. J. H. Ye and P. S. Fedkiw, *J. Electrochem. Soc.* **1994**, *141*, 1483-1492.

20. A. J. Bard and L. R. Faulkner. *Electrochemical Methods-Fundamentals and Applications, Second edition* **2001**, Chapter 9, 331-367.

APPENDICES

Appendix A. Conductivity Measurement Apparatus

Appendix A provides the description of equivalent circuit to analyze impedance data, photo of conductivity measurement apparatus, change in conductivity with time during equilibration of membrane with water vapor activity, and effect of thickness on water uptake and conductivity of Nafion membranes with 25 μm (NRE 211), 50 μm (NRE 212) and 175 μm (N117) thicknesses.

A.1. Equivalent Circuit for Impedance Data Analysis

In conductivity measurement of PEM, impedance data consist of PEM and PEM-interface systems. The following equivalent circuit $(R_1Q_1)(R_2Q_2)$ represents series combination of PEM and PEM-interface systems in which subscript 1 stands for PEM and subscript 2 stands for PEM-interface system. R stands for resistance and Q stands for constant phase element (CPE) accounting for non-ideal capacitive behavior.

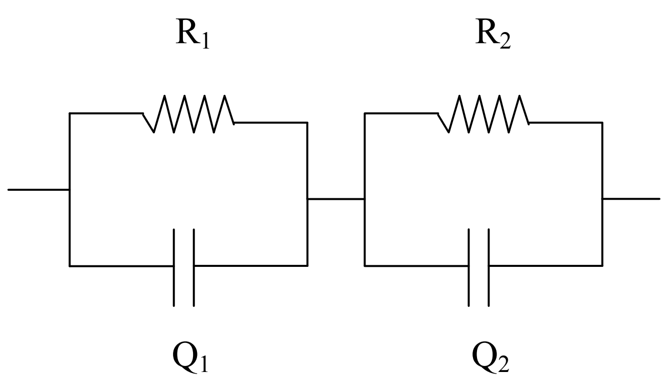

Equivalent Circuit (R_1Q_1)(R_2Q_2)

The following is analytical expression for PEM impedance in which replacing subscript 1 with subscript 2 represents PEM-interface system.

$$z(\omega)_{Equivalent} = z(\omega)_{PEM} + z(\omega)_{Interface} = z_{\mathrm{Re}}(\omega) - jz_{\mathrm{Im}}(\omega)$$

$$Z(\omega)_{PEM} = \frac{R_1 + R_1^2 Q_1^0 \omega^{n_1} \cos(\frac{n_1\pi}{2})}{1 + 2R_1 Q_1^0 \omega^{n_1} \cos(\frac{n_1\pi}{2}) + (R_1 Q_1^0 \omega^{n_1})^2} - j\frac{R_1^2 Q_1^0 \omega^{n_1} \sin(\frac{n_1\pi}{2})}{1 + 2R_1 Q_1^0 \omega^{n_1} \cos(\frac{n_1\pi}{2}) + (R_1 Q_1^0 \omega^{n_1})^2}$$

Equivalent circuit (R_1Q_1)(R_2Q_2) for modeling impedance spectra of PEM and PEM-interface systems obtained by EIS technique and two-probe method. R is resistance of PEM, and Q is constant phase element of PEM.

A.2. Photo of Conductivity Measurement Apparatus

Figure A.2 shows the photos of conductivity measurement apparatus. The conductivity measurement temperature is attained by submerging the whole apparatus in water bath. The six conductivity cells allow simultaneous study of six different PEMs or six same PEMs under identical measurement condition.

(b)

(a)

(c)

Figure A.2. (a) Photo of six identical conductivity cells attached on a performnated ceramic plate. **(b)** Photo of upper and lower blocks in conductivity cell. **(c)** Photo of assembled appratus.

A.3. Change in Conductivity with Time

Nafion membrane conductivity changes with time during equilibration of the membrane with water vapor activity at fixed temperature. To measure conductivity at equilibrium with water vapor activity, Nafion membrane conductivity was tracked with time for 48 hours to observe the change in conductivity with time. Conductivity was obtained when no significant change was observed. Figure A.3. shows the typical trend of conductivity with time during equilibration of membrane with water vapor activity.

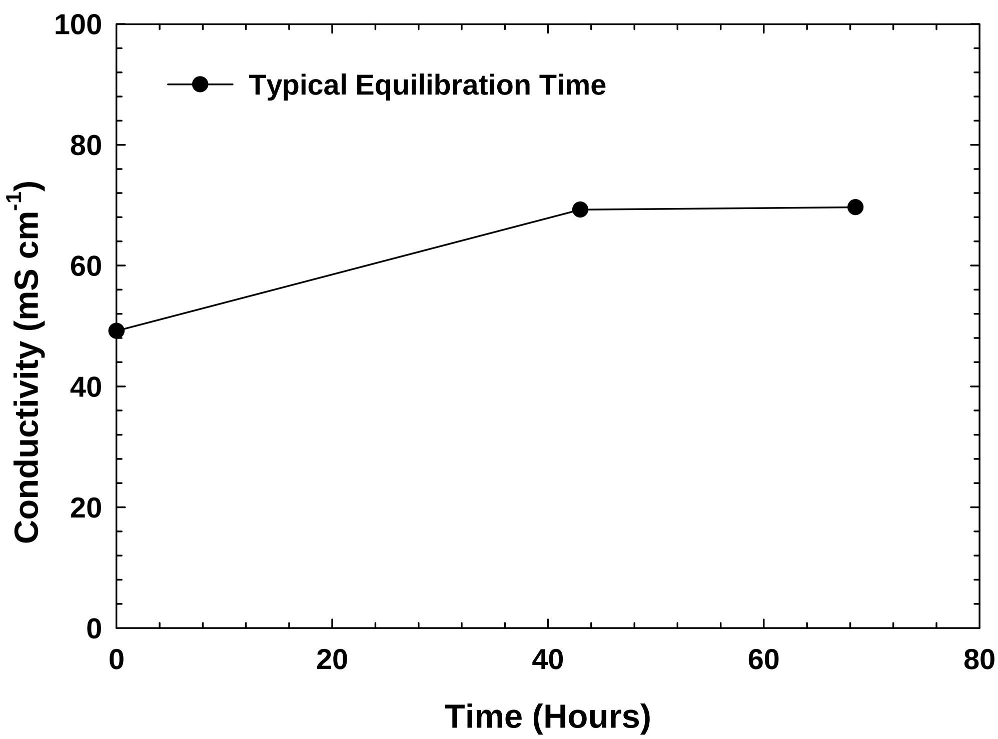

Figure A.3. Change in conductivity of Nafion 117 membrane with time at 25 °C and at 100% relative humidity. Typically, Nafion 117 membrane attains equilibration with water vapor in 48 hours at fixed temperature.

A.4. Effect of Thickness on Water Uptake and Conductivity of Nafion Membranes

There are some good incentives such as low cost and low-area specific resistance to use the polymer electrolyte membranes (PEMs) of low thicknesses in PEM fuel cells. Therefore, it is interesting to investigate the effect of thickness on the properties of PEMs. Under identical ion-exchange capacity, thickness of PEM can influence the water uptake and conductivity because extremely low thickness may be ineffective in supporting the ionic interaction and formation of hydrophilic-hydrophobic nanochannels that are believed to be responsible for proton conduction. Water uptake and conductivity are intrinsic properties of PEM and should be independent of PEM dimensions.

We suspect that processing condition may be responsible for membrane degradation leading to thickness-dependent intrinsic properties in PEM. This degradation could be severe in thinner membrane like NRE 211 and NRE 212 membranes, which have thicknesses of 25 μm and 50 μm, respectively and are fabricated through dispersion-casting of Nafion ionomer solution. If surface degradation is deeper into the bulk of the membrane, ability of membrane to support the water uptake and ionic conductivity could be diminished. To investigate the effect of thickness on PEM properties, water uptake and conductivity was measured for three types of Nafion membrane with three different thicknesses. Figures A.4.1-3 illustrate the effect of thickness on water uptake and conductivity of these Nafion membranes in which the thinnest membrane NRE 211 (25 μm) has the lowest water uptake and the thickest membrane N117 (175 μm) has the highest water uptake at all water vapor activities.

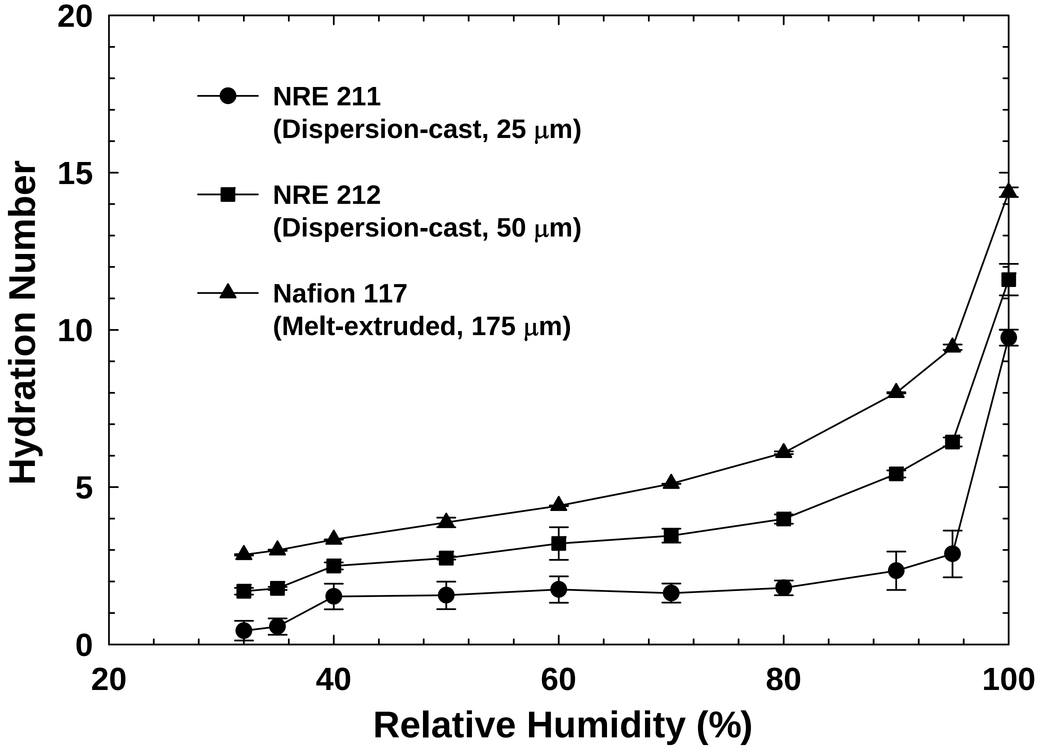

Figure A.4.1. Hydration number (number of H_2O per molecule of $-SO_3^-H^+$ group) in treated Nafion membranes at 20 °C. Membranes were treated in the following sequential way: boil in 3 wt% hydrogen peroxide solution for one hour, rinse with deionized water (18 MΩ), boil in deionized water for one hour, boil in 0.5 M sulfuric acid solution for one hour, boil in deionized water twice, and soak in deionized water at room temperature.

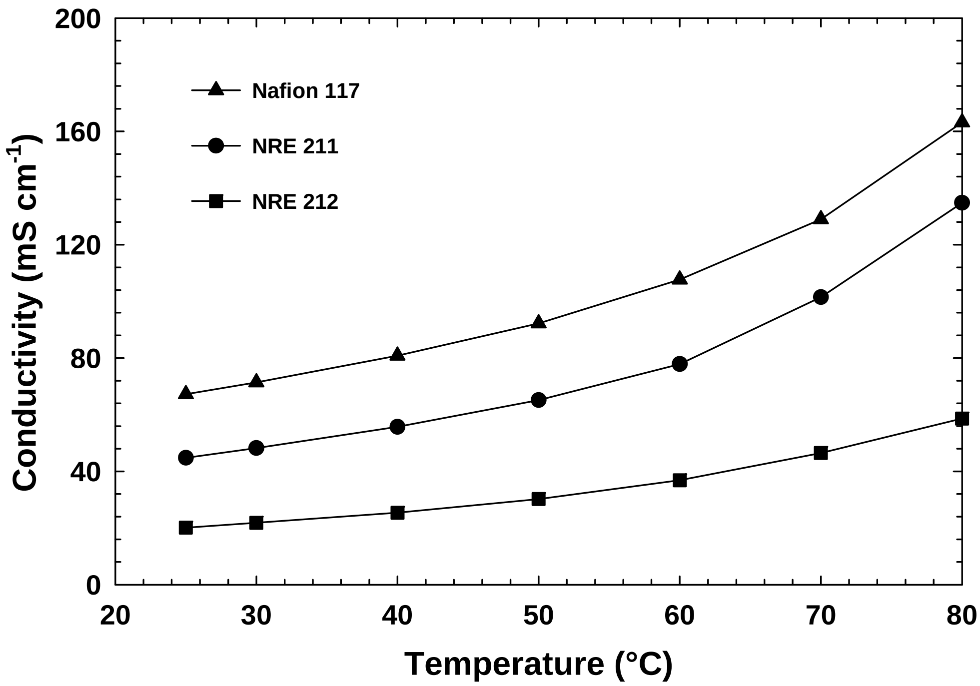

.

Figure A.4.2. Conductivity of as-received Nafion membranes at 100% relative humidity.

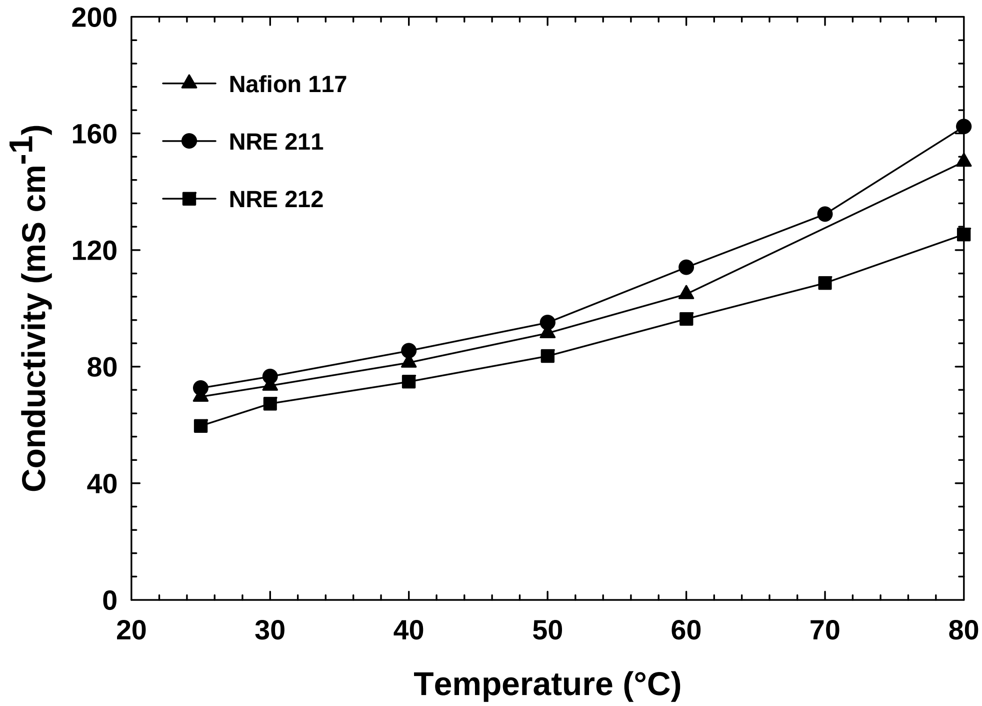

Figure A.4.3. Conductivity of treated Nafion membranes at 100% relative humidity. Membranes were treated in the following sequential way: boil in 3 wt% hydrogen peroxide solution for one hour, rinse with deionized water (18 MΩ), boil in deionized water for one hour, boil in 0.5 M sulfuric acid solution for one hour, boil in deionized water twice, and soak in deionized water at room temperature.

Nafion 117 membrane that is fabricated through melt-extrusion shows the highest conductivity among the three types of membranes when the membranes are in as-received form. Despite identical IEC, dispersion-cast membranes NRE 211 and NRE 212 exhibits water uptake and conductivity lower by 50 % of Nafion 117 membrane when these membranes are in as-received form. In case of conductivity, both dispersion-cast membranes in as-received form show consistently lower conductivity at all measurement temperatures. After treatment of these membranes with hydrogen peroxide and sulfuric acid, conductivity of NRE 211 and NRE 212 membranes improve and become comparable with that of Nafion 117. We suspect that curing of dispersion-cast membranes could be responsible for abnormal behavior in water uptake and conductivity. There is improvement in water uptake of NRE 211 and NRE 212 at 100% relative humidity. This effect of thickness study highlights the need to optimize the thickness of membrane to achieve optimal properties for their application in PEM fuel cells.

Appendix B. Methanol Permeability Apparatus

Appendix B presents the apparatus and procedure to measure methanol permeability across polymer electrolyte membranes. Methanol permeability was measured using a two-compartment diffusion cell in which methanol concentration in the receiving compartment was analyzed with a gas chromatograph.

B.1. Diffusion Cell

Figure B.1 shows the photo of diffusion cell that has two compartments. Membrane is clamped between the two compartments. The transmitting compartment is filled with methanol solution and the receiving compartment is filled with deionized water.

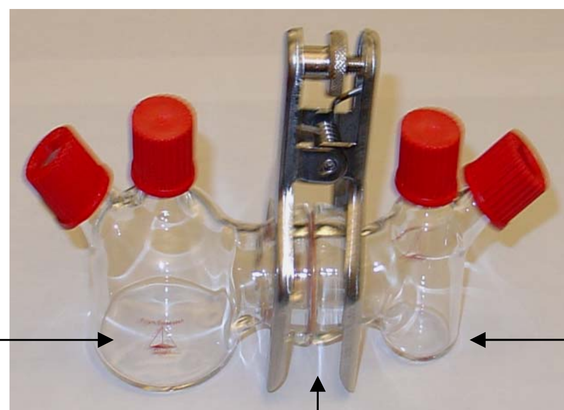

Figure B.1 Photo of diffusion cell.

B.2. Chromatograms

The methanol concentration in the receiving-compartment was analyzed with a HP 5890 gas chromatograph having the following features and conditions: injector inlet liner temperature maintained at 250 °C, flame ionization detector (FID) temperature maintained at 250 °C, hydrogen downstream pressure at 20 psig, air downstream pressure at 40 psig, a suitable polar column (Supelcowax[10], part number 24080-U, length of 30 meter, ID of 0.32 mm, and film thickness of 0.25 μm), column pressure at 10 psig, helium flow of 2 mL min^{-1} as the carrier gas, split vent flow of 40 ml min^{-1}, split ratio of 20, and manual injection of 0.5 μL sample with 5 μL capacity syringe.

The following oven-temperature profile was employed to separate methanol from water: equilibration time for 1.5 minutes, hold-time for 1 minute at 60 °C, ramp rate at 30 °C per minute from 60 to 150 °C, and hold-time for 3 minutes at 150 °C. In a typical chromatogram, a single peak observed at 1.88-1.93 minutes of elution time was assigned to methanol. The characteristic elution time of around 1.9 minutes was reconfirmed by injecting pure methanol liquid and pure methanol vapor under identical conditions.

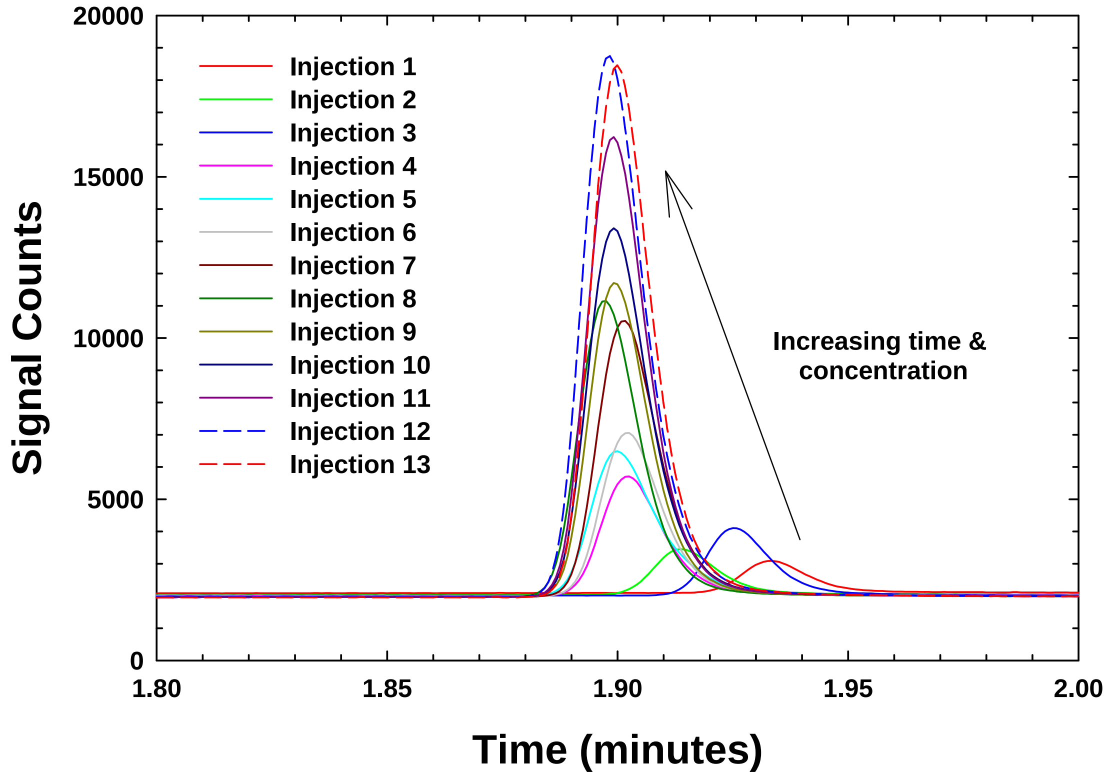

Figure B.2.1. Chromatograms of methanol samples from the receiving-compartment for Nafion 117 membrane.

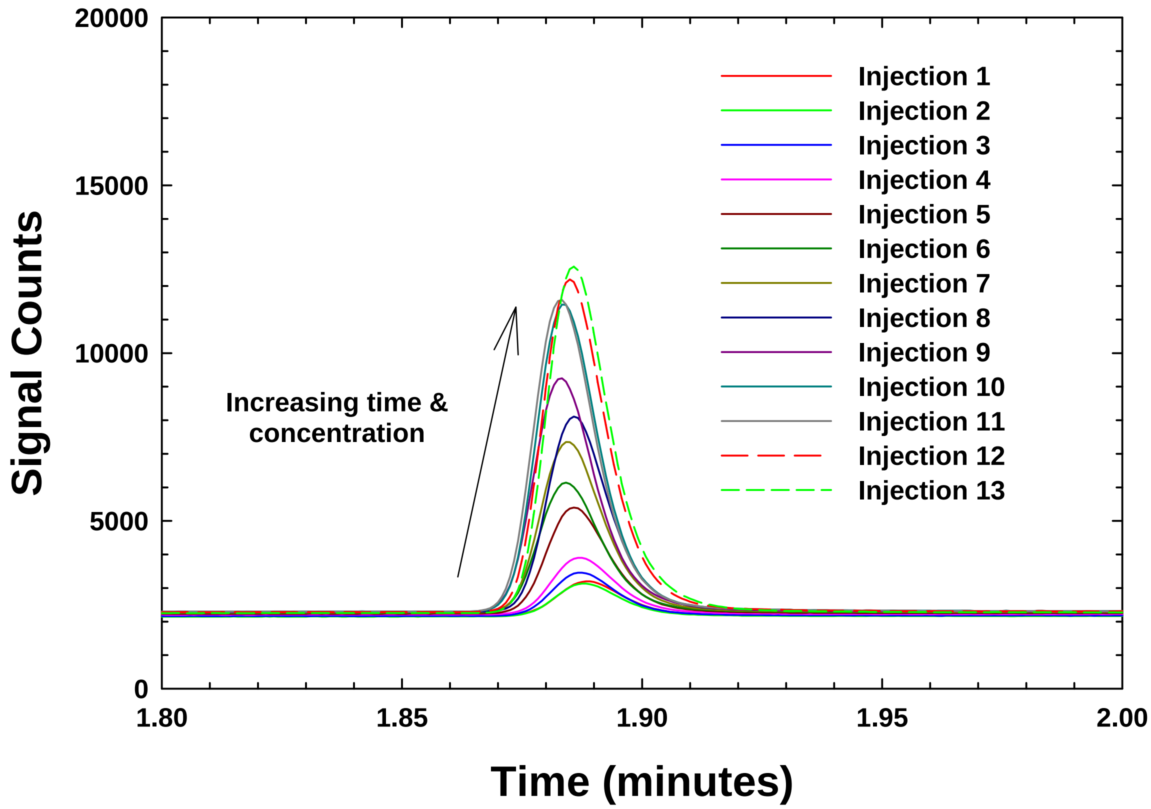

Figure B.2.2. Chromatograms of methanol samples from the receiving-compartment for crosslinked PEM with IEC of 1.16 meq g^{-1} and composition of sPFPE 4000 (60 wt%) and R_f-SSE (40 wt%).

Figures B.2.1 and B.2.2 show the typical chromatograms of methanol samples that were analyzed for methanol permeability of Nafion 117 and crosslinked sPFPE/R_f-SSE PEM. Characteristic time of around 1.9 minutes for each sample injection was observed (Figures B.2.1 and B.2.2). Independent of membrane compositions, methanol samples from the receiving compartment for each membrane qualitatively exhibited chromatograms similar to Figure B.2.2. For methanol analysis in the receiving-compartment, a calibration curve with a linear fit was generated from known concentrations of methanol solutions. A total 28 known methanol solution in the range of 0.0001-0.1 mol/L were prepared by serial dilution and analyzed by GC. The average of three chromatogram areas from three injections per concentration was used to generate the calibration curve that displayed a linear relationship between chromatogram area and methanol concentration.

In a typical methanol permeability experiment, a water-soaked membrane was clamped between the two compartments. After assembling the membrane, the receiving compartment was filled with deionized water and the transmitting compartment was filled with 1 mol/L methanol solution. The methanol concentration in the receiving-compartment was tracked with time for the first 30-40 minutes. Normally, 3-4 μL of samples were drawn from the receiving-compartment, withdrawal times of samples were recorded, and then samples were stored in fifteen numbered syringes each of 5 μL capacity. To prevent the loss of sample from the syringe during storage, the tip of each syringe was sealed with a septum. Storing the samples was essential because methanol concentration in the receiving-compartment was tracked for 30-40 minutes and GC analysis of all the samples required two to three hours. Only 0.5 μL out of 3-4 μL sample was injected into the GC injector after discarding excess sample.

B.3. Gas Chromatography Accessories and Parameters

Table B.3 HP 5890 Accessories and Parameters		
Supelcowax ™ 10 Column	30 meter, 0.32 mm ID, 0.25 μm film thickness	Part Number 24080-U
Supelco Septa	13 mm diameter, 0.060 inch thick	Part Number 27512
Inlet Liner ID	4 mm ID	Part Number 5183-4647
Hydrogen Gas Cylinder Downstream Pressure	20 psig	
Air Cylinder Downstream Pressure	40 psig	
Helium (Ultra Pure) Cylinder Downstream Pressure	60 psig	
Septum Purge Flow	3-5 ml/min	
Carrier Gas He Flow	2 ml/min	
Split Vent Flow	40 ml/min	
Purge Valve Position	On	
Split Ratio	20	
Injection Mode	Split	
Injector Temperature	250 °C	
Detector Temperature	250 °C	
Equilibration Time	1.5 minutes	
Column Initial Temperature	60 °C for 1 minute	
Temperature Ramp Rate	30 °C per minute	
Column Final Temperature	150 °C	
Hold time at 150 °C	3 minutes	
Total Time	10.7 minutes	

Appendix C. Synthesis and Characterization of Crosslinked PEMs

This section discusses the synthesis and characterization of crosslinked PEMs.

C.1. Synthesis of Difunctional sPFPE Crosslinker

The difunctional styrenyl-perfluoropolyethers (sPFPE) cross-linker was derived from perfluoropolyethers (PFPE) diols. The reaction involved the styrene-functionalization of PFPE diols with 4-vinylbenzyl chloride through a phase-transfer catalyzed reaction. Poly tetrafluoroethylene oxide-co-difluoromethylene oxide α, ω-diol (Fomblin ZDOL M_n = 2000, 2500, 3800, g/mol, CF_2CF_2O/CF_2O: 1/1; Fluorolink Modifier M_n = 1000, 1500, 2000 g/mol, CF_2CF_2O/CF_2O: 4/1) were purchased from Solvay Solexis. Solvent 1-1-1-3-3-pentafluorobutane (CAS No-406-58-6, $CF_3CH_2CF_2CH_3$, Solkane) was obtained from Microcare, Inc., (CT, USA). All other chemicals were purchased from Sigma Aldrich, Fisher Scientific, and Acros Organics and were used as received. Styrene linkages were incorporated onto both ends of the PFPE α, ω-diol by a base activated phase-transfer-catalyzed reaction.

In a typical synthesis for a fixed MW of PFPE, 30 g of PFPE α, ω-diol, 40 mL of 1-1-1-3-3-pentafluorobutane as solvent, and 1.5 g of tetrabutylammonium hydrogen sulfate as phase-transfer catalyst were added into a 250-mL capacity round-bottom-flask equipped with a magnetic stir bar. Aqueous KOH solution containing 15 g of anhydrous KOH in 30 mL of deionized water was added to the mixture in the reaction flask with stirring. The contents in the reaction flask were allowed to stir for one hour at 45 °C to distribute both aqueous and non-aqueous phases. After the gradual addition of 3.0 mL (3.25 g, 21.3 mmol) of 4-vinylbenzyl chloride for PPFE diol (M_n = 3800 g mol^{-1}, 7.9 mmol) and proportional amounts for other PFPE diols (M_n = 2000, 2500; 1000, 1500, 2000 g mol^{-1}), the reaction mixture was sealed and left to stir vigorously for 48 hours at 45 °C.

After completion of the reaction, 150 mL of 1-1-1-3-3-pentafluorobutane was added to dilute the product mixture that was highly viscous because of brown solids and other impurities. The diluted product mixture was filtered and then washed three times for one and half hours each with deionized water through gravimetric extraction. Stirring over anhydrous $MgSO_4$ for three hours at room temperature and subsequent filtration removed any residual water from the product mixture. After addition of decolorizing carbon, stirring the product mixture for twelve hours at room temperature and subsequent filtration through 0.22 μm filter removed the colored impurities. The final product distyrene-perfluoropolyether (sPFPE) was a transparent viscous liquid and was highly reactive because of styrene. The sPFPE was stored as a dilute solution in 1-1-1-3-3-pentafluorobutane at low temperatures using a glass container. At the time of use, the solvent 1-1-1-3-3-pentafluorobutane (boiling point 45 °C) was vacuum-evaporated to obtain sPFPE whose synthesis and chemical structure is shown in Figure C.1.1. Actual molecular weight of sPFPE was calculated from accounting the addition of two moles of 4-vinylbenzyl chloride for every one mole of PFPE diols. The calculated MWs are 1232 for 1000 g mol^{-1}, 1732 for 1500 g mol^{-1}, 2232 for 2000 g mol^{-1}, 2232 for 2000 g mol^{-1}, 2732 for 2500 g mol^{-1}, and 4232 for 4000 g mol^{-1} of PFPE diols. ^{1}NMR study shown in Figure C.1.2 confirmed the structure of fully styrenated PFPE.

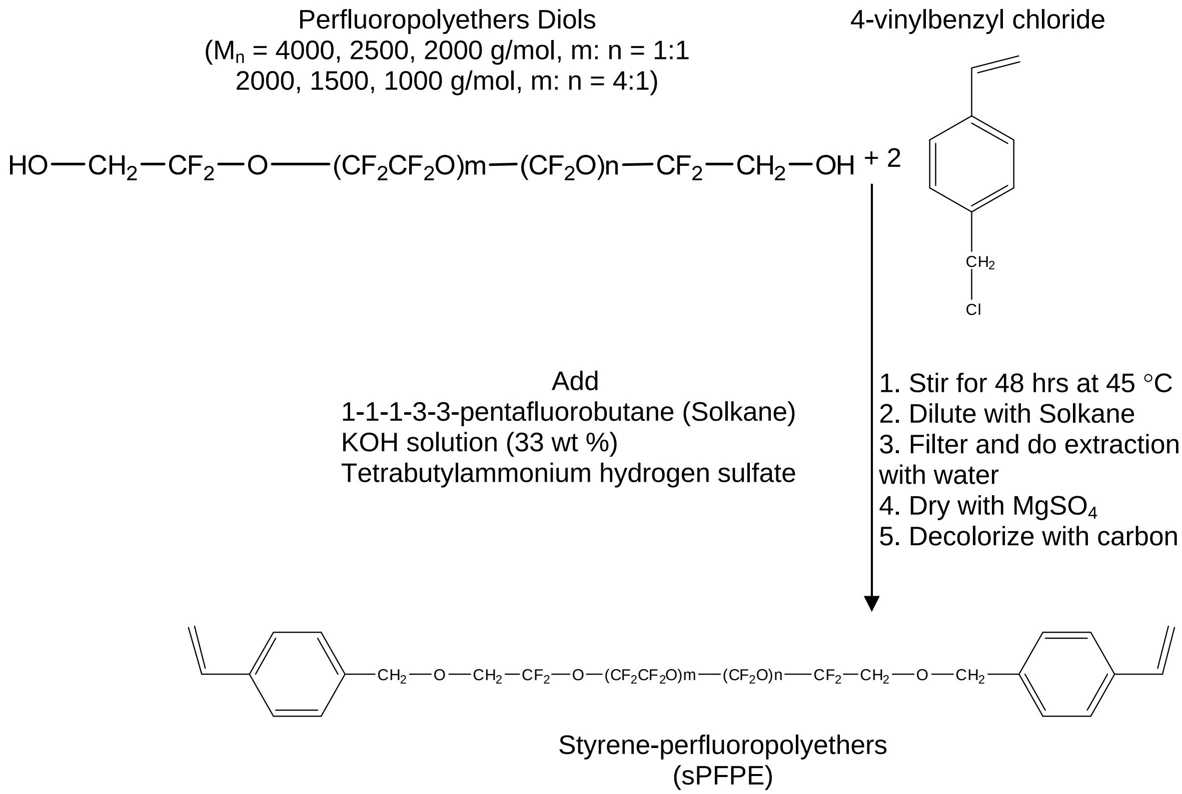

Figure C.1.1. Synthesis of sPFPE liquid crosslinker.

Nuclear Magnetic Resonance (NMR) spectra were collected using Bruker 400 MHz DRX spectrometer. Samples of sPFPE were dissolved in $CDCl_3$. 400 MHz ($CDCl_3$): δ 3.79 (2H, R_fCF_2-C$\boldsymbol{H_2}$-O-), 4.64 (2H, -O-C$\boldsymbol{H_2}$-*Φ*-), 5.26 and 5.77 (vinyl, -CH=C$\boldsymbol{H_2}$), 6.74 (vinyl, -C***H***=CH_2), 7.30-7.50 (4***H***, aromatic). ^{1}H-NMR confirmed that the hydroxyl groups of the PFPE diols were fully functionalized with 4-vinylbenzyl chloride. The resonance peak at 3.79 ppm identifies protons of PFPE methylene group that is next to the ether linkage (2H,

R_fCF_2-C$\boldsymbol{H_2}$-O-). The peak at 4.64 ppm identifies protons of methylene group that is in between the ether linkage and benzene ring (2H, -O-C$\boldsymbol{H_2}$-Φ-). The vinyl protons appear at 5.26 ppm and 5.77 ppm (vinyl, -CH=C$\boldsymbol{H_2}$), and at 6.74 ppm (vinyl, -C***H***=CH_2). The aromatic ring peaks appear at 7.25-7.40 ppm (4H, aromatic). Figure 4.1.3 shows the NMR spectra of sPFPE.

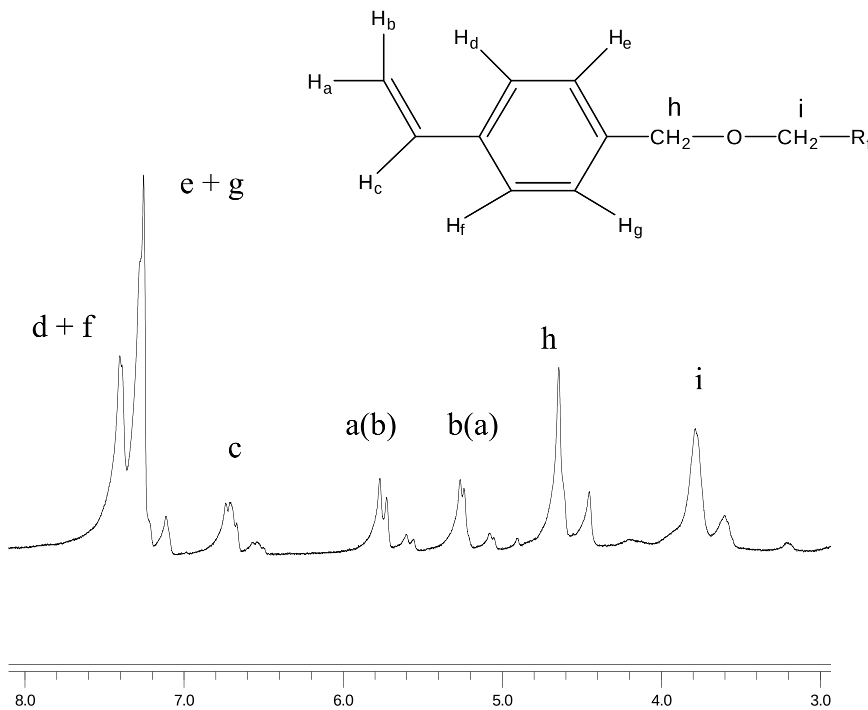

Figure C.1.2. ^{1}H NMR spectra of sPFPE crosslinker

C.2. Synthesis of Comonomer Styrene Sulfonate Ester

Sodium *p*-styrene sulfonate co-monomer is immiscible with sPFPE. To improve the compatibility of the sodium *p*-styrene sulfonate comonomer with sPFPE, a fluorinated ester that is compatible with sPFPE was synthesized using 4-vinylbenzene sulfonyl chloride and 3,3,4,4,5,5,6,6,7,7,8,8,8-tridecafluoro-1-octanol. For 4-vinylbenzene sulfonyl chloride synthesis, initially, a 250-mL capacity three-neck round-bottom-flask equipped with addition funnel was purged with dry argon for two hours to remove any moisture. After adding 35 mL of anhydrous *N, N,*-dimethylformamide (DMF) to the reaction flask through addition funnel, 26 g of sodium *p*-styrene sulfonate was added gradually into the reaction flask. The reagent sodium *p*-styrene sulfonate and solvent DMF were allowed to stir in order to obtain a homogeneous suspension. After one hour of stirring at room temperature, 70 mL of thionyl chloride ($SOCl_2$) was added dropwise to the resulting suspension. The homogenous reaction mixture was stirred for six hours at room temperature and then the product slurry was poured into ice-water to quench any unreacted thionyl chloride. The aqueous mixture was extracted three times with diethyl ether through gravimetric extraction. The combined diethyl layers were washed three times with a 10 wt% of NaCl aqueous solution, and dried over $MgSO_4$ for two hours all at room temperature. Finally, the solution was filtered to remove $MgSO_4$ and the diethyl ether was removed under vacuum to afford the 4-vinylbenzene sulfonyl chloride product as yellow oil. Figure C.2.1 shows the synthesis of 4-vinylbenzene sulfonyl chloride.

A fluorocarbon tail from 3,3,4,4,5,5,6,6,7,7,8,8,8-tridecafluoro-1-octanol was attached to the 4-vinylbenzne sulfonyl chloride in order to obtain 1-

(3,3,4,4,5,5,6,6,7,7,8,8,9,9,9-pentadecafluoro-nonane-1-sulfonyl)-4-vinyl benzene, the precursor styrene sulfonate ester (R_f-SSE), that is miscible with sPFPE. Initially, in a completely dry 250-mL three-neck round-bottom-flask, 8 g of 4-vinylbenzene sulfonyl chloride, 14 g of 3,3,4,4,5,5,6,6,7,7,8,8,8-tridecafluoro-1-octanol, 10 mL of triethylamine, and 20 mL of pyridine were added gradually and sequentially under continuous argon gas flow. The reaction mixture was allowed to stir for 24 hours at room temperature and then the reaction mixture was poured into an excess of dilute cold hydrochloric acid to neutralize unreacted triethylamine. The product slurry was extracted with diethyl ether three times and the combined ether layers were washed sequentially with deionized water, 10 wt% aqueous NaOH solution, and 10 wt% aqueous NaCl solution, all through gravimetric extraction. The product was then dried over $MgSO_4$ for two hours and filtered. Colored impurities were removed by stirring over decolorizing carbon for eight hours at room temperature and subsequent filtering. Finally, the diethyl ether solvent was removed under vacuum. Any residual diethyl ether was removed with drying in a vacuum oven at room temperature. The 1-(3,3,4,4,5,5,6,6,7,7,8,8,9,9,9-pentadecafluoro-nonane-1-sulfonyl)-4-vinyl-benzene (R_f-SSE) product is a waxy and yellowish solid. Figure C.2.1 shows the synthesis and structure of R_f-SSE. ^{1}H NMR spectra were collected using Bruker 400 MHz DRX spectrometer to confirm the linkage of vinyl and ester groups on R_f-SSE. Figure C.2.2 shows the NMR spectra of R_f-SSE.

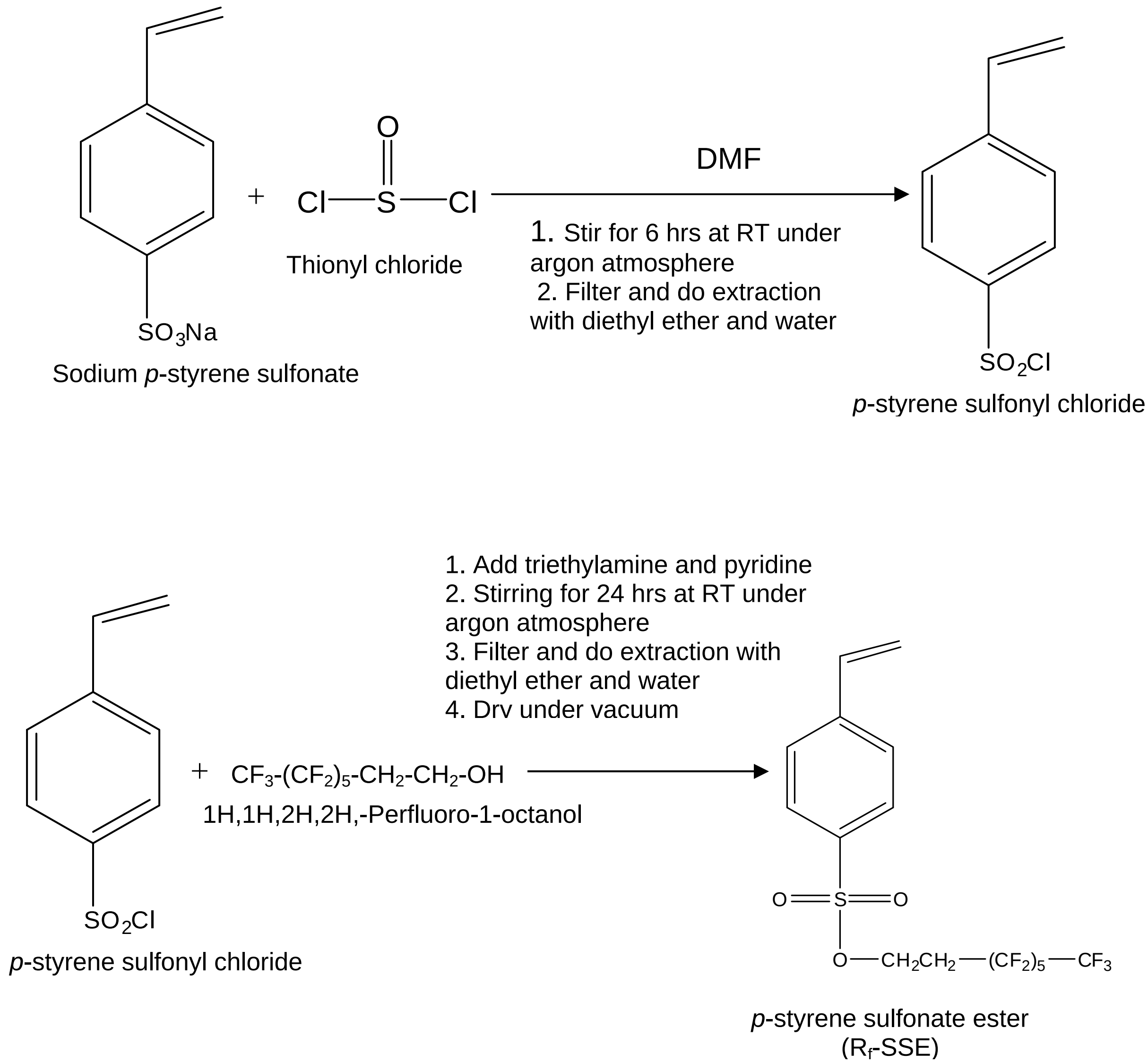

Figure C.2.1. Synthesis of co-monomer R_f-SSE

Samples of R_f-SSE were dissolved in $CDCl_3$ (Cambridge Isotope Labs). The peaks at 2.10 ppm (2H, CF_3-$(CF_2)_5$-C$\boldsymbol{H_2}$-CH_2-) and at 3.17 ppm (2H, CF_3-$(CF_2)_5$-CH_2-C$\boldsymbol{H_2}$-O-) correspond to methylene group protons from the fluorinated alcohol. The vinyl group protons appear at 4.80 ppm and 5.38 ppm (vinyl, -CH=C$\boldsymbol{H_2}$), and at 6.19 ppm (vinyl, -C***H***=CH_2). The aromatic ring peaks appear at 7.08-7.19 ppm (4H, aromatic).

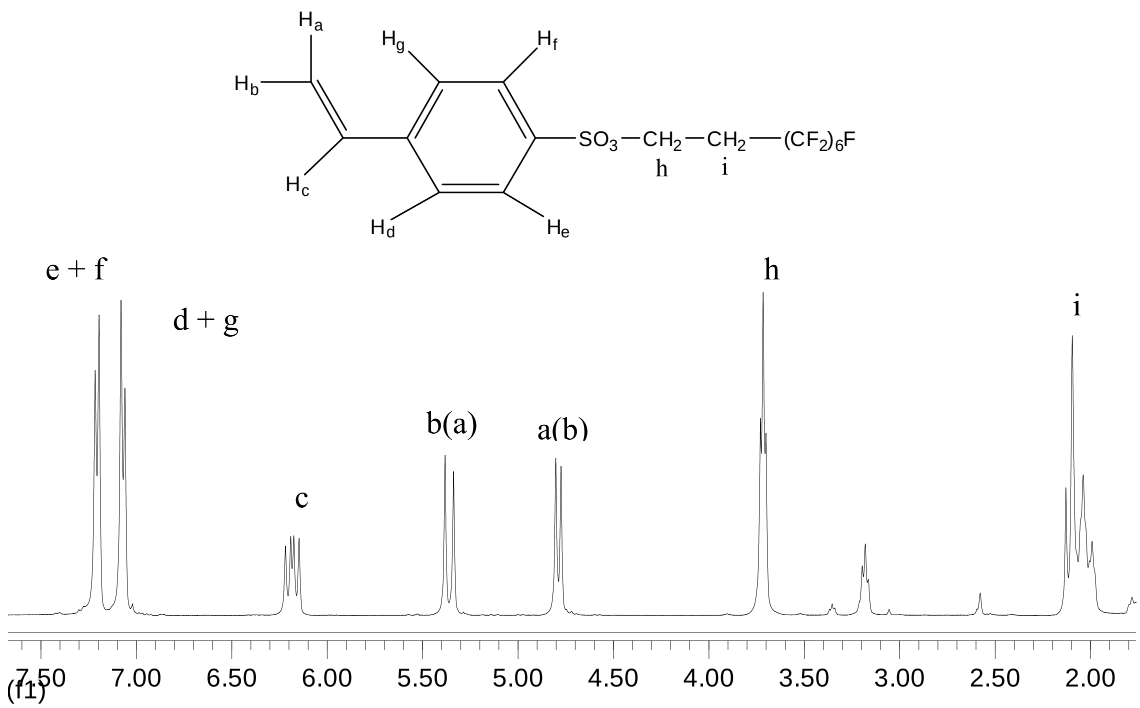

Figure C.2.2. ^{1}H NMR spectra of co-monomer styrene sulfonate ester (R_f-SSE).

C.3. FTIR-ATR Analysis on Crosslinked PEMs

FTIR analysis of the membrane surface before hydrolysis (when the membranes were in ester form) and after hydrolysis (when the membranes were in Na^+-salt form) confirmed that the ester group was converted to sulfonic acid. Figure C.3 shows the typical FTIR-ATR spectra of membrane in ester form before hydrolysis and Na-salt form after hydrolysis. A peak at 1400 cm^{-1} was observed and assigned to the ester group, corresponding to asymmetric stretch of the SO_2 groups in the sulfonate ester. After hydrolysis, disappearance of this peak confirmed that ester groups were fully converted into corresponding acid groups.

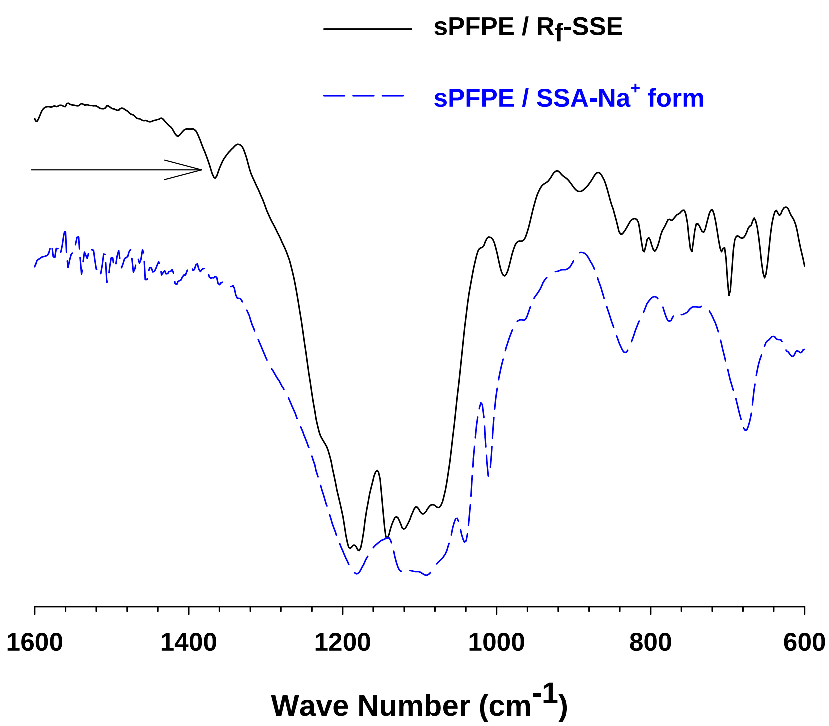

Figure C.3. FTIR-ATR spectra of crosslinked PEM before hydrolysis and after hydrolysis.

C.4. sPFPE MWs and Crosslink Density

Crosslink density is related to the molecular weights of crosslinkers. Reducing the MW of crosslinker increases the crosslinking and crosslink density. Figure C.4 shows behavior of sPFPE moles with crosslinker MW in which crosslink density is assumed to be inversely proportional to the MW of the crosslinker. The lowest MW crosslinker can be the most effective in incorporating the highest crosslinking in the membrane.

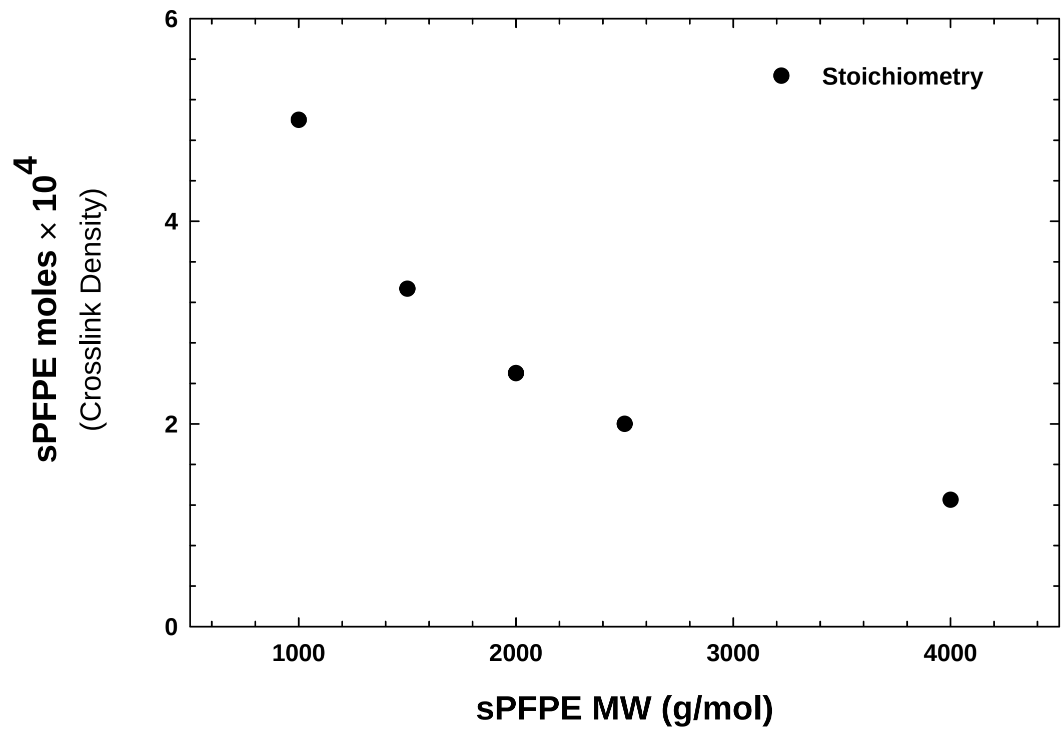

Figure C.4. Effect of crosslinker MWs on crosslink density. Molar amounts of crosslinker in the PEMs are related to crosslink density. Close symbols ● are calculated values from known compositions of PEMs.

C.5. sPFPE/ R_f-SSE Mole Ratio

Figure C.5 shows the mole ratio of crosslinker (4000 g/mol) and co-monomer as function of R_f-SSE weight content. It is clear that moles of R-SSE increases with increasing its weight in the crosslinked PEMs.

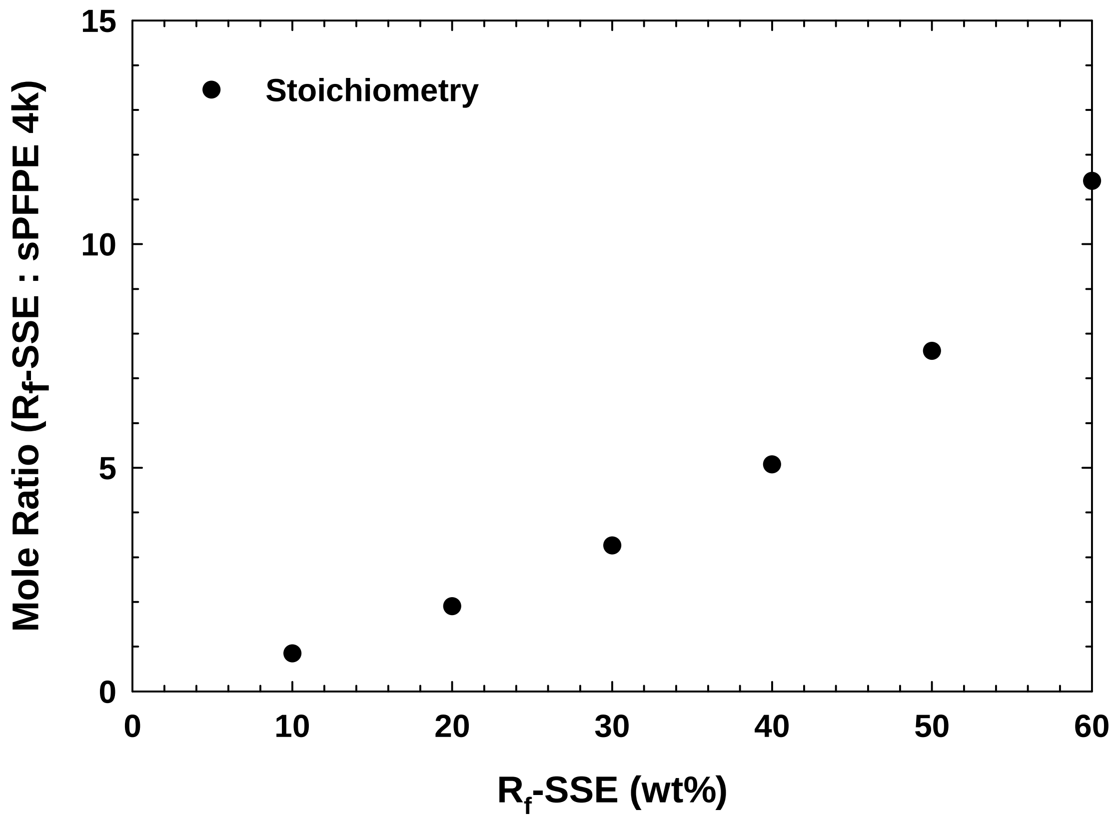

Figure C.5. Mole ratio of R_f-SSE to sPFPE (4000 g mol^{-1}) as function of R_f-SSE weight.

C.6. Methanol Solution Uptake

Decreasing the MW of the crosslinker reduces the methanol uptake. This reduction is attributed to increased crosslinking that prevents the solvent uptake. Figure C.6 shows the methanol solution uptake in crosslinked PEMs at fixed IEC of 1.74 meq g^{-1}.

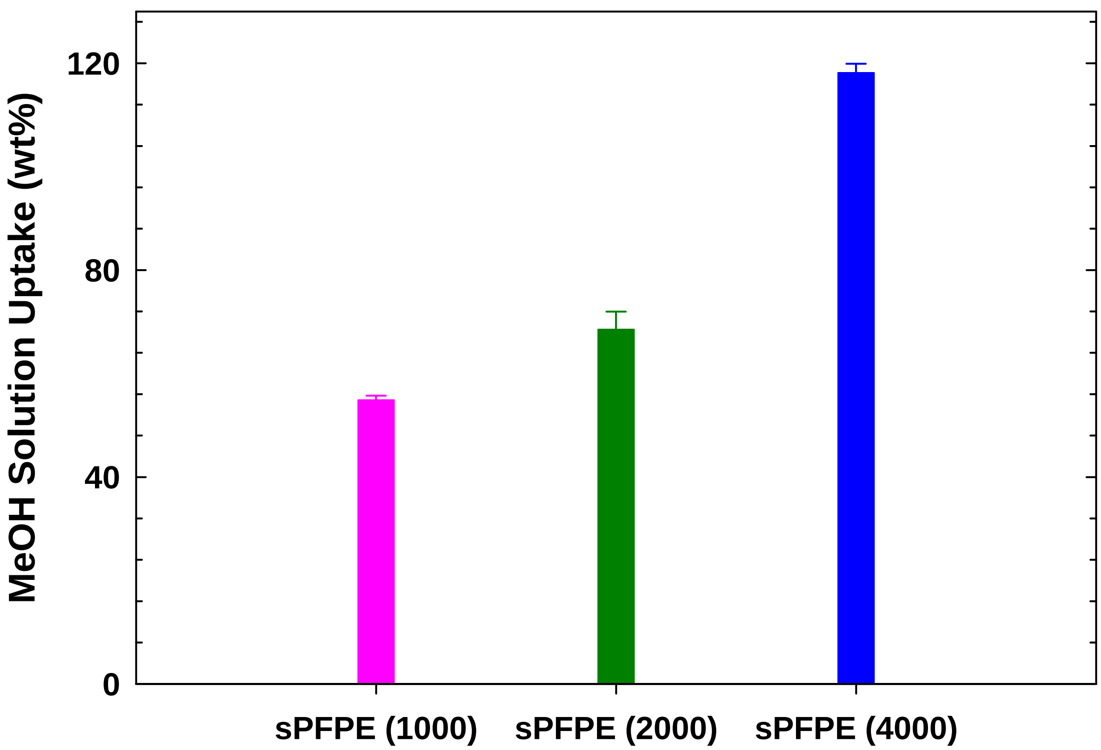

Figure C.6. Methanol solution uptake at room temperature in crosslinked PEMs at IEC of 1.74 meq g^{-1}.

C.7. Impedance Spectra of Crosslinked PEMs

Figure C.7 shows the typical impedance spectra of crosslinked PEM in which the equivalent circuit (R_1Q_1)(R_2Q_2) was fit to extract the bulk resistance of the membrane. This impedance spectra was collected at room temperature and in liquid water using EIS technique and two-probe method.

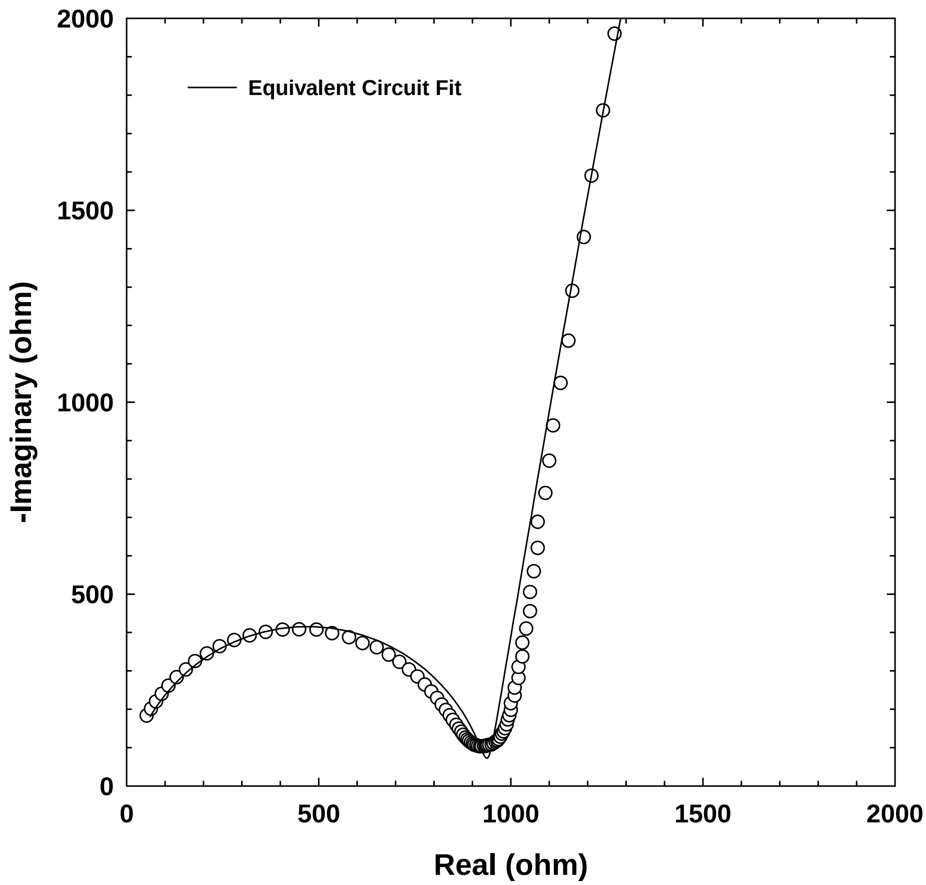

Figure C.7. Typical impedance spectra of crosslinked PEM.

C.8. Crosslinked PEM Conductivity Behavior with Time

Figure B.8 shows the change in conductivity of crosslinked PEM with time because of progress in water uptake at fixed relative humidity of 100% and temperature of 25 °C. In a typical experiment, ionic conductivity was tracked with time to estimate the equilibration of membrane with water vapor activity. Temperature was fixed and monitored closely to allow the membrane to equilibrate with target relative humidity. Typically, membranes attained equilibration with water vapor in 48 hours at any fixed temperature and relative humidity.

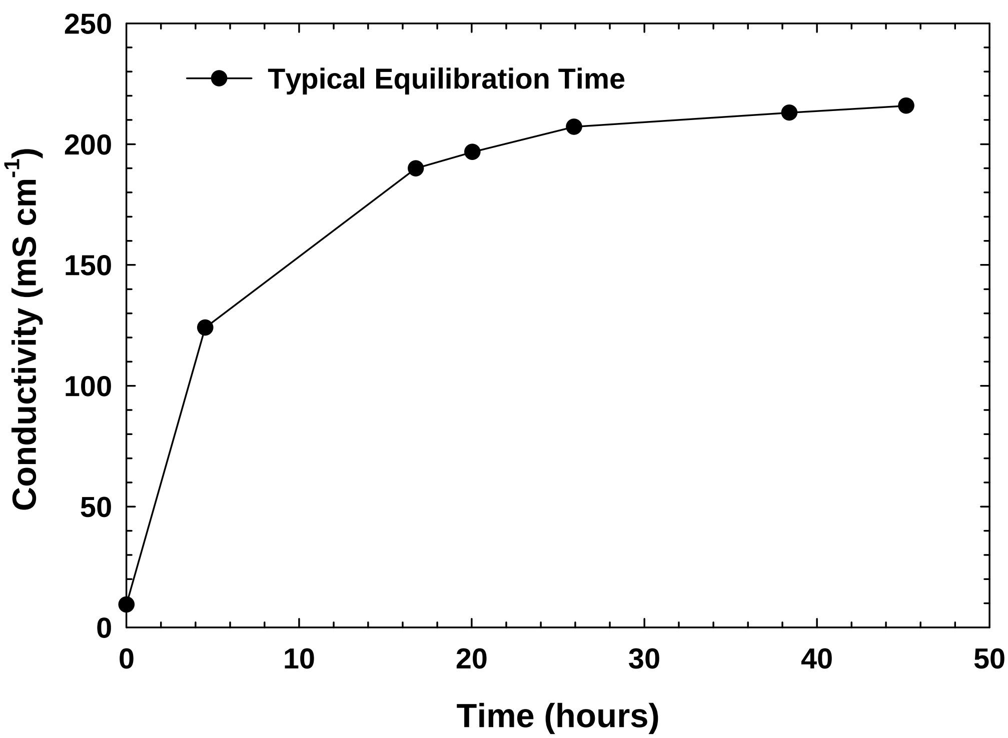

Figure C.8. Change in conductivity with time during equilibration of crosslinked PEM with water vapor activity (100% relative humidity and 25 °C).

C.9. Crosslinked PEMs Composition and Conductivity

Table C.9 Conductivity in Liquid Water and at RT			
Crosslinker MW (g/mol)	**Crosslinker Weight Content (wt%)**	**R_f-SSE (wt%)**	**Conductivity (S cm^{-1})**
4000	80	20	$9.53 \times 10^{-4} \pm 7.77 \times 10^{-5}$
4000	70	30	$2.88 \times 10^{-2} \pm 4.15 \times 10^{-3}$
4000	60	40	$9.53 \times 10^{-2} \pm 9.39 \times 10^{-3}$
4000	50	50	$1.25 \times 10^{-1} \pm 7.75 \times 10^{-3}$
2500	80	20	$5.75 \times 10^{-4} \pm 6.57 \times 10^{-5}$
2500	70	30	$1.11 \times 10^{-2} \pm 1.24 \times 10^{-3}$
2500	60	40	$5.79 \times 10^{-2} \pm 5.34 \times 10^{-3}$
2000	80	20	$6.00 \times 10^{-4} \pm 2.06 \times 10^{-4}$
2000	70	30	$2.79 \times 10^{-2} \pm 7.51 \times 10^{-4}$
2000	60	40	$7.30 \times 10^{-2} \pm 6.54 \times 10^{-3}$
2000	85	15	$5.86 \times 10^{-4} \pm 2.42 \times 10^{-4}$
2000	80	20	$6.56 \times 10^{-3} \pm 4.23 \times 10^{-4}$
2000	70	30	$3.40 \times 10^{-2} \pm 3.58 \times 10^{-4}$
2000	60	40	-
2000	50	50	$1.17 \times 10^{-1} \pm 7.30 \times 10^{-3}$
1500	85	15	$3.84 \times 10^{-4} \pm 4.20 \times 10^{-5}$
1500	80	20	$4.46 \times 10^{-4} \pm 6.82 \times 10^{-5}$
1500	70	30	$3.87 \times 10^{-2} \pm 1.33 \times 10^{-3}$
1500	60	40	$8.47 \times 10^{-2} \pm 3.54 \times 10^{-4}$
1500	50	50	$1.12 \times 10^{-1} \pm 2.18 \times 10^{-3}$
1000	85	15	$3.65 \times 10^{-4} \pm 6.48 \times 10^{-5}$
1000	80	20	$4.15 \times 10^{-4} \pm 9.85 \times 10^{-5}$
1000	70	30	$2.20 \times 10^{-2} \pm 5.02 \times 10^{-3}$
1000	60	40	$7.29 \times 10^{-2} \pm 5.45 \times 10^{-3}$
1000	50	50	$9.55 \times 10^{-2} \pm 6.29 \times 10^{-3}$

C.10. Combination of Low and High MW Crosslinkers

Incorporating low MW crosslinker with high MW crosslinker decreases the conductivity because of increased crosslinking. Figure C.7 shows the effect of low MW crosslinker sPFPE (1000 g mol^{-1}) on conductivity of crosslinker PEMs.

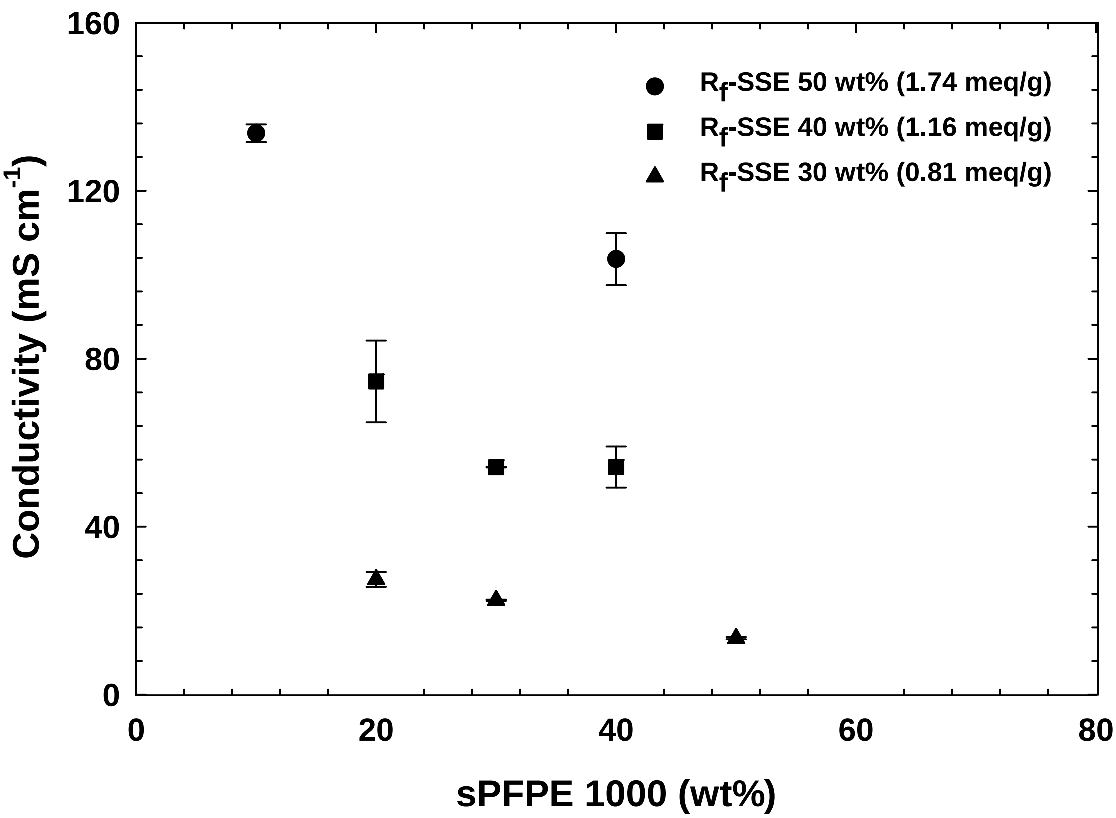

Figure C.10. Ionic conductivity in liquid water and at room temperature for crosslinked PEMs as function of sPFPE 1000 weight content. The remaining weight content of PEM was from sPFPE 4000.

C.11. Selectivity of Crosslinked PEMs

Crosslinked PEMs have showed higher selectivity than that of Nafion 117 membrane. Figure C.11 shows that crosslinking is effective in reducing the permeability that leads to high selectivity.

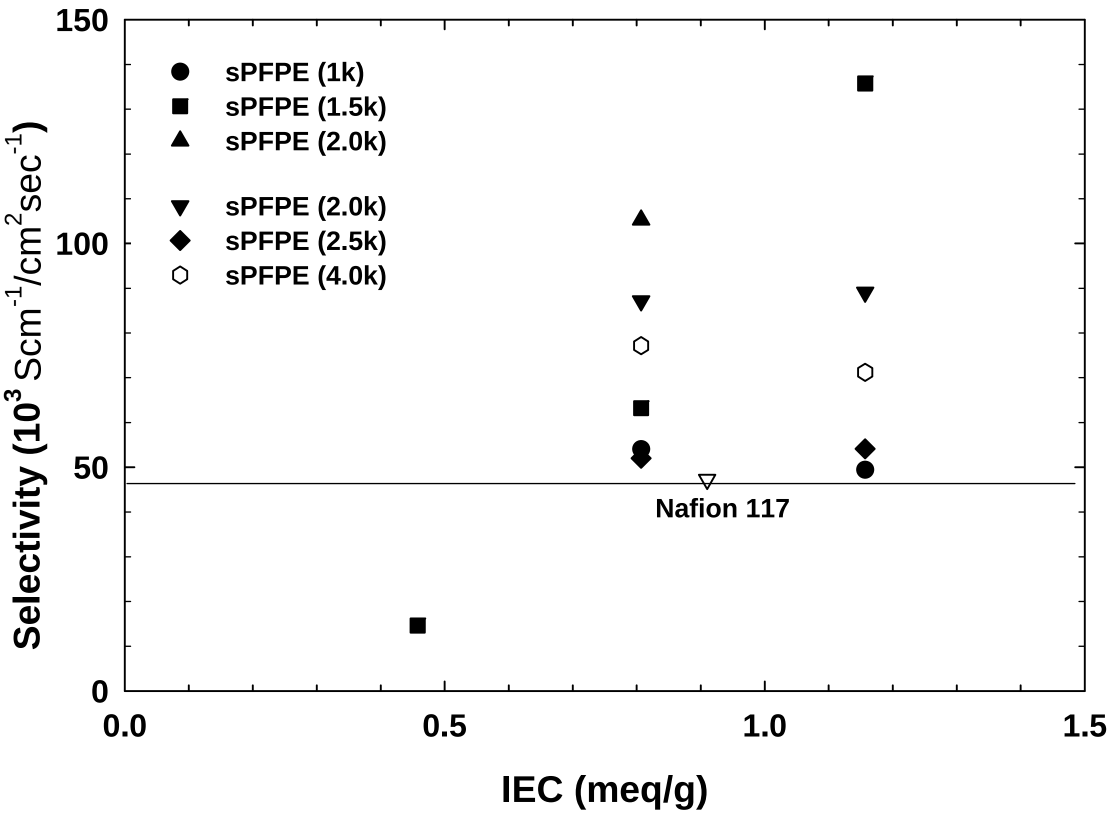

Figure C.11. Selectivity as function of IEC.

Appendix D. Composite PEMs based on ePTFE and sPFPE/R_f-SSE

Composite PEMs were derived from imbibing the porous-expanded PTFE film with sPFPE/R_f-SSE mixture followed by crosslinking through photocuring, hydrolysis and ion-exchange.

D.1. Conductivity of Composite PEMs

Composite PEMs based on expanded-PTFE (ePTFE) are mechanically robust, are chemically inert in acidic environment, are inexpensive to manufacture, have low-dimensional change, and have low-area specific resistance because of low thickness. Because of ePTFE availability, composite PEMs incur lower manufacturing cost than freestanding PEMs. Under identical IEC, composite PEMs have several advantages over free-standing PEMs. However, conventional composite PEMs suffer from some shortcomings such as insufficient impregnation of pores during their preparation, delamination of imbibing material from the pores, and lack of mechanical strength in the imbibing material.

For complete impregnation of pores, imbibing materials should have low-surface energy to overcome the capillary forces in order to impregnate the pores uniformly and entirely. Chemical crosslinking of impregnating material can prevent the delamination from the pores and provide sufficient mechanical strength to the composite PEMs. A liquid precursor approach based on low-surface energy of PFPE has advantage over other traditional methods because low-surface energy of PFPE can ensure complete impregnation of pores at affordable condition.

In this work, porous ePTFE film was soaked in target sPFPE/R_f-SSE mixture and was allowed to contain the liquid mixture in its pores. Usually, the mixture contained high amount of R_f-SSE to achieve comparable IEC with that of Nafion membrane. To obtain composite PEMs in acid form, ePTFE film that was soaked in sPFPE/R_f-SSE liquid mixture was prepared following the synthesis procedure of free-standing cross-linked PEMs. Bubble point test confirmed that composite PEMs held 50 psig of pressure for several hours. Bubble point test also showed that pores were completely impregnated with liquid sPFPE/R_f-SSE mixture.

Water uptake and conductivity were measured to characterize the composite PEMs relative to Nafion 117 membrane. At room temperature, composite PEMs absorbed 51 ± 10 wt% water from water vapor at 100% relative humidity and 81 ± 9 wt % water from liquid water. Water uptake in composite PEMs was two to three times higher than that of Nafion 117. Such high-water uptake was achieved due to high IEC resulting from 70 wt% of R_f-SSE in the liquid mixture. Expectedly, composite PEMs exhibited conductivity of three times higher than that of Nafion 117 at 100% relative humidity. At 100% relative humidity, conductivity increased by two times from 200 to 490 mS cm^{-1} for temperatures of 25 to 80 °C. Figure D.1 shows the conductivity results of composite PEMs and Nafion 117 membrane. Increase in ionic conductivity with temperature is typical. We confirmed that ionic conductivity followed the Arrhenius behavior with activation energy of 16.7 kJ mol^{-1} that is higher than that of Nafion 117 (11.3 kJ mol^{-1}). High-activation energy may be due to rearrangement of ionic groups and pore walls at high temperature.

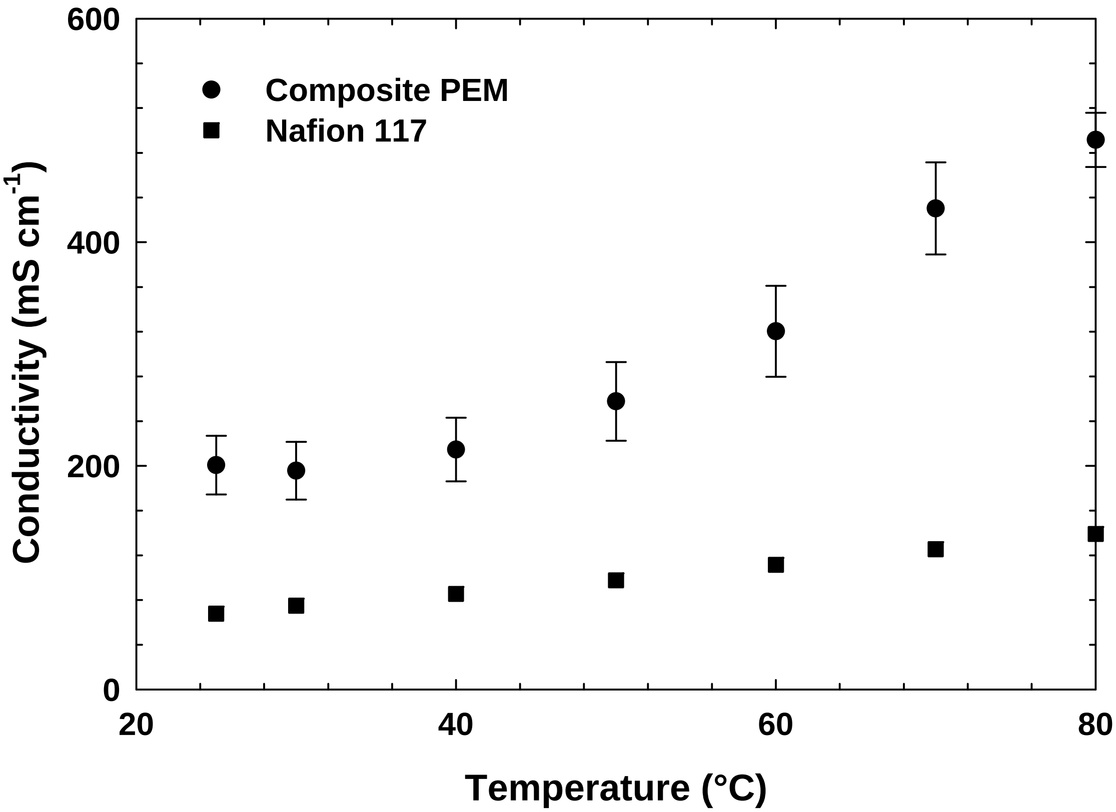

Figure D.1. Conductivity of composite PEMs at 100% relative humidity. The composition of liquid precursor that was imbibed in ePTFE was 30 wt% of sPFPE (4000) and 70 wt% of R_f-SSE.

Appendix E. Equipment and Instruments

This section provides the specifications of equipment and instruments.

E.1 Equipment and Instruments

Digital Micrometer-Mitutoyo Corporation, Japan, Model: IDC –112CEB, Code No. 54B 144B, S/N: 400396, Range 0-12.7 mm, Accuracy 0.001 mm

Potentiostat-Zahner/BAS, Model IM6e, 14007, Thales Software

Temperature Bath-Neslab Instrument, INC, S/N-19831049, Model-RTE-111, Refrigerant –R-134A, Pressure Range 150-300 psi, Temperature Range –25 –150 °C. Temperature Stability +/-0.01 C, Bath Volume 7 liters, Flow Rate 15 liter/min at 0 meter 0 liter/min at 4.9 meter.